Investigations of Structural, Dielectric and Electrical Properties of Rare Earth Doped Layered Ferroelectric Ceramics

THESIS

Submitted in partial fulfillment

of the requirements for the degree of

DOCTOR OF PHILOSOPHY

by

RAJESH KANNAN B

ID. No. 2011PHXF029H

Under the supervision of

Dr. B. Harihara Venkataraman

BITS Pilani

Pilani | Dubai | Goa | Hyderabad

BIRLA INSTITUTE OF TECHNOLOGY AND SCIENCE, PILANI

Hyderabad Campus, Hyderabad, INDIA

2016

BIRLA INSTITUTE OF TECHNOLOGY AND SCIENCE, PILANI

Hyderabad Campus, Hyderabad

CERTIFICATE

This is to certify that the thesis entitled **"Investigations of Structural, Dielectric and Electrical Properties of Rare Earth Doped Layered Ferroelectric Ceramics"** was submitted by **Rajesh Kannan B** ID. No. **2011PHXF029H** for the award of Ph. D. degree of the Institute embodies original work done by him under my supervision.

Signature of the supervisor :

Name in capital letters : Dr. B. HARIHARA VENKATARAMAN

Designation : Assistant Professor

Date :

Acknowledgement

First and foremost I wish to thank my supervisor Dr. B. HariharaVenkataraman, Assistant Professor, Department of Physics, BITS-Pilani Hyderabad, for his active guidance, continuous support and constant motivation throughout this journey. I am extremely obliged to Doctoral Advisory Committee (DAC) members, Prof. Souri Banerjee and Prof. Kannan Ramaswamy, Department of Physics, BITS -Pilani Hyderabad for their valuable suggestions on the research work whenever needed. My sincere thanks to Prof. Bijendra Nath Jain, former vice chancellor of BITS, for providing necessary support to accomplish my research work. My heart felt gratitude to Prof. V. S. Rao, Director (BITS - Pilani, Hyderabad Campus) and present vice chancellor of BITS for his constant support and encouragement throughout the course of the research work. I am grateful to Prof. M. M. S. Anand, Registrar, Prof. S. K. Verma, Dean, Academic Research (Ph.D. Programme), Prof. M. B. Srinivas, Dean, General Administration and Prof. Vidya Rajesh, Associate Dean, Academic Research (Ph.D. Programme) BITS - Pilani, Hyderabad, for extended their kind cooperation. I sincerely thank Dr. Aravinda N Raghavan, Assistant Professor and Head, Department of Physics, BITS - Pilani Hyderabad for providing infrastructural facilities to execute the research work. I am greatly indebted to Dr. A.R. James, Scientist-F, Defence Metallurgical Research Laboratory, (Ministry of Defence) for his kind assistance in ferroelectric hysteresis characterization. I specially thank Prof. N. Rajesh, Chemistry Department for his kind encouragement and support during my entire stay in our campus. I deeply acknowledge **Department of Science and Technology,** New Delhi, India for funding the project (SR/FT/CS-065/2009) and fellowship.

Last but not least, I thank my Mother and God almighty for standing with me in all my steps.

Rajesh Kannan B

April, 2016

ABSTRACT

In recent years, bismuth layered ferroelectric materials such as $SrBi_2Ta_2O_9$ (SBT), $BaBi_2Nb_2O_9$ (BBN), $Bi_4Ti_3O_{12}$ (BIT) and $SrBi_2Nb_2O_9$ (SBN) have attracted much attention due to its potential applications in nonvolatile random access memory (NVRAM) devices. Lead zirconate titanate, $PbZrTiO_3$ (PZT) was the prominent material for the NVRAM application owing to its low switching field, high remnant polarization and low processing temperature. However, the PZT material undergoes severe fatigue failure and retention loss on conventional silicon substrate with platinum (Pt) electrodes. The renewed interest stems from the Aurivillius family of layered ferroelectric materials (e.g. SBT, BBN, BIT, and SBN) because of their fatigue-free behavior and low coercive field. But the drawbacks of these layered ferroelectric materials are low remnant polarization, high processing temperature and high dc conductivity. It was known that the physical properties of these layered ferroelectric materials could be enhanced by doping the suitable cations in the crystal lattice. The emergence of lanthanum ion doped bismuth titanate has fuelled considerable interest to investigate the influence of trivalent rare earth ions on the physical properties of bismuth based layered ferroelectric compounds. It is widely accepted that the Bi_2O_2 layers have a significant influence on the polar and electrical conductivity properties of bismuth based layered structures. It is expected that by substituting Bi^{3+} (ionic radius = 0.103 nm) ion with a slightly smaller rare earth cation such as Sm^{3+} ion (ionic radius = 0.098 nm) could significantly increase the structural distortion in the crystal structure and thereby enhancing the polar properties. However, the studies are limited concerning the improvement of dielectric properties of the layered perovskite ferroelectrics such as SBT and BBN through the substitution of Bi^{3+} ions in Bi_2O_2 layer by samarium ion (Sm^{3+}). Molten salt synthesis (MSS) is one of the effective routes for synthesizing ceramic powders at relatively lower temperatures. By this fabrication route, one can achieve improved homogeneity, purity and good control over particle sizes as compared to that of the conventional solid state reaction route. Since, there seems to be no attempts made to synthesize samarium ion doped layered ferroelectric compounds such as strontium bismuth tantalate and barium bismuth niobate via molten salt synthesis route, the present investigations in the thesis have been taken up to substitute Bi^{3+} by Sm^{3+} in the crystal lattice of SBT and BBN layered ferroelectric compounds fabricated by molten salt synthesize method and study its influence on the

structural, dielectric, electrical conductivity and ferroelectric properties in order to exploit these materials for aforementioned applications.

Polycrystalline $Sr(Bi_{0.9}Sm_{0.1})_2Ta_2O_9$ (SBSmT) ceramics were fabricated via the promising low temperature molten salt synthesis route using potassium chloride (KCl) as a flux material. The mono-phasic perovskite crystal structure was confirmed by the X-ray powder diffraction patterns. The scanning electron microscopic studies revealed the presence of plate shaped morphological features of the SBSmT ceramics. Interestingly, the dielectric constant of the SBSmT ceramics in the frequency range of 100 Hz - 1 MHz could be tuned as a function of sintering duration. It is observed that the SBSmT ceramics sintered at 1323 K for 10 h exhibited higher dielectric constant (ε'_r= 76) at 100 kHz than those of ceramics sintered at other durations. The magnitude of the electrical conductivity of the order of 10^{-7} - 10^{-9} S/cm at 300 K indicates that the conductivity mechanism might be attributed to the migration of oxygen ion vacancies in these ceramics. However, systematic efforts have been made to investigate the influence of samarium on the physical properties of $SrBi_2Ta_2O_9$ and $BaBi_2Nb_2O_9$ ceramics by adding an excess amount of 5 wt % bismuth oxide to the initial mixture of reactants during calcination to compensate bismuth vaporization at high temperatures and the details of which are discussed in the remaining chapters.

Layered $Sr(Bi_{1-x}Sm_x)_2Ta_2O_9$ ceramics with x ranging from 0 - 0.10 (10 mol%) were fabricated by the low temperature molten salt synthesis route. X - ray powder diffraction studies revealed that the single phase orthorhombic layered perovskite structure is retained in all these compositions. Scanning electron microscopic studies on these ceramics confirmed the presence of well packed equiaxed plate shaped grains. The dielectric and electrical conductivity properties were studied in the 100 Hz – 1 MHz frequency range at 300 K. Interestingly, the 10 mol% samarium doped $SrBi_2Ta_2O_9$ ceramics exhibited high dielectric constant (ε'_r = 155) and low dielectric loss (0.00298) compared to those of other compositions. The ferroelectric property of $SrBi_2Ta_2O_9$ ceramics is superior for higher concentration of samarium content. The electrical conductivity of undoped and samarium doped ceramics increased linearly with increase in frequency.

The dielectric and electrical conductivity measurements were carried out in the 100 Hz - 1 MHz frequency range at various temperatures for undoped and samarium doped $SrBi_2Ta_2O_9$ ferroelectric ceramics. A decrease in dielectric constant maximum (ε_m) and a downward shift in the Curie transition temperature (T_c) have been observed with the increase

in samarium concentration. The frequency dependence real and imaginary parts of dielectric constant of these ceramics exhibited low frequency dielectric dispersion. Interestingly, temperature and frequency dependent dielectric constant plots indicated that the formation of oxygen ion vacancies have been inhibited by samarium doping in SBT lattice. The activation energy values obtained from the Arrhenius plot have confirmed the existence of motion of oxygen ion vacancies in these ceramics.

Barium bismuth samarium niobate $Ba(Bi_{1-x}Sm_x)_2Nb_2O_9$ (x = 0, 0.03, 0.05, and 0.10) ceramics have been fabricated successfully via molten salt synthesis route. The X - ray diffraction analysis revealed the existence of bismuth layered perovskite phase with orthorhombic crystal structure in all the compositions studied. The dielectric and electrical conductivity properties were carried out in the 100 Hz – 1 MHz frequency range at 300 K. The dielectric constant and dielectric loss were found to decrease from 186 to 180 and 0.0966 to 0.0755 respectively with increase in samarium content at 100 kHz.

The temperature dependence of dielectric and electrical conductivity properties of polycrystalline $BaBi_2Nb_2O_9$ and $Ba(Bi_{0.9}Sm_{0.1})_2Nb_2O_9$ ceramics investigated at various frequencies have revealed the characteristic features of relaxor behaviour. The incorporation of Sm^{3+} for Bi^{3+} has induced a downward shift in the dielectric maximum temperature (438 K - 393 K) with the decrease in dielectric constant maximum (372 - 212) at 100 kHz. The estimated degree of diffuseness (γ) was found to be 2.17 for $BaBi_2Nb_2O_9$ and 1.93 for $Ba(Bi_{0.9}Sm_{0.1})_2Nb_2O_9$ ceramic samples. The activation energy obtained from the Arrhenius plot revealed the existence of motion of oxygen ion vacancy in these ceramics.

Table of Contents

List of Tables

List of Figures

List of Abbreviations

XRD	: X-ray powder diffraction
SEM	: Scanning electron microscope
SBT	: Strontium bismuth tantalate
BBN	: Barium bismuth niobate
SBSmT	: Samarium doped strontium bismuth tantalate
BBSmN	: Samarium doped barium bismuth niobate
PZT	: Lead zirconium titanate
BIT	: Bismuth titanate
SBN	: Strontium bismuth niobate
MSS	: Molten salt synthesis
NVRAM	: Non-volatile random access memory
BLSFs	: Bismuth layered structured ferroelectrics
LFDD	: Low frequency dielectric dispersion
BBT	: Barium bismuth titanate

List of Symbols

ε_r	: Dielectric constant
P_s	: Spontaneous Polarization
T_c	: Curie transition temperature
χ	: Dielectric susceptibility
ε_0	: Permittivity of free space
α	: Total polarizability
$n(T)$	: Temperature dependent exponent that determines the interaction of dipoles
$a(T)$	: Strength of polarizability

Chapter 1

Introduction

1. **Introduction**

This chapter primarily describes the underlying phenomenon of dielectric and ferroelectric properties of materials. In addition to the principles and phenomena, the modelling of dielectric behaviour of ferroelectric materials by Jonscher's universal formalism has also been briefly discussed. Subsequently, the interesting aspects of the crystal structure and physical properties of Aurivillius family of layered ferroelectric ceramics, reported in the literature have been dealt.

1.1. Ferroelectric materials

Ferroelectric materials exhibit spontaneous polarization that could be reversed by an externally applied electric field. The polarization response of ferroelectric materials with respect to the electric field is non-linear leading to the occurrence of ferroelectric hysteresis loop [1-3]. These materials are being widely used in a range of applications which include sensors, actuators, non-linear optical devices and optical modulators [4-8]. Ferroelectric phenomenon was first discovered in Rochelle salt single crystals in 1921 by J. Valasek [9] followed by the observation of the same phenomenon in potassium dihydrogen phosphate, KH_2PO_4 [10]. A theory on the phase transition of hydrogen bonded compounds was published in 1941 by Slater that stimulated a great interest in ferroelectricity among the physicists. The anomalous dielectric behaviour of $BaTiO_3$ had been simultaneously observed by Ogawa, Wainer and Solomon, Wul and Goldman and later Von Hippel et.al confirmed the ferroelectric nature of $BaTiO_3$[11-21]. Presently, bismuth layered ferroelectric compounds and tetragonal tungsten bronze structures are at the helm of emerging technologies and the application ranges from capacitors to ferroelectric non - volatile random access memories.

1.2. Crystal symmetry requirements and Classification of materials

In general, basic crystal systems could be classified into 32 point groups based on the symmetry operations such as translation, rotation, mirror planes and inversion. Out of the 32 crystal classes, 11 point groups are centrosymmetric and 21 point groups are non-centrosymmetric. The centrosymmetric point groups cannot possess polar properties since they lack a point of inversion symmetry. The remaining 21 are non-centrosymmetric and 20 of these are piezoelectric in which 10 point groups exhibit pyroelectric activity. A special category of materials designated as ferroelectrics are the subgroup of spontaneously polarized pyroelectrics (Figure 1.1) [22]. Hence, all the ferroelectrics are pyroelectrics and all the pyroelectrics are piezoelectrics but the reverse is not applicable. The inherent characteristic features for the ferroelectrics are (i) existence of spontaneous polarization and (ii) polarization reversibility with an applied electric field [23].

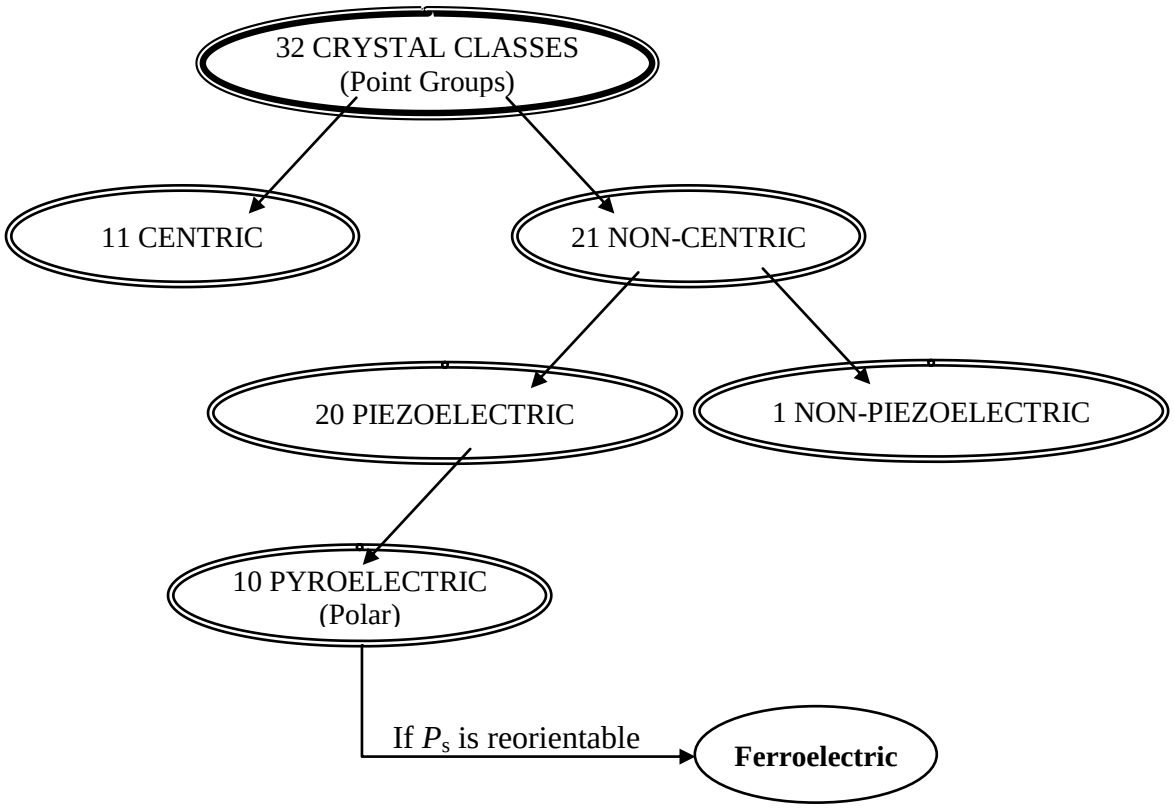

Figure 1.1. Classification of materials[22]

1.3. Ferroelectric domains

Ferroelectric materials comprise of regions with uniformly oriented polarization vectors, which are called ferroelectric domains. These domains are separated by domain walls and the thickness of the domain wall is quite small. For instance, the thickness of the $BaTiO_3$ domain wall is about 2 Å. The wall that separates the relative orientation in the polarization vectors between two domain walls by 90° are called 90° domains and those which distinguish the relative orientation between two domain walls by 180° are called 180° domains (Figure 1.2). One can observe the domains by etching the surface of ferroelectric materials with a suitable etchant. The consequence of domain wall switching in ferroelectric materials leads to the occurrence of the ferroelectric hysteresis loop [24].

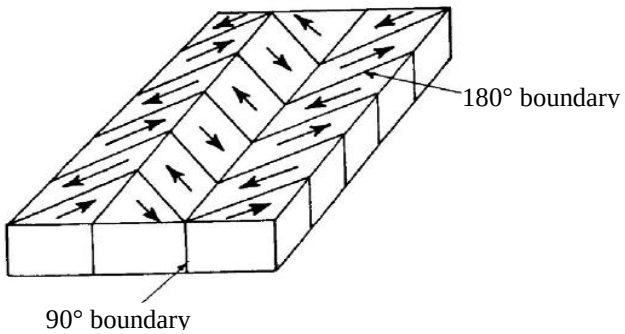

Figure 1.2. Schematic illustration of 90° and 180°domain walls [24]

1.4. Ferroelectric phase transitions

The intrinsic ferroelectric property of a ferroelectric disappears above the transition temperature called Curie temperature T_c. Above T_c, the material remains in a para electric state and the crystal structure becomes centrosymmetric. The dielectric, optical and elastic properties of a ferroelectric material exhibits anomalies in the vicinity of Curie temperature. The temperature dependence of the dielectric constant above T_c obey the Curie- Weiss law,

$$\varepsilon_r - 1 = C \,/\, (T - T_\theta)$$

Where C is a material specific Curie-Weiss constant, T is an absolute temperature, measured in Kelvin and T_θ is the Curie - Weiss temperature. For first order transition, $T_\theta < T_c$ and for the second order transition, $T_\theta = T_c$. In second order phase transition, spontaneous polarization (P_s) decreases continuously from a maximum to zero as T approaches the T_c whereas in the first order transition, P_s acquires a zero value at T_c [25-30].

Diffuse phase transition

Diffuse phase transition (DPT) is usually characterized by the broadening in the temperature dependent dielectric curve and frequency dispersion of both ε′ and tanδ in the transition region. The diffuseness of a phase transition could be estimated by

$$\left(\frac{1}{\varepsilon'} - \frac{1}{\varepsilon'_{max}}\right) = C^{-1}(T - T_{max})^{\upsilon}$$

where ε' is the relative dielectric constant at temperature T, ε'_{max} is the relative dielectric constant at the transition temperature T_c, ν is the critical exponent and C is the Curie constant. A value of ν = 1 implies that the material obeys the ideal Curie-Weiss behavior, whereas ν =2 indicates a completely diffuse transition (i.e., relaxor behavior).The diffuseness in the phase transition arises due to the compositional fluctuations of cations in the crystal lattice and crystallite size distribution [31].

1.5. Polarization switching and hysteresis loop

The inherent interesting characteristics feature of the ferroelectrics is the property of reversal or change in polarization direction by an applied electric field that leads to a hysteresis in the

polarization and electric field relation. The parameters such as remnant polarization, coercive field and saturation polarization could be determined from the hysteresis loop [32].

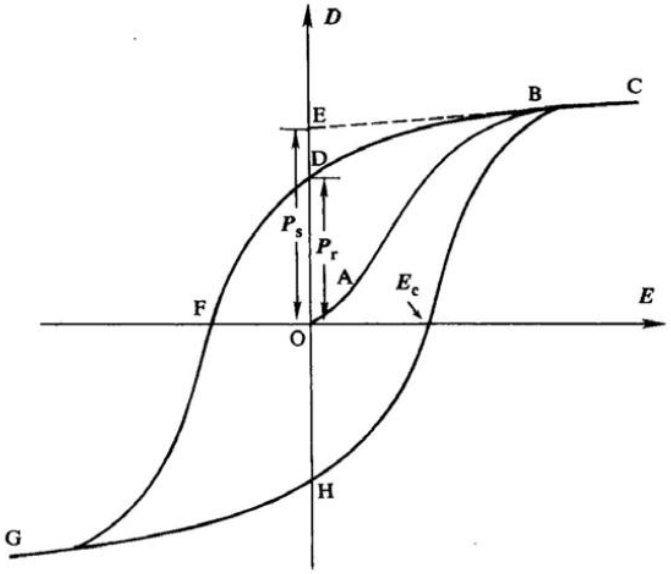

Figure 1.3. A typical P-E hysteresis loop in ferroelectrics[32].

Figure 1.3 illustrates a typical ferroelectric hysteresis loop. The domains start to align in the positive direction as the electric field strength is increased that leads to a rapid increase in the polarization and at very high fields the polarization reaches a saturation value. Some of the domains remain aligned in the positive direction at zero external field and hence the material will exhibit a remnant polarization (P_r). The external field required to reduce the polarization to zero is called coercive field. On further increasing the field in the negative direction, the direction of polarization flips and hence a hysteresis loop is obtained [33].

1.6. Classification of ferroelectrics

Ferroelectric materials are generally classified into order-disorder and displacive type ferroelectrics [34].

(i) Order-disorder class: In this class of ferroelectrics, the motion of protons is related to the polar property. Potassium dihydrogen phosphate (KDP) and triglycine sulphate (TGS) are the classical examples for this category.

(ii) Displacive class: This class of ferroelectrics includes ionic crystal structures pertaining oxygen octahedra and the distortion in the oxygen octahedral causes the ferroelectricity. The structures incorporating oxygen octahedra are mainly perovskites and bismuth layer - structured (Aurivillius) compounds.

Since the focus of the present research investigations is mainly concerned with the physical properties of bismuth layered ferroelectric compounds, the discussion is related to these compounds. Ferroelectric bismuth layered compounds were first reported by Aurivillius in 1949. These compounds are being widely used for their potential applications in the ferroelectric non-volatile random access memory device applications due to their large spontaneous polarization, low leakage current and high transition temperatures. The general formula for Aurivillius family of layered oxides is $(Bi_2O_2)^{2+}$ $(A_{n-1}B_nO_{3n+1})^{2-}$ where A is the 12 - fold coordinated cation such as Ca^{2+}, Sr^{2+}, Ba^{2+}, Pb^{2+}, Bi^{3+} etc, B is the octahedra site occupied by cations like Fe^{3+}, Ti^{4+}, Nb^{5+}, Ta^{5+} and W^{6+} and n is an integer indicating the number of perovskite slabs interleaved in between $[Bi_2O_2]^{2+}$ layers. The crystal structures of Bi_2WO_6, Bi_3TiNbO_9 and $Bi_4Ti_3O_{12}$ determined by R. E. Newnham are shown in (Figure 1.4). In these crystal structures, the octahedral shape of the oxygen framework in the perovskite slabs of the parent structure remains intact and the origin of ferroelectricity in these compounds mainly arises from the displacement of Bi atoms along a - axis in the perovskite A sites with respect to the chains of octahedra [34].

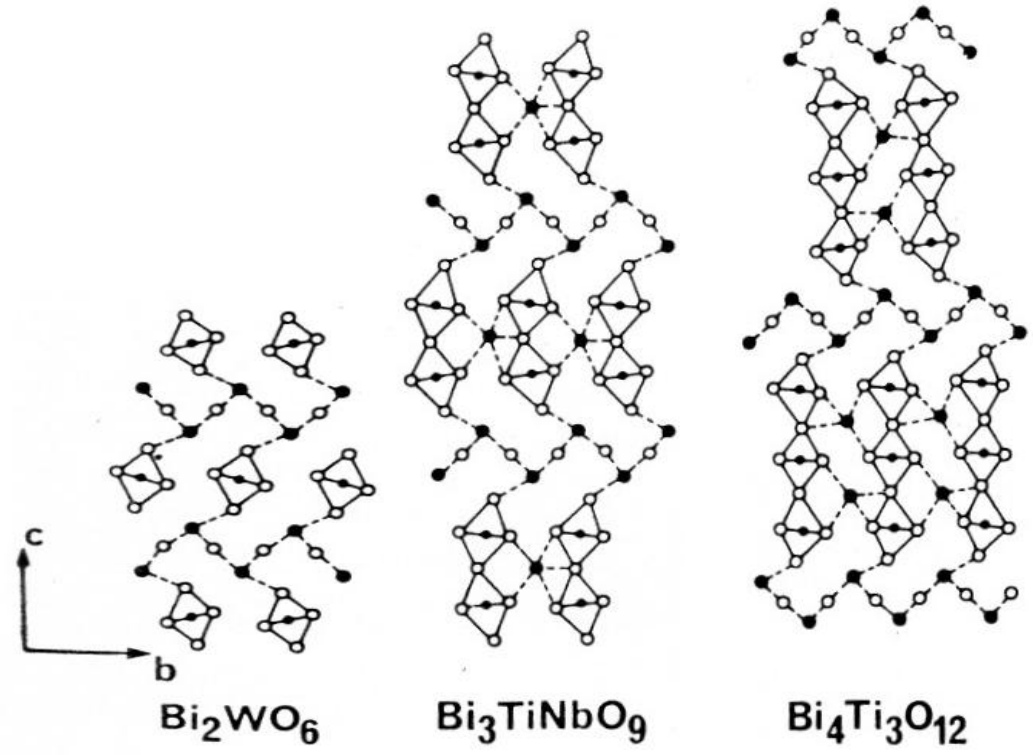

Figure 1.4. (011) sections of: (a) Bi_2WO_6 (n=1); (b) Bi_3TiNbO_9 (n=2); (c) $Bi_4Ti_3O_{12}$ (n=3) real structures. Dashed lines indicate strong Bi-O bonds.

1.7. Ferroelectric ceramics

A ferroelectric ceramic is a polycrystalline material in which individual grains are single crystals of a ferroelectric phase and these grains are separated by well-defined grain boundaries. In ceramic materials, the grains are randomly oriented and it is possible to orient the grains to produce textured specimens with special fabrication processing technique. Normally, the thickness and composition of the grain boundaries control the interaction between the grains. The material properties between the ferroelectric grains and the grain boundaries could differ and hence grain boundaries play a significant role in determining the macroscopic properties of the polycrystalline ceramics. Depending on the fabrication techniques, the grain sizes of ferroelectric ceramics differ from 0.01 μm to 10 μm [35].

1.8. Dielectric properties of ferroelectric ceramics

Dielectrics are insulators in which the electrons are very tightly bound with atoms or molecules. The dielectric properties such as dielectric constant, dielectric loss and dielectric strength have been of most concern for prominent applications as capacitors in electronic circuits and as electrical insulators.

The capacitance of a dielectric material could be correlated with the charge stored inside the capacitor by Q = CV, where V is the applied voltage and C is the capacitance. For a parallel plate capacitor, the capacitance is directly proportional to the area and inversely proportional to the thickness as $C = \varepsilon_r \varepsilon_0 A / d$, where ε_r is the relative permittivity of the material, ε_0 is the free space permittivity and A is the area of the capacitor and d is the thickness.

When a dielectric is placed in an external electric field, it becomes polarized. The polarization P is defined as the net dipole moment per unit volume

$$\vec{P} = \vec{p}/\Delta V$$

If N is the total number of molecules in unit volume and if each has a moment p, then the polarization is given by,

$$\vec{P} = N\vec{p}$$

The displacement vector and the electric field could be interrelated by the following equation,

$$\vec{D} = \varepsilon_0 \vec{E} + \vec{P}$$

The dielectric constant (ε) is related to the dielectric susceptibility (χ) by the relation,

$$\varepsilon = 1 + 4\pi\chi$$

Moreover, dielectric constant is a complex quantity consists of real and imaginary components

$$\varepsilon^* = \varepsilon' - i\varepsilon''$$

Dielectric loss or loss tangent is given by

$$tan\ \delta = \varepsilon'' / \varepsilon'$$

where ε' and ε'' are real and imaginary part of the dielectric constant. The loss tangent is related to the quality factor of the material by $Q = 1/\ tan\ \delta$.

1.9. Polarization

The dipole moment per unit volume P is proportional to the applied electric field in the polar materials for uniform isotropic medium.ie.,

$$\vec{P} = \chi\varepsilon_0 \vec{E}$$

where χ is the dielectric susceptibility and ε_0 is the permittivity of free space. In dielectric materials, different kinds of polarization mechanism (Figure 1.5) exist due to the presence of various charge carrier species. The electronic polarization is prevalent in all the materials and it arises by the displacement of center of gravity of the negative electron clouds with respect to the positive nucleus of the atom under the influence of an external applied electric field. On the other hand, in an ionic lattice, the relative displacement of positive and negative ions in opposite direction produces the ionic polarization. In polar molecules, the dipoles tend to align along the direction of the electric field and eventually produce the orientation polarization which is a function of frequency and the temperature. The space charge polarization arises owing to the accumulation of charges (i.e., free charge carriers) at the electrodes or at the interfaces in multiphase dielectrics [36].

The total polarizability of the material is the sum of all these individual polarizabilities and it could be written as $\alpha = \alpha_e + \alpha_i + \alpha_o + \alpha_s$ where α_e is the electronic, α_i is the ionic, α_o is the orientation, and α_s is the space chare polarizability.

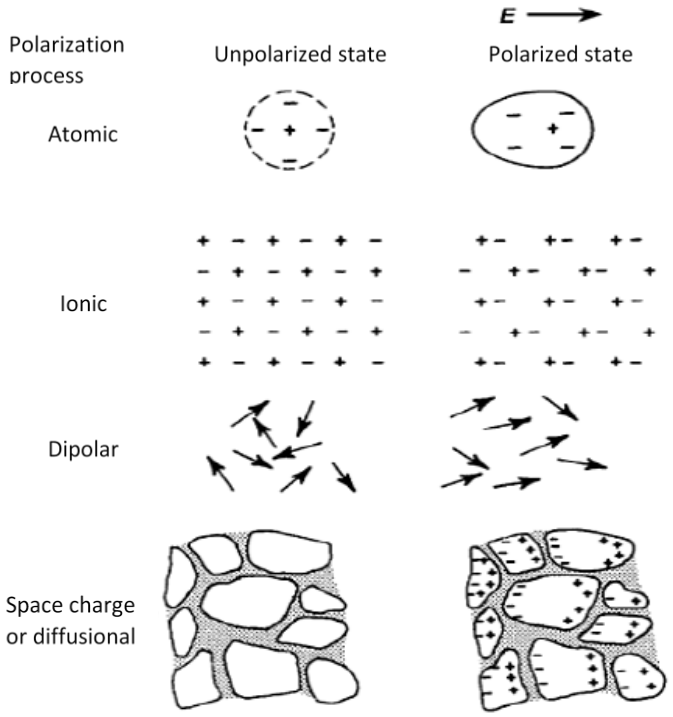

Figure 1.5. Different kinds of polarization mechanism

1.10. Dipolar responses

The dielectric constant of the material with non-negligible conductivity has two contributions from (i) intrinsic polarization and (ii) charge carrier polarization and the net dielectric is governed by

$$\varepsilon_r{}' = \varepsilon_r{}'_{(lattice)} + \varepsilon_r{}'_{(carrier)}$$

where $\varepsilon_r{}'_{(lattice)}$ represents the lattice response due to permanent dipoles and $\varepsilon_r{}'_{(carrier)}$ represents the carrier response associated with long range migration. The materials with significant ionic conductivity do not reflect the lattice contribution since the polarization associated with mobile charge carriers is prevalent. Jonsher introduced a model to separate out the lattice and charge carrier polarization of the material by the following dielectric dispersion relations

$$\varepsilon_r' = \varepsilon_\infty + \sin\left(\frac{n(T)}{2}\right)\omega^{n(T)-1}a(T)/\varepsilon_0$$

$$\varepsilon_r'' = \frac{\sigma}{\varepsilon_0\omega} + \sin\left(\frac{n(T)}{2}\right)\omega^{n(T)-1}a(T)/\varepsilon_0$$

where ε_∞ is the high frequency value of dielectric constant, $n(T)$ is the temperature dependent exponent and $a(T)$ is the strength of polarizability arising from the universal mechanism [8]. The first term in the above equations represent the lattice response and the dc conduction part. The second terms in both the equations represent the charge carrier contribution of the observed dielectric constants.

1.11. Scope of the present work

In recent years, bismuth layered ferroelectric materials such as $SrBi_2Ta_2O_9$ (SBT), $BaBi_2Nb_2O_9$ (BBN), $Bi_4Ti_3O_{12}$ (BIT) and $SrBi_2Nb_2O_9$ (SBN) have attracted much attention due to its potential applications in nonvolatile random access memory (NVRAM) devices [37-40]. Lead zirconate titanate, $PbZrTiO_3$ (PZT) was the prominent material for the NVRAM application owing to its low switching field, high remnant polarization and low processing temperature [41,42]. However, the PZT material undergoes severe fatigue failure and retention loss on conventional silicon substrate with platinum (Pt) electrodes [43,44]. The renewed interest stems from the Aurivillius family of layered ferroelectric materials (e.g. SBT, BBN, BIT, and SBN) because of their fatigue-free behavior and low coercive field. But the drawbacks of these layered ferroelectric materials are low remnant polarization, high processing temperature and high dc conductivity [45 - 47].

It was known that the physical properties of these layered ferroelectric materials could be enhanced by doping the suitable cations in the crystal lattice. A partial replacement of scandium (Sc^{3+}) in the 'B' site has improved the physical properties of $SrBi_2Ta_2O_9$ ferroelectric ceramics [48]. It was observed that the dielectric loss reduced significantly with yttrium (Y^{3+}) ion substitution in the A-site of SBT ceramics ($Sr_{1-x}Y_xBi_2Ta_2O_9$). The Y^{3+} ion substitution has also improved the ferroelectric properties and the maximum value of remnant polarization observed for the composition, x = 0.05 is due to the cation vacancies introduced into the lattice structure [49]. The substitution of Sr^{2+} ion (ionic radius = 0.144 nm) by Eu^{3+} (ionic radius = 0.138 nm) has significantly enhanced the photoluminescence intensity of the SBT film with negligible change of the remnant polarization [50]. The remnant polarization

value for the c-axis oriented thin film has been determined at room temperature and it is found that the reduction of remnant polarization value might be attributed to the enhancement of coercive field at lower temperature. The partial substitution of V^{5+} ion in the niobium site of SBN ceramics has enhanced the dielectric and ferroelectric properties [51]. The crystal structure and ferroelectric properties of $ABi_2Ta_2O_9$ (A = Ca, Sr, Ba) ceramics have been investigated in detail. It is observed that the lattice mismatch between TaO_2 and AO planes in the perovskite-type unit of ATa_2O_7 increased as the size of the A-site cation decreases from Ba^{2+} to Ca^{2+} and also the structural distortion becomes more pronounced [52]. The distortion induced in the crystal structure leads to the higher Curie transition temperature and larger spontaneous ferroelectric polarization. The dielectric non-linearity in the layered ferroelectric ceramics of BBN and SBT has been studied by analyzing the polarization loop and also by measuring the dielectric permittivity as a function of frequency. In the case of BBN, the system has a broad phase transition manifesting the essential features of the slow relaxation process of polarization; but in SBT the polarization process is driven by the rearrangement of the domain structure [53]. The investigation of the microstructure and the electrical properties of Aurivillius phase ferroelectric solid solutions of $(CaBi_2Nb_2O_9)_{1-x}$ $(BaBi_2Nb_2O_9)_x$ $(0 \leq x \geq 1)$ have been carried out and it is observed that the Curie transition temperature decreased with the substitution of Ba^{2+} ion on the A- site of the perovskite blocks [54]. It is also noticed that the effect of sintering temperature has a strong influence on the grain structure, dielectric properties and Ba^{2+} ion fluctuations in BBN ceramics [55].

The theoretical study of the oxygen ion vacancy formation and its effect on spontaneous polarization in BIT ceramics has been investigated by the first-principle theoretical calculation [56]. The combination of first-principle calculation with shell-model techniques offered a multiscale approach to investigate the finite-temperature properties of Aurivillius compounds [57]. The grain orientation dependent ferroelectric properties of Sm^{3+} doped BIT thin films were studied in detail and it is noticed that the highly oriented (117) film showed $2P_r$ value of 54 $\mu C/cm^2$. It was also reported in the literature that the leakage current could be suppressed by the Nd substitution in the BIT thin films [58]. The structural dependence of the ferroelectrics properties of BIT ceramics has been studied by the substitution of various rare earth ion dopants in the bismuth site [59]. The influence of oxygen ion vacancies and crystallinity on the polarization switching and relaxation dynamics of Nd-substituted BIT thin films on platinum electrodes has been investigated in detail [60]. The substitution of Pr^{3+} into the BIT ($Bi_{4-x}Pr_xTi_3O_{12}$: BPT) crystal structure has caused the micro structural transformation

from platelet-like to equiaxed structure which increased the density of the material and thereby enhancing the physical properties [61]. The lattice vibration modes of $Bi_{4-x}La_xTi_3O_{12}$ ceramics were also studied as a function of La content. The frequency of the rigid mode due to the vibration between $(Bi_2Ti_3O_{10})^{2-}$ and $Bi_2O_2^{2+}$ layers was found to be stable when $x < 0.75$ and decreased with increasing x when $x \geq 1.00$ [62]. The substitution of Bi^{3+} ion by La^{3+} has improved the fatigue-free behavior of bismuth titanate ferroelectric ceramics due to the charge-compensating role of the (Bi_2O_2) layers and also the high structural stability of the perovskite layers [63].

The emergence of lanthanum ion doped bismuth titanate has fuelled considerable interest to investigate the influence of trivalent rare earth ions on the physical properties of bismuth based layered ferroelectric compounds. It is widely accepted that the Bi_2O_2 layers have a significant influence on the polar and electrical conductivity properties of bismuth based layered structures. It is expected that by substituting Bi^{3+} (ionic radius = 0.103 nm) ion with a slightly smaller rare earth cation such as Sm^{3+} ion (ionic radius = 0.098 nm) could significantly increase the structural distortion in the crystal structure and thereby enhancing the polar properties. However, the studies are limited concerning the improvement of dielectric properties of the layered perovskite ferroelectrics such as SBT and BBN through the substitution of Bi^{3+} ions in Bi_2O_2 layer by samarium ion (Sm^{3+}). On the other hand, the fabrication process for most of the layered ferroelectric compounds are based on the conventional solid state reaction route which often leads to the compositional and structural inhomogeneities owing to the high calcination and sintering temperatures and thus worsening the microstructural and subsequently the physical properties of the ferroelectric materials. This makes it necessary to look for alternative routes of synthesizing these families of layered ferroelectric compounds such as molten salt synthesis method. Molten salt synthesis (MSS) is one of the effective routes for synthesizing ceramic powders at relatively lower temperatures. By this fabrication route, one can achieve improved homogeneity, purity and good control over particle sizes as compared to that of the conventional solid state reaction route. Since, there seems to be no attempts made to synthesize samarium ion doped layered ferroelectric compounds such as strontium bismuth tantalate and barium bismuth niobate via molten salt synthesis route, the present investigations have been taken up to substitute Bi^{3+} by Sm^{3+} in the crystal lattice of SBT and BBN layered ferroelectric compounds fabricated by molten salt synthesize method and study its influence on the structural, dielectric, electrical conductivity

and ferroelectric properties in order to exploit these materials for aforementioned applications.

Chapter 1 primarily deals with a brief introduction to the underlying phenomenon of dielectric and ferroelectric properties of materials. In addition to the principles and phenomena, the modelling of dielectric behaviour of ferroelectric materials by Jonscher's universal formalism has also been discussed. The interesting aspects of the crystal structure and physical properties of Aurivillius family of layered ferroelectric ceramics, reported in the literature have been dealt.

In **Chapter 2**, the experimental techniques that have been employed to synthesize and characterize the layered ferroelectric ceramic materials under investigations are described. The details pertaining the materials fabrication techniques adopted to fabricate polycrystalline ceramics has been discussed. The structural and microstructural characterization of these materials was carried out by X - ray powder diffraction and scanning electron microscopy techniques. The dielectric and electrical conductivity measurements on these materials are reported. The ferroelectric properties of the materials under investigations were demonstrated by the Sawyer-Tower techniques.

Chapter 3 deals with the fabrication and characterization of samarium doped $SrBi_2Ta_2O_9$ ceramics. Polycrystalline $Sr(Bi_{0.9}Sm_{0.1})_2Ta_2O_9$ (SBSmT) ceramics were fabricated via the promising low temperature molten salt synthesis route using potassium chloride (KCl) as a flux material. The mono-phasic perovskite crystal structure is confirmed by the X-ray powder diffraction patterns. The scanning electron microscopic studies revealed the presence of plate shaped morphological features of the SBSmT ceramics. Interestingly, the dielectric constant of the SBSmT ceramics in the frequency range of 100 Hz - 1 MHz could be tuned as a function of sintering duration. It is observed that the SBSmT ceramics sintered at 1323 K for 10 h exhibited higher dielectric constant (ε'_r= 76) at 100 kHz than those of ceramics sintered at other durations. The magnitude of the electrical conductivity of the order of 10^{-7} - 10^{-9} S/cm at 300 K indicates that the conductivity mechanism might be attributed to the migration of oxygen ion vacancies in these ceramics. Systematic efforts have been made to investigate the influence of samarium on the physical properties of $SrBi_2Ta_2O_9$ and $BaBi_2Nb_2O_9$ ceramics by adding an excess amount of 5 wt % bismuth oxide to the initial mixture of reactants during calcination to compensate bismuth vaporization at high temperatures and the details of which are discussed in the forthcoming chapters.

The structural, dielectric and ferroelectric properties of rare earth doped strontium bismuth tantalate ceramics are described in **Chapter 4**. Layered $Sr(Bi_{1-x}Sm_x)_2Ta_2O_9$ ceramics with x ranging from 0 - 0.10 (10 mol%) were fabricated by the low temperature molten salt synthesis route. X - ray powder diffraction studies revealed that the single phase orthorhombic layered perovskite structure is retained in all these compositions. Scanning electron microscopic studies on these ceramics confirmed the presence of well packed equiaxed plate shaped grains. The dielectric and electrical conductivity properties were studied in the 100 Hz – 1 MHz frequency range at 300 K. Interestingly, the 10 mol% samarium doped $SrBi_2Ta_2O_9$ ceramics exhibited high dielectric constant (ε'_r = 155) and low dielectric loss (0.00298) compared to those of other compositions. The ferroelectric property of $SrBi_2Ta_2O_9$ ceramics is superior for higher concentration of samarium content. The electrical conductivity of undoped and samarium doped ceramics increased linearly with increase in frequency.

Chapter 5 deals with the dielectric and electrical conductivity measurements carried out on undoped and samarium doped SBT ceramics at various frequencies and temperature of interest, whose fabrication, structural, microstructural and ferroelectric properties were dealt in the previous chapter. Undoped and samarium doped $SrBi_2Ta_2O_9$ ferroelectric ceramics have been fabricated by the molten salt synthesis route. The dielectric and electrical conductivity measurements were carried out in the 100 Hz - 1 MHz frequency range at various temperatures. A decrease in dielectric constant maximum (ε_m) and a downward shift in the Curie transition temperature (T_c) have been observed with the increase in samarium concentration. The frequency dependent real and imaginary parts of dielectric constant of these ceramics exhibited low frequency dielectric dispersion. Interestingly, temperature and frequency dependence dielectric constant plots indicated that the formation of oxygen ion vacancies have been inhibited by samarium doping in SBT lattice. The activation energy values obtained from the Arrhenius plot have confirmed the existence of motion of oxygen ion vacancies in these ceramics.

Chapter 6 describes the fabrication and characterization of samarium doped barium bismuth niobate relaxor ferroelectric ceramics. Barium bismuth samarium niobate $Ba(Bi_{1-x}Sm_x)_2Nb_2O_9$(x = 0, 0.03, 0.05, and 0.10) ceramics have been fabricated successfully via molten salt synthesis route. The X - ray diffraction analysis revealed the existence of bismuth layered perovskite phase with orthorhombic crystal structure in all the compositions studied.

The dielectric and electrical conductivity properties were carried out in the 100 Hz - 1 MHz frequency range at 300 K. The dielectric constant and dielectric loss were found to decrease from 186 to 180 and 0.0966 to 0.0755 respectively with increase in samarium content at 100 kHz.

Chapter 7 presents the temperature and frequency dependence of dielectric and conductivity characteristics of undoped and samarium doped BBN relaxor ferroelectric ceramics whose fabrication, structural and microstructural properties have been discussed in the previous chapter. The polycrystalline $BaBi_2Nb_2O_9$ and $Ba(Bi_{0.9}Sm_{0.1})_2Nb_2O_9$ ceramics have been fabricated via the molten salt synthesis route. The temperature dependence of dielectric and electrical conductivity properties of BBN and BBSmN ceramics investigated at various frequencies have revealed the characteristic features of relaxor behaviour. The incorporation of Sm^{3+} for Bi^{3+} has induced a downward shift in the dielectric maximum temperature (438 K - 393 K) with the decrease in dielectric constant maximum (372 - 212) at 100 kHz. The estimated degree of diffuseness (γ) was found to be 2.17 for BBN and 1.93 for BBSmN ceramic samples. The activation energy obtained from the Arrhenius plot revealed the existence of motion of oxygen ion vacancy in these ceramics.

References

[1] M. E. Lines, A. M. Glass, Principles and applications of ferroelectrics *and related materials*. Oxford University Press, (1977).

[2] E. Fatuzzo, W. J. Merz, *Ferroelectricity*, North-Holland (1967).

[3] J. C. Burfoot, *Ferroelectrics*, Van Nostrand, New York (1967).

[4] U. Chon, H.M. Jang, M.G. Kim, C.H. Chang, *Phys. Rev. Lett.* **89** (087601), 1 (2002).

[5] A. Roy, A. Dhar, S.K. Ray, *J. Appl. Phys*. **104** (064103),1 (2008) .

[6] B.H. Venkataraman, K.B.R. Varma, *Ferroelectrics*. **33**, 39 (2006).

[7] A.Z. Simões, B.D. Stojanovic , M.A. Ramirez, A.A. Cavalheiro, E. Longo, J.A. Varela,. *Ceram. Int.* **34**, 257 (2008).

[8] C.L.Diao, J.B. Xu, H.W. Zheng, L. Fang, Y.Z. Gu, W.F. Zhang,. *Ceram. Int.* **39**, 6991 (2013).

[9] J. Valasek, *Phys. Rev*., **17**, 475 (1921).

[10] G. Busch, *Ferroelectrics*, **74**, 267 (1987).

[11] W. Kanzig, *Ferroelectrics and Antiferroelectrics*, Academic Press, New York (1957).

[12] J. F. Nye, *Physical Properties of Crystals*, Oxford University Press, Oxford (1957).

[13] E. Fatuzzo, W. J. Merz, *Ferroelectricity*, North-Holland (1967).

[14] J. C. Burfoot, *Ferroelectrics*, Van Nostrand, New York (1967).

[15] J. B. Grindlay, *An Introduction to Phenomenological Theory of Ferroelectricity*, Pergamon Press, Oxford (1970).

[16] B. Jaffe, W. R. Cook, H. Jaffe, *Piezoelectric Ceramics*, London and New York (1971).

[17] T. Mitsui, I. Tatsuzaki, E. Nakamura, *An Introduction to the Physics of Ferroelectrics*, Gordon and Breach, London (1976).

[18] W. G. Cady, *Piezoelectricity*, McGraw - Hill, New York (1946).

[19] M. E. Lines and A. M. Glass, *Principles and Applications of Ferroelectrics and Related Materials*, Clarendon Press, Oxford (1977).

[20] H. D. Megaw, *Ferroelectricity in Crystals*, Methuen and Co., London (1957).

[21] F. Jona, G. Shirane, *Ferroelectric Crystals*, Pergamon Press, Oxford (1962).

[22] G. Busch, *Ferroelectrics*, **71**, 43 (1987).

[23] M. S. Vijaya, G. Rangarajan, *Materials Science*. Tata McGraw-Hill Publishing Company Limited, New Delhi, India 364 (2004).

[24] L. Solymar, D.Walsh, *Electrical properties of materials*, 7th edn. Oxford University Press, New Delhi, India (2004).

[25] S. O.Kasap, *Principles of electronic materials and devices*, 3rd edn. Tata McGraw-Hill Publishing Company Limited, New Delhi, India (2007).

[26] A. J. Moulson, J. M.Herbert, *Electroceramic, materials, properties and applications* 2nd ed. Wiley, Chichester, England.91 (2003).

[27] M. M.Vijatovi, J.D. Bobi, B. DStojanovi, *History and Challenges of Barium Titanate: Part I. Science of Sintering.* **40**,155 (2008).

[28] C. D. Chandler, C. Roger, M. J .H.-Smit, *Chemical Review*. **93**, 1205 (1993).

[29] U. A. Joshi, S.Yoon, S.Baik, J.S.Lee, *Journal of Physical Chemistry B*.**110**,12249 (2006).

[30] A. Jamal, M.Naeem,Y.Iqbal, *Journal of the Pakistan Materials Society*.**2**,2 (2008).

[31] R.Asiaie, W.Zhu, A,Sheikh, P.K Dutta, *Chemistry of Materials*. **8**, 226 (1996).

[32] B. Jaffe and W. R. Cook, *Piezoelectric Ceramics*, no. 3. London: Academic Press, 1971.

[33] B. Jaffe and W. R. Cook, no. 3. London: Academic Press (1971).

[34] B. S. Kang, J. Yoon, T. W. Noh, T. K. Song, S. Seo, Y. K. Lee, and J. K. Lee, Appl. Phys. Lett. **82**, 103 (2003).

[35] Y. Matsuo and H. Sasaki, *J. Am. Ceram. Soc.* **49**, 229 (1966)

[36] S. Singha and M. J. Thomas, Dielectrics and Electrical Insulation, IEEE Transactions **15**, 1 (2005).

[37] U. Chon, H.M. Jang, M.G. Kim, C.H. Chang, *Phys. Rev. Lett.* **89** (087601), 1 (2002).

[38] A. Roy, A. Dhar, S.K. Ray, *J. Appl. Phys.* **104** (064103), 1 (2008).

[39] A.Z. Simões, B.D. Stojanovic , M.A. Ramirez, A.A. Cavalheiro, E. Longo, J.A. Varela, *Ceram. Int.* **34**, 257 (2008) .

[40] C.L.Diao, J.B. Xu, H.W. Zheng, L. Fang, Y.Z. Gu, W.F. Zhang, *Ceram. Int.***39**, 6991 (2013).

[41] Y. Wang, C. Ganpule, B.T. Liu, H. Li, K. Mori, B. Hill, M. Wutting, R. Ramesh, J. Finder, Z. Yu, R. Droopad, K. Eisenbeiser, *Appl. Phys. Lett.* **80**, 97 (2002).

[42] Y.-X. Wang, W.-L. Zhong, C.-L. Wang, P.-L. Zhang, *Chin. Phys. Lett.***18**, 826 (2001).

[43] C. Zhao, Q. Zhu, D. Wu, A. Li, *J. Phys. D: App. Phys.***42** (185412), 1 (2009).

[44] C.-A Paz de Araujo, J.D. Cuchiaro, L.D. Mcmillan. M.C. Scoot, J.F. Scott, *Nature*. **374,** 627 (1995).

[45] Y.Shimakawa, Y. Kubo, Y. Nakagawa, S. Goto, T. Kamiyama, H. Asano, F. Izumi, *Phys. Rev. B.***61,**6559 (2000).

[46] J.F. Scott, *Ann. Rev. Mater. Sci.* **28,** 79 (1998).

[47] K. Kato, C. Zheng, J.M. Finder, S.K. Dey, Y. Torii, *J. Am. Ceram. Soc.* **81,**1869 (1998).

[48] T.Sivakumar, M.Itoh, *Chemistry of Materials*. **23**, 129 (2011).

[49] K .Aizawa, Y.Ohtani, *Japanese Journal of Applied Physics*. **47**, 7549 (2008).

[50] Y.Ohtani, *Japanese Journal of Applied Physics*, **47**, 7594 (2008).

[51] S.Jain, A. K.Jha, *Journal of Electroceramics,* **24**,58 (2010).

[52] Y.Shimakawa, Y.Kubo,Y. Nakagawa, S.Goto, T.Kamiyama, H.Asano, *Physical Review B,* **61**, 6559 (2000).

[53] K. Bormanis,A. Kalvane, A. I.Burkhanov, Y. V.Kochergin, *International Conference on Solid Dielectrics*, Potsdam, Germany, July 4-9, IEEE, 1(2010).

[54] H.Zhang, H.Yan, M. J.Reece, *Journal of Applied Physics*, **108**, 0141091 (2010).

[55] M.Adamczyk, Z. Ujmay, M.Pawelczy, L.Szymczak, L.Kozielski, *Phase Transitions*, **79**,435 (2006).

[56] T.Hashimoto, H. Moriwake, *Physical Review B,* **78**, 0921061 (2008).

[57] R.Machado, M.Sepliarsky, M. G. Stachiotti, *Journal of Materials Science*, **45**, 4912. (2010).

[58] C.Zhao, Q.Zhu, D.Wu, A.Li, *Journal of Physics D: Applied Physics*, **42**, 1854121 (2009).

[59] C.Zhao, Q.Zhu, D.Wu, A.Li, *Journal of Physics D: Applied Physics*, **42**, 1854121 (2009).

[60] J. H.Lee, R. H.Shin, W.Jo, *Physical Review B,* **84**,0941121 (2011).

[61] W.Krengvirat, S.Sreekantan, A.B.M. Noor,A.Matsuda, C.Chinwanitcharoen, *Journal of the Ceramic Society of Japan*, **120**,58 (2012).

[62] D.Wu, B.Yang, A. Li *Phase Transitions*, **82**,146 (2012).

[63] A. Z. Simoes, B. D.Stojanovic , M.A.Ramirez , A.A. Cavalheiro , E.Longo, J.A. Varela, *Ceramics International*, **34**, 257 (2008).

CHAPTER 2

Materials and Methods

2. **Materials and Methods**

In this chapter, the experimental techniques that have been employed to synthesize and characterize the layered ferroelectric ceramic materials under investigations are described. The details pertaining to the materials fabrication techniques adopted to fabricate polycrystalline ceramics is discussed. The structural and microstructural characterizations of these materials were carried out by X-ray powder diffraction and scanning electron microscopy techniques. The dielectric and electrical conductivity measurements on these materials are reported. The ferroelectric properties of the materials under investigations were demonstrated by the Sawyer - Tower techniques.

2.1. Materials fabrication (polycrystalline ceramics)

Molten salt synthesis (MSS) method has been adopted to fabricate polycrystalline layered ferroelectric ceramics at relatively lower temperatures than conventional solid state reaction route. In this method, the inorganic oxide materials are well mixed with flux salt and heated slightly above the melting temperature of the flux salt [1]. The oxides react together in the molten state of the salt and the product phases are formed via the nucleation and the growth process as indicated in the schematic representation (Figure 2.1).

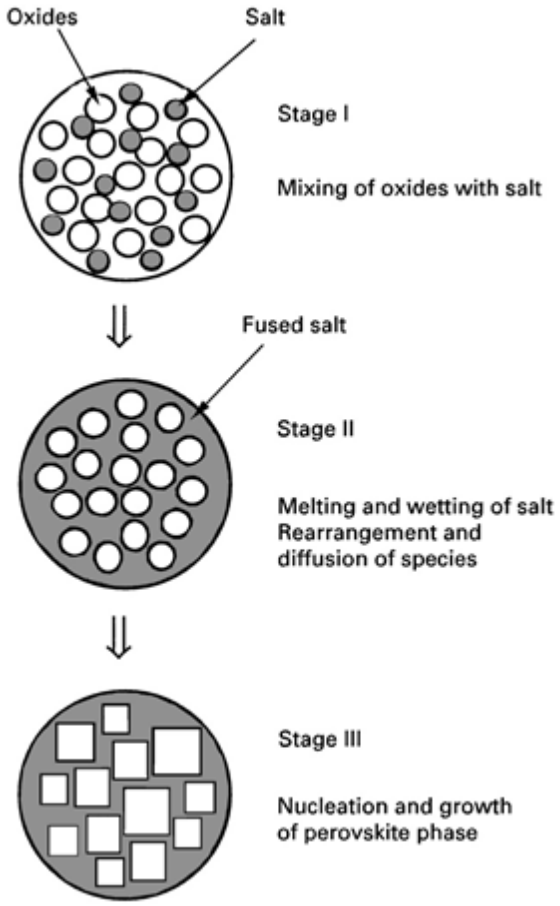

Figure 2.1. Schematic diagram of the molten salt synthesis process for oxide materials [1]

A stoichiometric mixture of reagent grade (purity > 99.9%) oxides, carbonates were mixed thoroughly with flux salt using mortar and pestle and these powders were calcined at appropriate temperatures. Subsequently, these calcined powders were cold pressed at 300 K for a few minutes at the pressure of 225 kg/cm^2 and subjected to the conventional sintering process at 1323 K for 10 h. The following compounds that have been fabricated in the present investigations are (i) $Sr(Bi_{1-x}Sm_x)_2Ta_2O_9$ (x = 0.00 - 0.10) and (ii) $Ba(Bi_{1-x}Sm_x)_2Nb_2O_9$ (x = 0.00 - 0.10)

2.2. Structural and microstructural characterization

The structural phase analysis of the polycrystalline calcined powders and sintered ceramics was confirmed via powder X-ray diffraction (XRD) technique using Cu-Kα radiation (Pan Analytical XPERT - PRO diffractometer). This X-ray powder diffraction technique was also employed to determine the degree of orientation of the calcined and sintered ceramic samples. In order to identify the crystalline phases present in the samples, the obtained XRD patterns for various samples were compared with those of standard JCPDS pattern.

The comparison of XRD patterns, of the sintered ceramics with as-prepared polycrystalline powder over the 2θ range of 10° to 70°, enabled to evaluate the degree of grain - orientation. The degree of grain orientation (f) was estimated by Lotgering's method [2].

$$f = \frac{P - P_0}{1 - P_0}$$

where $P = \Sigma I_{00l} / \Sigma I_{hkl}$ for the given oriented sample (i.e., sintered pellet) and $P_0 = \Sigma I_{00l} / \Sigma I_{hkl}$ for the non-oriented sample (i.e., calcined polycrystalline powder). The surface morphological features of calcined powders and sintered ceramic samples were monitored by scanning electron microscope (SEM; JSM - 6390).

2.3. Density measurement

The densities of the sintered ceramic samples were determined by the Archimedean principle using an 'Essae' electronic balance. For this measurement, de-ionised water was used as the liquid medium. The following formula has been used for calculating the densities of the ceramic pellets.

$$\rho = \frac{W_1}{(W_1 - W_2)} \text{ x 1 g/cm}^3$$

where ρ is the density of the sample, W_1 is the weight of the sample in air, W_2 is the weight of the sample in water.

2.4. Dielectric constant measurements

The capacitance (c_p) and the dielectric loss (D) measurements were carried out using a LCR meter (Waynekerr : 43100) in the frequency range 100 Hz - 1 MHz with a signal strength of

1 V_{rms} at different temperatures (300 K - 673 K). The temperature variation of the dielectric constant was carried out to assess the Curie temperature in these ceramics. For temperature variation measurements, an indigenously built furnace associated with Eurotherm temperature controller and interface (RS 232) were employed (Figure 2.2). The samples were heated at the rate of 1 K/min. The real and imaginary parts of the dielectric constants were determined by the following formula

$$\varepsilon_r' = C_p d \,/\, \varepsilon_0 A$$

$$\varepsilon_r'' = \varepsilon_r' \tan \delta$$

where, d is the thickness and A is the area of the sample and ε_0 is the permittivity of the free space (8.854 x 10^{-12} F/m).

Figure 2.2. Experimental setup of LCR meter (Waynekerr : 43100)

2.5. Ferroelectric measurements (The Sawyer-Tower circuit (P vs E hysteresis loop))

The ferroelectric hysteresis loops could be obtained by placing the crystal under an applied electric field in a Sawyer-Tower circuit and this circuit is represented schematically in Figure 2.3. An ac signal generator provides a potential difference to the sample and to the X-plate of the oscilloscope. The resulting polarization P leads to a charge Q, which is fed to the amplifier, where Q = PA and A being the electrode area of the sample. By assuming an ideal operational amplifier with large inverting gain, negligible input admittance and 'C' initially discharged, the output voltage is V = - Q /C indicating that output is proportional to the polarization. It is customary to calibrate the vertical axis of the plot in terms of polarization P rather than Q as P = Q /A (A is the electrode area of the ferroelectric) and the horizontal axis is defined in terms of E rather than V (E = V / d) where d is the thickness of the ferroelectric material).

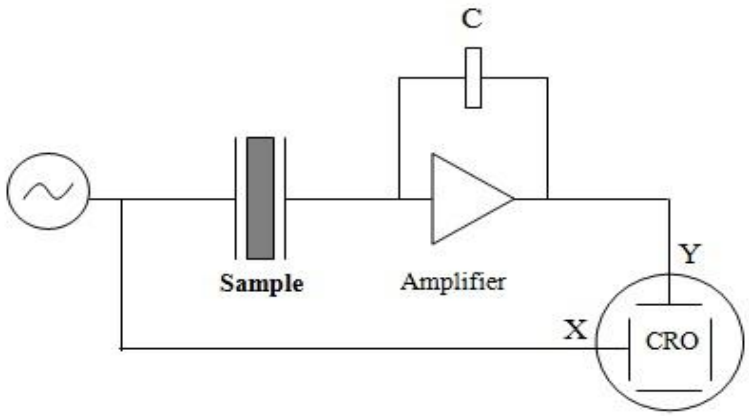

Figure 2.3. The Sawyer - Tower circuit [3]

In the present research work, polarization versus electric field measurements (P vs E hysteresis loops) were carried out using a Piezoelectric Evaluation System, TF analyzer 2000 with triangular waveform. This system could be employed for comprehensive electrical characterization of ferroelectric bulk ceramic samples over a wide electric field range.

References

[1] K. H. Yoon, Y.S. Cho, D.H. Kang, *Journal of Materials Science*, **33**, 2977 (1998).

[2] F. K. Lotgering, *J. Inorg. Nucl.Chem*. **9**, 113 (1959).

[3] B.H. Venkataraman, *Multifunctionalities of ceramics and glass nanocrystal composites of V_2O_5 doped Aurivillius family of ferroelectric oxides*, (2005).

CHAPTER 3

Structural and Dielectric Properties of Strontium Bismuth Samarium Tantalate Layered Perovskites

3. **Structural and Dielectric Properties of Strontium Bismuth Samarium Tantalate Layered Perovskites**

This chapter deals with the fabrication and characterization of samarium doped $SrBi_2Ta_2O_9$ ceramics. Polycrystalline $Sr(Bi_{0.9}Sm_{0.1})_2Ta_2O_9$ (SBSmT) ceramics were fabricated via the promising low temperature molten salt synthesis route using potassium chloride (KCl) as a flux material. The mono-phasic perovskite crystal structure is confirmed by the X-ray powder diffraction patterns. The scanning electron microscopic studies revealed the presence of plate shaped morphological features of the SBSmT ceramics. Interestingly, the dielectric constant of the SBSmT ceramics in the frequency range of 100 Hz - 1MHz could be tuned as a function of sintering duration. It is observed that the SBSmT ceramics sintered at 1323 K for 10 h exhibited higher dielectric constant (ε'_r= 76) at 100 kHz than those of ceramics sintered at other durations. The magnitude of the electrical conductivity of the order of 10^{-7} - 10^{-9} S/cm at 300 K indicates that the conductivity mechanism might be attributed to the migration of oxygen ion vacancies in these ceramics.

3.1. Introduction

Layered ferroelectric materials have attracted much attention in recent years for multifarious applications such as optical switches, pyroelectric based infrared detectors, piezoelectric, and non-volatile random access memory (NVRAM) devices [1-5]. The renowned material for the NVRAM application is $PbZr_{1-x}Ti_xO_3$ (PZT) [6,7]. The Aurivillius family of layered ferroelectric materials such as $SrBi_2Ta_2O_9$ (SBT), $Bi_4Ti_3O_{12}$ (BIT), and $SrBi_2Nb_2O_9$ (SBN) replaced the PZT material by the inherent properties of high fatigue resistance and relatively low leakage current [8, 9]. These layered ferroelectric materials consist of two perovskite like structures interleaved between the Bi_2O_2 layers are associated with two major drawbacks: High processing temperature and low remnant polarization [10-12]. It was expected that by substituting Bi^{3+} ion in the crystal lattice of layered ferroelectric materials with trivalent rare earth ions such as Sm^{3+} could significantly increase the structural distortion in the crystal structure due to the large difference in the eightfold coordination ionic radii and thereby enhancing the polar properties [13-15]. Most of the layered ferroelectric compounds have been synthesized based on the conventional solid state reaction route which often leads to the structural and compositional inhomogeneity due to the high calcination and sintering temperatures [16]. Alternatively, the molten salt synthesis route has been determined to be a simple and effective route for synthesizing ceramic powders at relatively low temperatures and one can achieve improved homogeneity and good control over particle sizes, which will have a direct influence on the physical properties [17-22]. It has been known in the literature that the sintering conditions also play a vital role in tailoring the microstructure and the dielectric properties of the ceramic materials [23-25]. With this background and keeping the technological importance of layered ferroelectric materials in view, our approach has been to replace Bi^{3+} partially by samarium in $SrBi_2Ta_2O_9$ and visualize the effect of samarium doping of various concentrations on the physical properties of $SrBi_2Ta_2O_9$ ceramics. To begin with, we have investigated the structural, microstructural and dielectric properties of 10 mol.% samarium doped $SrBi_2Ta_2O_9$ ceramics sintered at different durations which were fabricated by the molten salt synthesis route and hence the present chapter describes the details pertaining to these aspects of SBSmT ceramics.

3.2. Strontium Bismuth Tantalate

The crystal structure of $SrBi_2Ta_2O_9$ has orthorhombic symmetry with $a = 5.5306$ Å, $b = 5.5344$ Å and $c = 24.9839$ Å (Figure 3.1), and it exhibits ferroelectricity at room temperature. The crystal structure consists of two perovskite like blocks $(SrTa_2O_7)^{2-}$ that are interleaved between the Bi_2O_2 layers along the c-axis. The non - centrosymmetric orthorhombic structure of SBT is responsible for its ferroelectric nature. Atomic displacement along the a-axis induces non-centrosymmetric space group from its parent centrosymmetric (I4/mmm) group that causes the ferroelectric polarization. The contribution of each constituent ion to the total spontaneous ferroelectric polarization is calculated from the atomic displacements is 18.2 μC/cm^2 [26]. The reported ferroelectric to paraelectric phase transition temperature for SBT is 583 K.

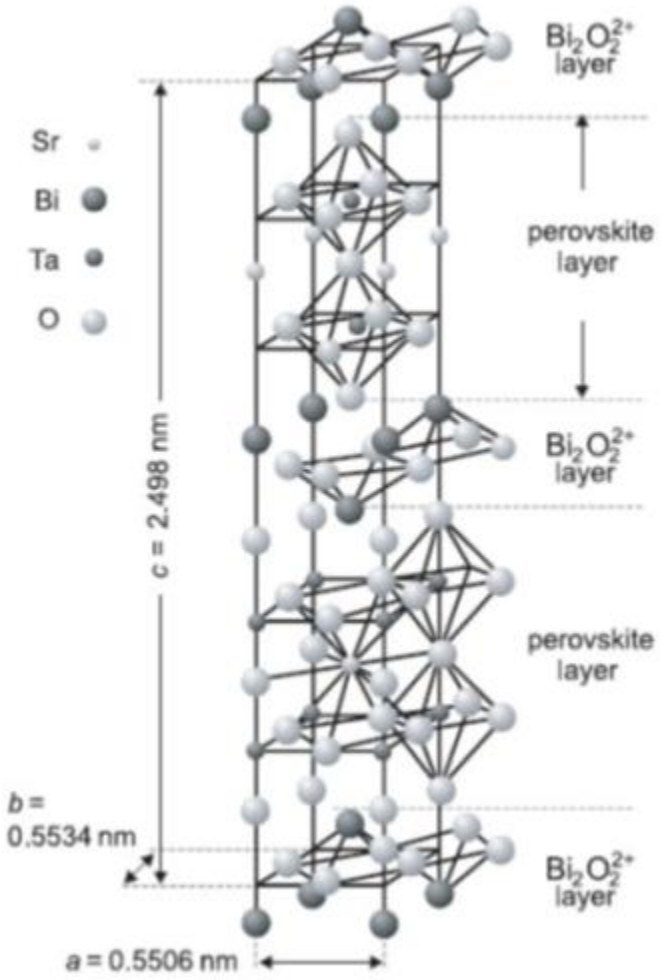

Figure 3.1. Crystal structure of $SrBi_2Ta_2O_9$[32]

3.3. Structural Analyses

The strontium bismuth samarium tantalate polycrystalline powders in the composition of $Sr(Bi_{1-x}Sm_x)_2Ta_2O_9$ with x = 0.00 and 0.10 (10 mol.%) were fabricated from a stoichiometric mixture of reagent grade strontium carbonate ($SrCO_3$), bismuth oxide (Bi_2O_3), tantalum pentoxide (Ta_2O_5), and samarium oxide (Sm_2O_3) via the molten salt synthesis route using KCl as a flux material. Furthermore, these reactant materials were uniformly ground in the acetone medium with KCl in the molar ratio of 1:5 and calcined at 1073 K in air for 4h with the heating rate of 3 K/min. Further, these calcined powders were washed with hot deionized water several times to remove the KCl salt and subsequently these powders were cold pressed at the room temperature for few minutes at a pressure of 225 kg/ cm^2. These ceramic samples were sintered at optimized temperature, 1323 K for different soaking durations (6 h, 8 h, 10 h and 12 h) to visualize the effect of duration of sintering on the microstructure and physical properties. The as-prepared powders and the sintered samples were subjected to the X-ray diffraction studies and the c - axis orientation factors (f) were calculated by using the Lotgering's method [27]. The X - ray powder diffraction patterns

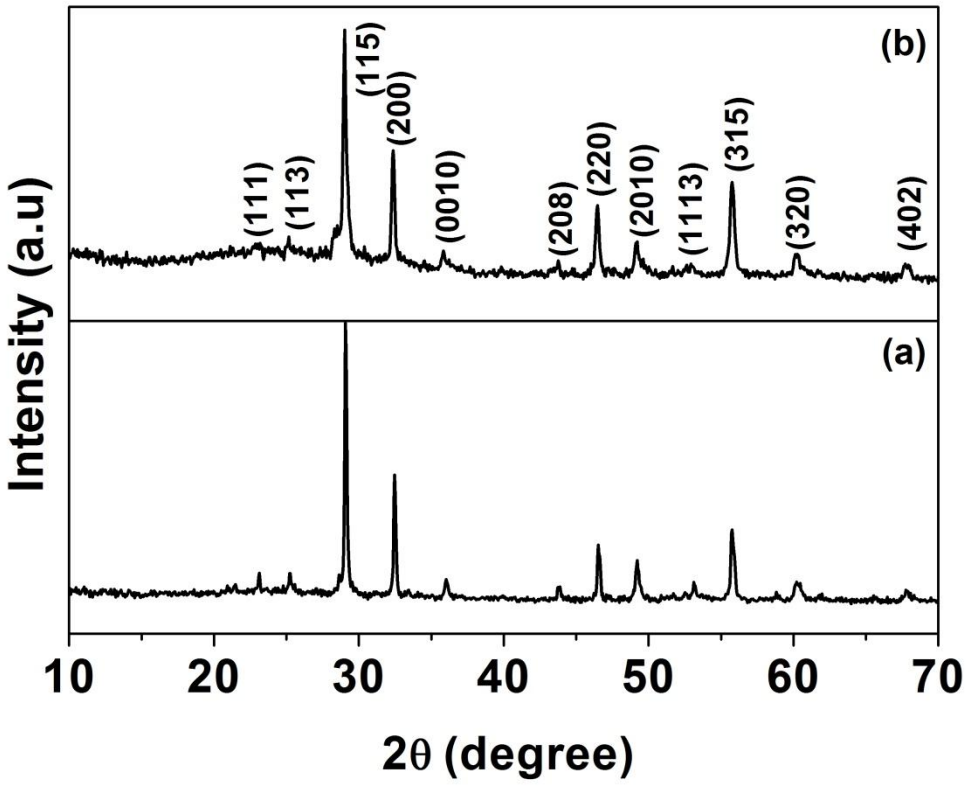

Figure 3.2. The XRD patterns recorded for (a) undoped and (b)10 mol. % samarium doped SBT polycrystalline powders.

obtained for an undoped (Figure. 3.2(a)) and SBSmT (Figure. 3.2(b)) polycrystalline powders confirm the formation of single phase layered perovskites. These XRD patterns are indexed to an orthorhombic unit cell and the obtained lattice parameters (Table. 3.1) are in close agreement with those reported in the literature [28]. It is interesting to note that the crystallinity of the layered perovskite $SrBi_2Ta_2O_9$ phase has been achieved at lower temperatures (1073 K/4h) and also at shorter duration compared to that of the solid state reaction route (1373 K/12h).

Table 3.1. Unit cell parameters of undoped and samarium doped SBT polycrystalline powders.

Composition	a(Å)	b(Å)	c (Å)
$SrBi_2Ta_2O_9$	5.5176	5.5133	24.9454
$Sr(Bi_{0.9}Sm_{0.1})_2Ta_2O_9$	5.5246	5.5290	24.9639

The average crystallite size (D) is calculated based on the crystalline planes (115), (200), (220), (2010) and (315) by the following Scherrer formula [29] for undoped and SBSmT polycrystalline samples are found to be 48 nm and 35 nm.

$$D = \frac{k\lambda}{\beta \cos\theta}$$

where k (0.94) is the shape factor, λ is the X- ray wavelength of Cu - Kα radiation (1.5406 Å), θ is the Bragg angle and β is the full width at half maximum of the peak. The decrease in crystallite size of SBSmT polycrystalline powders could be due to the ionic radii difference between bismuth and samarium ion in the SBT crystal lattice.

Figure 3.3(a-e) shows the XRD pattern recorded for the randomly oriented SBSmT calcined powder (Figure. 3.3(a)) along with those obtained for the polycrystalline ceramic pellets sintered at 1323 K for different durations (6 h, 8 h , 10 h and 12h). The d - spacings that are associated with all these XRD patterns of the sintered samples are found to be corresponding to the layered perovskite SBT crystal structure without any secondary phase formation. The full width at half maximum of the Bragg peaks of these sintered samples are sharper compared to that of the SBSmT powder samples which reveals that there is an occurrence of grain growth during the sintering process.

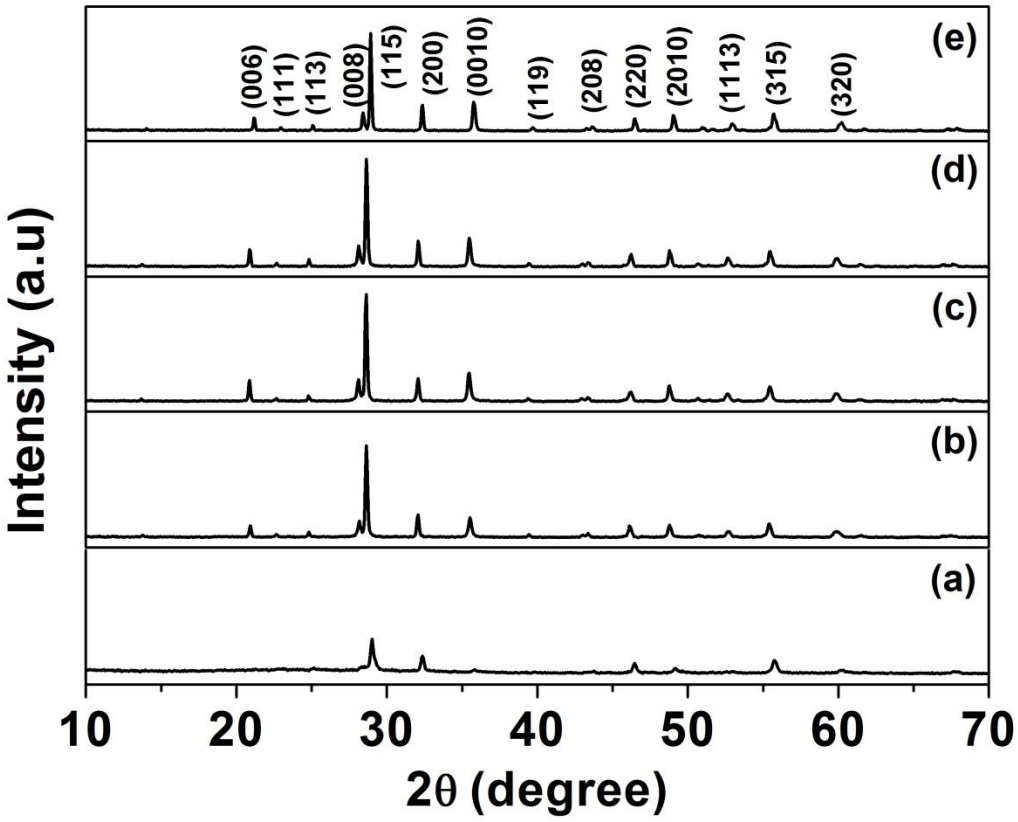

Figure 3.3. The XRD patterns recorded for the 10 mol.% samarium doped SBT samples for (a) calcined polycrystalline powder (b) 1323 K/ 6h (c) 1323 K / 8 h (d) 1323 K / 10h and (e) 1323 K /12h.

It is also interesting to note that the X-ray intensities corresponding to (00*l*) planes for these sintered pellets are slightly stronger than those of the SBSmT calcined powder samples indicating the c-axis preferred orientation. The values of the c-axis orientation factor (f) calculated based on the Lotgering's method for all the sintered samples varies from 0.17 to 0.19 as tabulated in Table 3.2.

Table 3.2. Orientation factor (f), Orthorhombic distortion ($^{b}/_{a}$) and dielectric constant (ε'_r) for the SBSmT samples sintered at various durations.

Sintering condition	Orientation factor (f)	$^{b}/_{a}$	ε'_r at 100 kHz
1323 K /6h	0.17	1.0001	71
1323 K/ 8 h	0.19	1.0007	70
1323 K/ 10 h	0.18	1.0010	76
1323 K/ 12 h	0.19	0.9995	59

3.4. Microstructural Analyses

The scanning electron micrographs of the calcined powders are shown in the Figure. 3.4 (a) and 3.4 (b). Both the micrographs revealed the presence of plate shaped morphology. This plate shaped morphology is a characteristic grain growth of the Aurivillius family of oxides and it occurs due to the anisotropic nature of the crystal structure [30].

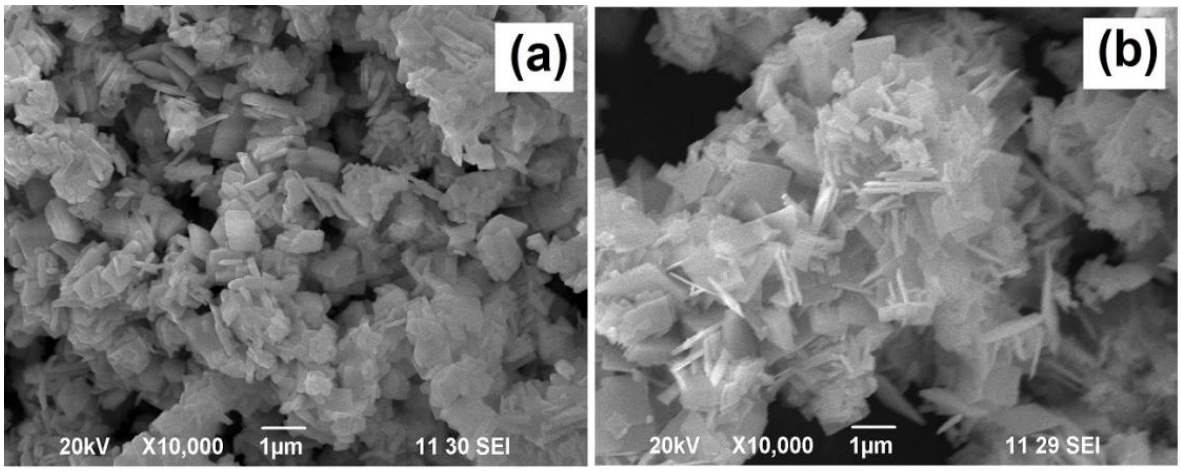

Figure 3.4. The scanning electron micrographs obtained for (a) undoped and (b) 10 mol.% samarium doped SBT polycrystalline powders calcined at 1073 K for 4h.

The scanning electron micrographs recorded for the SBSmT samples sintered at 1323 K for 6 h, 8 h, 10 h and 12h are depicted in Figure 3.5 (a-d). These micrographs indicated the existence of plate shaped SBSmT grains associated with considerable porosity due to the high volatile nature of the bismuth at high temperatures during the sintering process and the relative density value of all these ceramic samples is found to be 80% of the theoretical value. The c-axis is found to be perpendicular to the major faces of these grains showing a preferential grain orientation in the XRD pattern. The average grain size of these sintered pellets calculated from the SEM micrographs is around 0.6 μm - 0.8 μm. It seems the duration of sintering does not have any significant effect on the microstructure though there is a slight increase in the grain size.

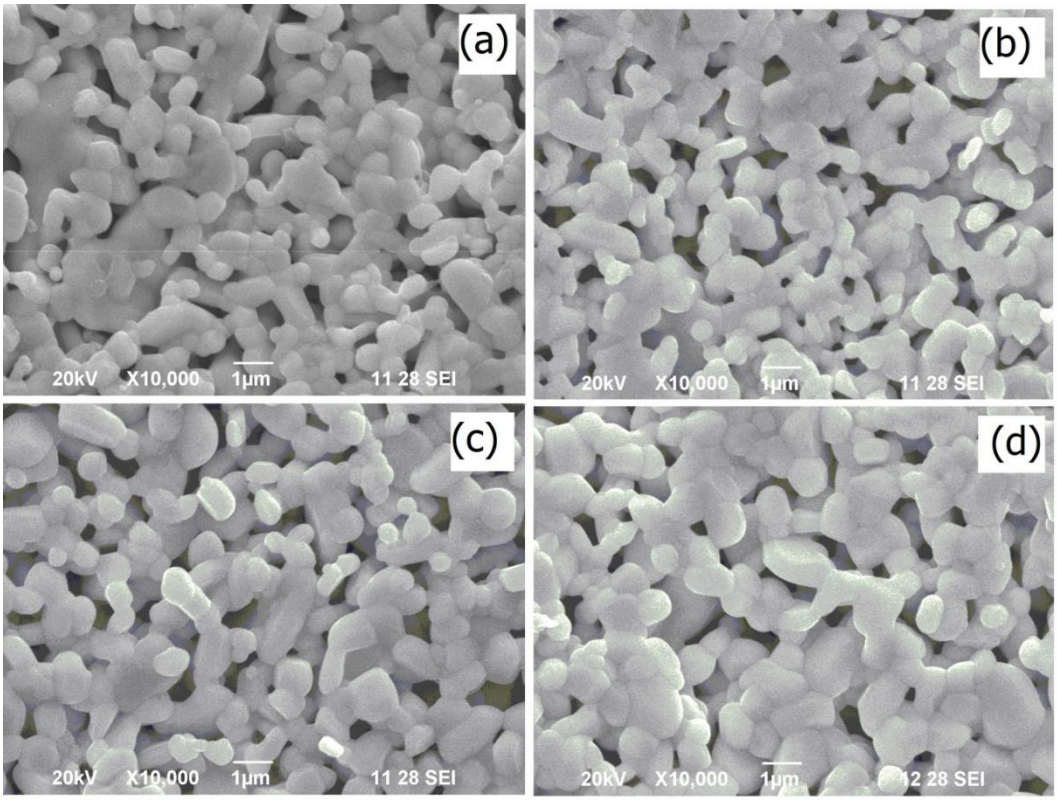

Figure 3.5. The scanning electron micrographs for the SBSmT pellets sintered at 1323 K for different durations (a) 6 h (b) 8 h (c) 10 h and (d) 12 h.

3.5. Dielectric and Conductivity Studies

The frequency dependence of the dielectric constant (ε'_r) at 300 K for the SBSmT ceramic samples sintered at different durations is shown in Figure 3.6. In all these samples, the dielectric constant does not show any appreciable dispersion with frequency suggesting that the polarization mechanism could be originated from the bound charges in the lattice and hence the effect of space charge polarization due to the oxygen ion vacancy charge carriers is not very significant. This observation suggested that the molten salt synthesis route might have assisted in minimizing the creation of oxygen ion vacancies in SBSmT ceramics by reducing the formation temperature of the compound. It is observed in Figure 3.6 that the dielectric constant for the sample sintered at 1323 K for 10 h is higher than those of other samples at all the frequencies under study. For instance, the value of the dielectric constant measured at 100 kHz for the SBSmT sintered ceramic samples is tabulated in Table 3.2.

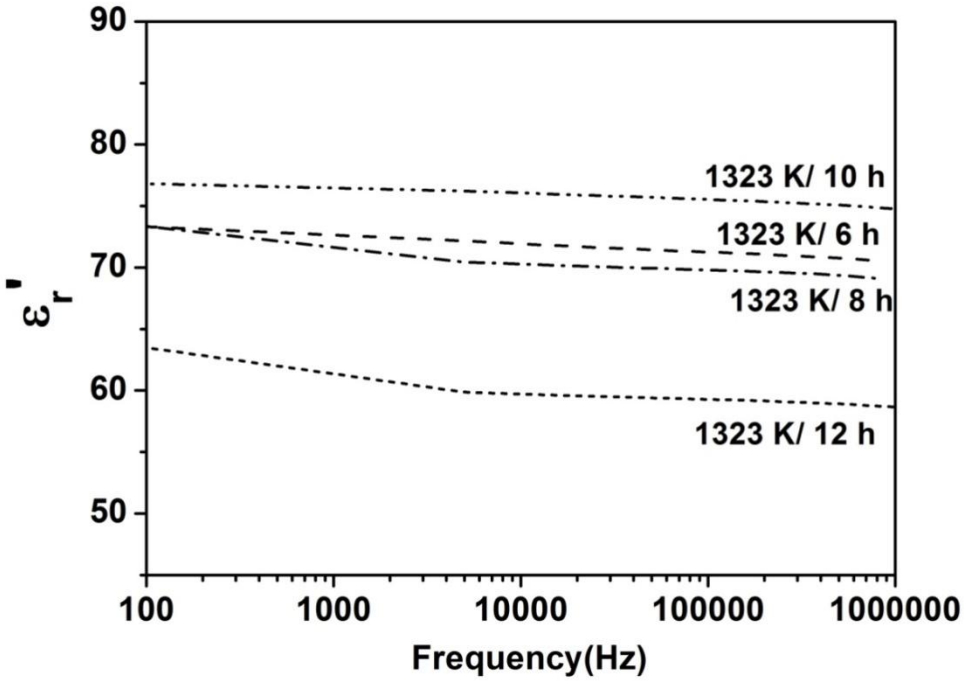

Figure 3.6. The frequency dependence dielectric constant for the SBSmT samples sintered at various durations.

In these families of layered ferroelectric materials, the origin of ferroelectricity mainly arises from the structural distortion of the TaO_6 perovskite blocks in the crystal structure associated with noncentrosymmetric space group. The atomic displacement along the a - axis from the equilibrium position in the crystal structure induces the spontaneous ferroelectric polarization [10]. Hence, we believe that the observed high value of the orthorhombic distortion for the sample sintered at 1323 K for 10 h (Table 3.2) accounted for the incidence of higher dielectric constant due to the increase in the lattice polarizability of the material.

Figure 3.7 shows the variation of real part of the ac conductivity as a function of frequency at 300 K for SBSmT ceramic samples sintered at different durations. The ac conductivity spectra of all these samples obey Jonscher's law [31].

$$\sigma = \sigma_o + A\omega^n$$

where σ_o is the dc conductivity, A is the temperature dependent parameter, n is the value between 0 and 1 and ω is the angular frequency.The conductivity increases with the increase in frequency for all these samples, varying approximately as a power of frequency (ω^n). However, the trend of the curve does not vary much with the increase in the sintering

duration. The oxygen ion vacancies might be the responsible charge carrier species for the existence of electrical conductivity of the order of 10^{-7} to 10^{-9} S / cm in all these samples.

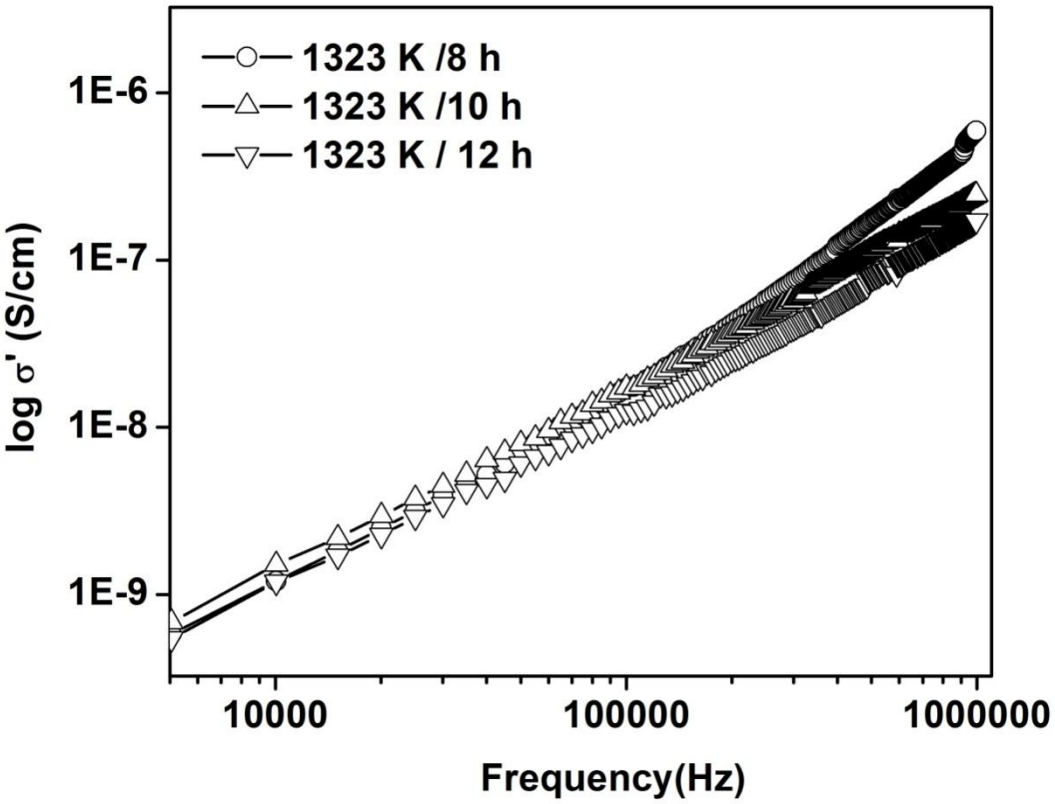

Figure 3.7. Double logarithmic plot of ac conductivity vs frequency at different sintering durations of SBSmT ceramics.

3.6. Conclusions

The $Sr(Bi_{0.9}Sm_{0.1})_2Ta_2O_9$ ferroelectric ceramics synthesized by low temperature molten salt synthesis route has exhibited single phase perovskite crystal structure. The average grain size of these ceramic samples has been found to vary between 0.6 - 0.8 µm. The frequency dependent dielectric constants of the SBSmT ceramics are influenced by the sintering duration. The electrical conductivity is found to be increasing with increase in frequency for these SBSmT ceramics. However, systematic efforts have been made to investigate the influence of samarium on the physical properties of $SrBi_2Ta_2O_9$ and $BaBi_2Nb_2O_9$ ceramics by adding an excess amount of 5 wt % bismuth oxide to the initial mixture of reactants during calcination to compensate bismuth vaporization at high temperatures and the details of which are discussed in the forthcoming chapters.

References

[1] U. Chon, H.M. Jang, M.G. Kim, C.H. Chang, *Phys. Rev. Lett.* **89** (087601), 1 (2002).

[2] A. Roy, A. Dhar, S.K. Ray, *J. Appl. Phys*. **104** (064103), 1 (2008).

[3] B.H. Venkataraman, K.B.R. Varma, *Ferroelectrics*. **33**, 39 (2006).

[4] A.Z. Simões, B.D. Stojanovic , M.A. Ramirez, A.A. Cavalheiro, E. Longo, J.A. Varela,. *Ceram. Int* .**34**, 257 (2008).

[5] C.L.Diao, J.B. Xu, H.W. Zheng, L. Fang, Y.Z. Gu, W.F. Zhang,. *Ceram. Int.* **39**, 6991 (2013).

[6] Y. Wang, C. Ganpule, B.T. Liu, H. Li, K. Mori, B. Hill, M. Wutting, R. Ramesh, J. Finder, Z. Yu, R. Droopad, K. Eisenbeiser, *Appl. Phys. Lett.***80**, 97(2002).

[7] Y.-X. Wang, W.-L. Zhong, C.-L. Wang, P.-L. Zhang, *Chin. Phys. Lett.***18**, 826 (2001).

[8] C. Zhao, Q. Zhu, D. Wu, A. Li, *J. Phys. D: App. Phys.***42** (185412), 1 (2009).

[9] C.-A Paz de Araujo, J.D. Cuchiaro, L.D. Mcmillan. M.C. Scoot, J.F. Scott, *Nature* .**374,** 627(1995).

[10] Y.Shimakawa, Y. Kubo, Y. Nakagawa, S. Goto, T. Kamiyama, H. Asano, F. Izumi, *Phys. Rev. B.***61,** 6559 (2000).

[11] J.F. Scott, *Ann. Rev. Mater. Sci.***28,** 79 (1998).

[12] K. Kato, C. Zheng, J.M. Finder, S.K. Dey, Y. Torii, *J. Am. Ceram. Soc.***81,** 1869 (1998).

[13] N.Sharanappa, S.Madolappa, R. Sagar, R.L. Raibagkar, *Ferroelectrics Lett* .**39**, 81 (2012).

[14] Sugandha, A.K. Jha, *Ferroelectrics*. **447**, 136 (2013).

[15] J.D. Bobić, M.M.V Petrović, J. Banys, B.D. Stojanović, *Ceram. Int.* **39,** 8049 (2013).

[16] L. B. Kong, T.S Zhang, J. Ma, Y.C.F. Boey, *Prog. Mater. Sci.* **53,** 207 (2008).

[17] S. Zhao, Q. Li, Y. Feng, C. Nan, *J. Phys. Chem. Solids* 7**0,** 639 (2009).

[18] Z. Ming-Lei, W. Chun-Lei, Z. Wei-Lei, W. Jin-Feng, L. Zheng-Fa, *Chin. Phys. Lett.* 20, 290 (2003).

[19] C. Sikalidas, *Advances in Ceramics - Synthesis and Characterization, Processing and Specific Applications*, InTech, 75 (2011).

[20] T. Kimura, T. Yamaguchi, *Ceram. Int* .**9,** 13 (1983).

[21] T. Kimura, T. Takahashi, T. Yamaguchi, *J. Mater. Sci.* **15,** 1491 (1980).

[22] B.R. Kannan, B.H. Venkataraman, *Ceram. Int.* **40**, 16365 (2014).

[23] D.Bochenek, Z.Surowiak, J.K. Kowalski, J.P. Vejpravova,.*J. Electroceram.* **25,**122 (2010).

[24] H. Naceur, A. Megriche, M.-EL. Maaoui, *Journal of Advanced Ceramics* **3,** 17 (2014).

[25] P. Sittiketkorn, T. Bongkarn, *Ferroelectrics Lett* .**40**, 77 (2013).

[26] R. Machado, M. G. Stachiotti, and R. L. Migoni, A. H. Tera, *Physical Review B.* **70**, 214112 (2004).

[27] F.K. Lotgering, *J. Inorg. Nucl. Chem.* **9,** 113 (1959).

[28] S. Maity, D. Bhattacharya, S.K. Ray, *J. Phys. D: Appl. Phys.***44** (095403), 1 (2011).

[29] H.P. Klug, L.E. Alexander, *X-ray diffraction procedures for polycrystalline and amorphous materials, Wiley*, New York, 491.(1954).

[30] A.Watcharapasorn, P. Siriprapa, S. Jiansirisomboon, *J. Eur. Ceram. Soc.***30,** 87 (2010).

[31] B.H. Venkataraman, K.B.R. Varma, *Solid State Ionics.***167,**197 (2004).

[32] B. S. Kang, J. Yoon, T. W. Noh, Appl. Phys. Lett. **82**, 103 (2003).

CHAPTER 4

Fabrication, Structural, Microstructural and Dielectric Properties of Samarium Doped Strontium Bismuth Tantalate Ceramics

4. Fabrication, Structural, Microstructural and Dielectric Properties of Samarium Doped Strontium Bismuth Tantalate Ceramics

The structural, dielectric and ferroelectric properties of rare earth doped strontium bismuth tantalate ceramics are described in this chapter. Layered $Sr(Bi_{1-x}Sm_x)_2Ta_2O_9$ ceramics with x ranging from 0 - 0.10 (10 mol%) were fabricated by the low temperature molten salt synthesis route. X - ray powder diffraction studies revealed that the single phase orthorhombic layered perovskite structure is retained in all these compositions. Scanning electron microscopic studies on these ceramics confirmed the presence of well packed equiaxed plate shaped grains. The dielectric and electrical conductivity properties were studied in the 100 Hz – 1 MHz frequency range at 300 K. Interestingly, the 10 mol% samarium doped $SrBi_2Ta_2O_9$ ceramics exhibited high dielectric constant (ε_r = 155) and low dielectric loss (0.00298) compared to those of other compositions. The ferroelectric property of $SrBi_2Ta_2O_9$ ceramics is superior for higher concentration of samarium content. The electrical conductivity of undoped and samarium doped ceramics increased linearly with increase in frequency.

4.1. Introduction

Bismuth containing layered structured ferroelectric materials (BLSFs) have been investigated extensively for non-volatile random access memories (NVRAM), piezoelectric sensors and microelectromechanical based device applications [1-4]. $PbZr_{1-x}Ti_xO_3$ (PZT) is one of the renowned materials for NVRAM device application owing to its versatile properties. It belongs to the perovskite crystal structure with high remnant polarization and low switching field [5, 6]. However, PZT material tends to degrade with platinum electrodes after 10^8 cycles of polarization switching [7, 8]. In comparison, the Aurivillius family of layered ferroelectric materials such as SBT, BIT, and SBN have attractive superior characteristics which include fatigue - free behaviour [9-11]. Among these materials, $SrBi_2Ta_2O_9$ is proved to be one of the potential candidates for NVRAM device application because of its excellent properties such as low leakage current and high fatigue free endurance up to 10^{12} polarisation cycles [12, 13]. But the SBT crystal structure comprising of two perovskite like blocks $(SrTa_2O_7)^{2-}$ that are interleaved between the $(Bi_2O_2)^{2+}$ layers along the c-axis suffers from the following major drawbacks: High dielectric loss, low remnant polarization and high processing temperature [14]. One of the effective approaches to improve the dielectric and ferroelectric properties has been to partially substitute bismuth by samarium in SBT lattice. Since the ionic radius of samarium (0.108 nm) is smaller than bismuth (0.117 nm) ion, it is expected that the partial substitution of bismuth ions by trivalent samarium ions would have a profound influence on the physical properties.

The conventionally synthesized layered ferroelectric ceramics would normally exhibit compositional and structural inhomogeneities owing to the high calcination and sintering temperatures. In order to achieve improved homogeneity and good control over particle sizes, low temperature molten salt synthesis technique has been adopted [15–17]. T. Kimura et al have reported the formation of homogenous powders of $Bi_4Ti_3O_{12}$ [18], ferrites [19] and Bi_2WO_6 [20] by molten salt synthesis route. Moreover, ferroelectric oxide powders with anisotropic particle morphologies (i.e textured microstructures) could also be prepared by this technique which helps in attaining the grain - oriented ceramics [21, 22]. Hence, there seems to be no other reports exist on the fabrication of samarium ion doped strontium bismuth tantalate compound via molten salt synthesis route, the objective of the present investigations has been to visualize the effect of partial substitution of bismuth sites by samarium on the structural, microstructural, dielectric, electrical conductivity and ferroelectric properties of

SBT ceramics by molten salt synthesis technique and the results obtained on the aforementioned studies are reported in this chapter.

4.2. Structural Analyses

Polycrystalline strontium bismuth samarium tantalate (SBSmT) ceramic powders with the composition of $Sr(Bi_{1-x}Sm_x)_2Ta_2O_9$ (x = 0.00, 0.03, 0.05, 0.10, mol%) were prepared by molten salt synthesis route using KCl as a flux material. The stoichiometric mixture of strontium carbonate ($SrCO_3$), bismuth oxide (Bi_2O_3), samarium (III) oxide (Sm_2O_3) and tantalum pentoxide (Ta_2O_5) were uniformly mixed with KCl in the molar ratio of 1:5. In the present study, the molten KCl salt has been chosen as a flux material since it is readily available, inexpensive and highly soluble in water. This salt also plays a vital role in determining the reaction rate and reaction temperature. The optimization of the reactants versus different salt ratio (1:3, 1:5 and 1:7) was carried out based on the crystallinity of the polycrystalline SBSmT powders from the XRD patterns. The molar ratio of 1:5 has been arrived at for the fabrication process since the synthesized polycrystalline SBSmT powders corresponding to this ratio exhibited high crystallinity without any secondary peaks compared to that of other molar ratios. An excess amount of 5 wt.% bismuth oxide was added to the initial mixture to compensate bismuth vaporization at high temperatures. These reactants were calcined at 1073 K for 4 h with the heating rate of 3 K/min and subsequently the calcined powders were leached in hot deionized water for several times to remove KCl salt. The cold pressed pellets were subjected to conventional sintering process in air at 1323 K for 10 h. The phase formation of the calcined powders and sintered ceramic samples was confirmed via X-ray diffraction (XRD) using Cu Kα radiation.

Figure 4.1 shows the XRD patterns obtained for the polycrystalline undoped and samarium doped SBT powders. These XRD patterns revealed that the single phase layered perovskite structure without any detectable impurity phase is retained in all the compositions under study and the crystalline peaks could be indexed to an orthorhombic unit cell. The XRD patterns recorded for the polycrystalline SBT ceramic samples containing different concentrations of samarium sintered at 1323 K for 10 h are depicted in Figure 4.2.

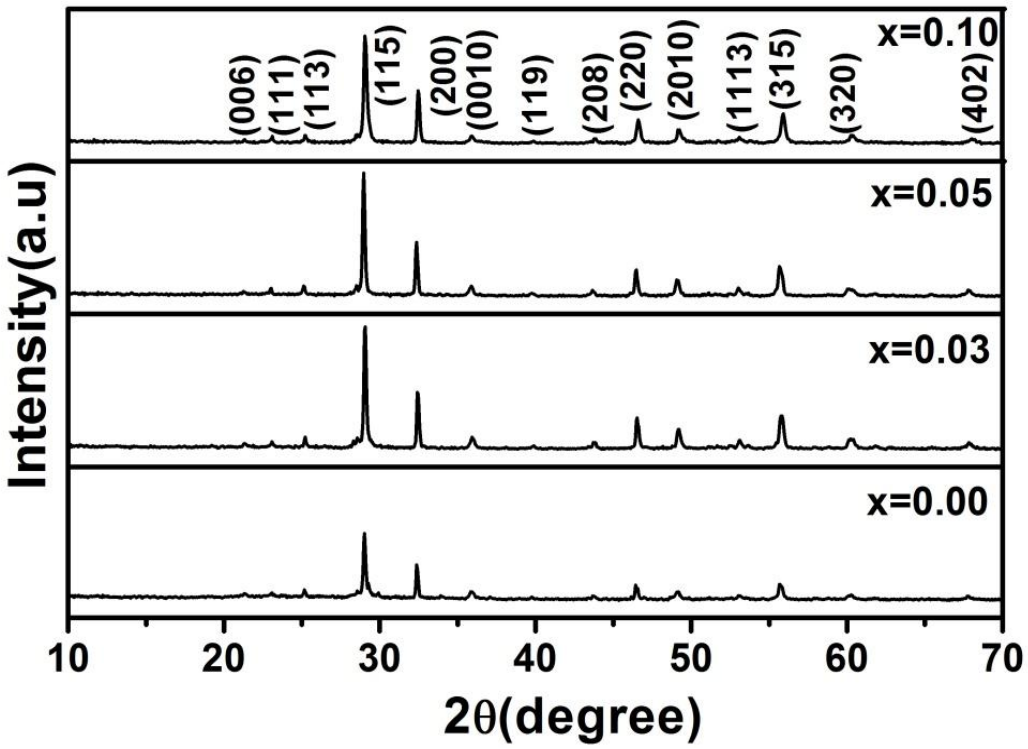

Figure 4.1 XRD patterns recorded for the polycrystalline powders of various concentrations of samarium

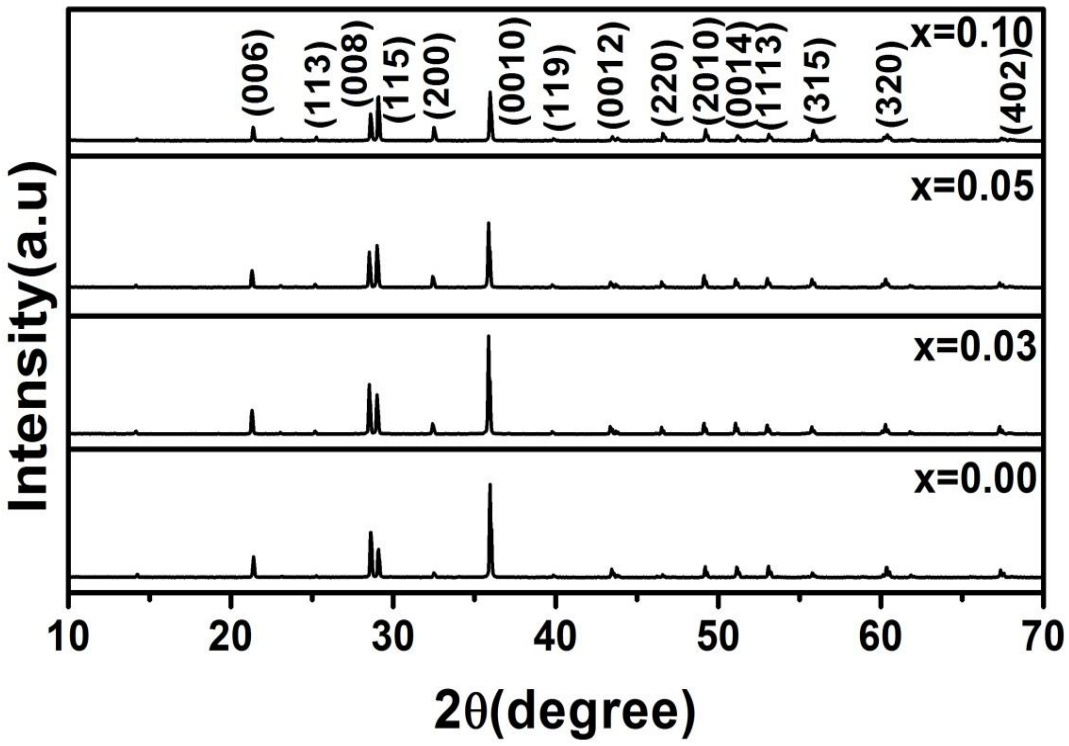

Figure 4.2. XRD patterns recorded for the sintered SBT ceramics for various concentrations of samarium

The d - spacing that are associated with all these XRD patterns of the sintered samples are found to be corresponding to the layered perovskite SBT crystal structure. The full width at half maximum (FWHM) of the Bragg peaks of these sintered samples are sharper compared to that of the respective SBSmT powder samples which reveals that there is an occurrence of grain growth during the sintering process. It is also interesting to note that the XRD peak intensities corresponding to (006), (008), and (0014) planes for these sintered samples are slightly stronger than those of the SBSmT calcined powder indicating the c-axis preferred orientation. In the Aurivillius family of layered ferroelectric oxides, grain growth along the c - axis is more prevalent and it could be caused by the anisotropic nature of the crystal structure. These crystal structures are also associated with a stronger bonding along the a - b axis and much weaker bonding between perovskite slabs along the c - axis which would have led to the faster grain growth with the observed preferred c - axis orientation [23].

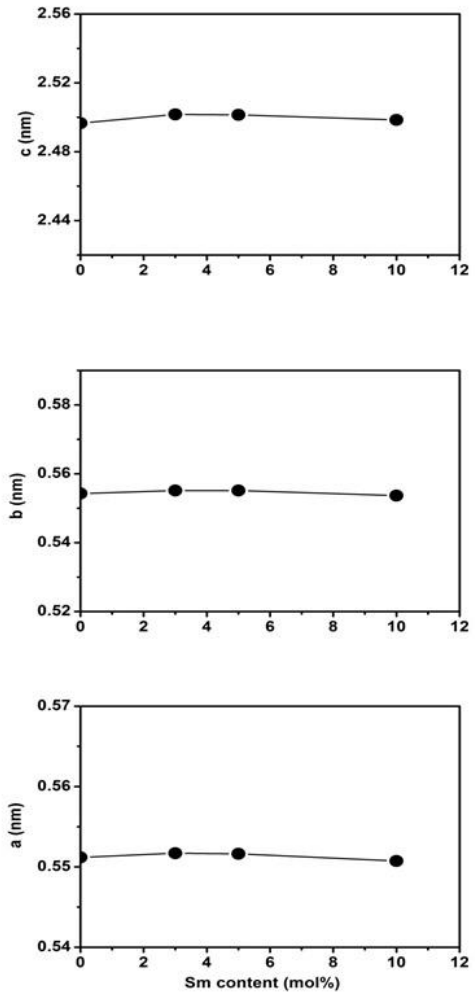

Figure 4.3. Variation of lattice parameters as a function of samarium content

The degree of c - axis grain orientation (f) in the sintered samples of pure SBT ceramics is found to be 57% by Lotgering's method. The X-ray diffraction patterns have also revealed that the c - axis orientation factor decreases with the increase in samarium content and it reaches a value of 37% for x = 0.10. However, there is a slight increase in intensity of the (200) peak with increase in samarium content. We believe that the decrease in the c - axis orientation associated with the increase in the a - axis orientation with increasing samarium content would lead to the formation of more or less equiaxed SBT grains and thereby enhancing the uniformity of the microstructure. The variation in lattice parameters with increase in samarium content is depicted in Figure 4.3. It is observed that there is a slight change in the lattice parameters with the doping of samarium in the crystal lattice of SBT ceramics due to the difference in ionic radii between bismuth and samarium ions.

4.3. Microstructural Analyses

Figure 4.4 (a-d) depicts the scanning electron micrographs obtained for the sintered samples of SBT and SBSmT ceramics. The SEM recorded for pure SBT and doped (SBSmT) samples demonstrated the presence of tightly packed equiaxed plate shaped grains with the relative density value of 93% and 96%. This plate like morphology is typical of Aurivillius family of oxides and is due to the anisotropic nature of the crystal structure [24]. The c - axis is found to be major faces of these grains showing a preferential orientation in XRD pattern. This observed preferential c - axis grain growth/orientation has been considered to be the characteristic grain growth of Aurivillius family of ferroelectric materials. Since the surface free energy of the layered perovskite is low along the c-axis, it tends to rearrange the solid particles of the SBSmT samples to attain maximum packing and a minimum of resultant pore surface along the pressing axis during the initial stage of the sintering. These micrographs also indicated that the grain size decreases from $1\mu m$ to 0.69 μm as the samarium content increased from x = 0.03 to x = 0.10 and this observation suggested that the samarium doping has influenced the grain growth of the SBT ceramics. In the bismuth based layered ferroelectric compounds ($SrBiNb_2O_9$ and $SrBiTa_2O_9$), the volatilization of bismuth at high temperatures leads to the formation of bismuth and oxygen ion vacancies. These vacancies are the responsible diffusing species for the material transport during the grain growth process. The observed retardation in the grain growth rate could be attributed to the partial substitution of samarium for bismuth in SBT has suppressed the volatilization of bismuth and thereby resulting in the reduction of diffusion ion transport in the material. On the other hand,

the microstructural property could also be correlated to the particle transport mechanism between the grains during the sintering process. Since the diffusivity of samarium ion is lower than that of bismuth, the particle transport between the adjacent SBT grains would have reduced which leads to the retardation in the grain growth rate with increase in samarium content [25, 26].

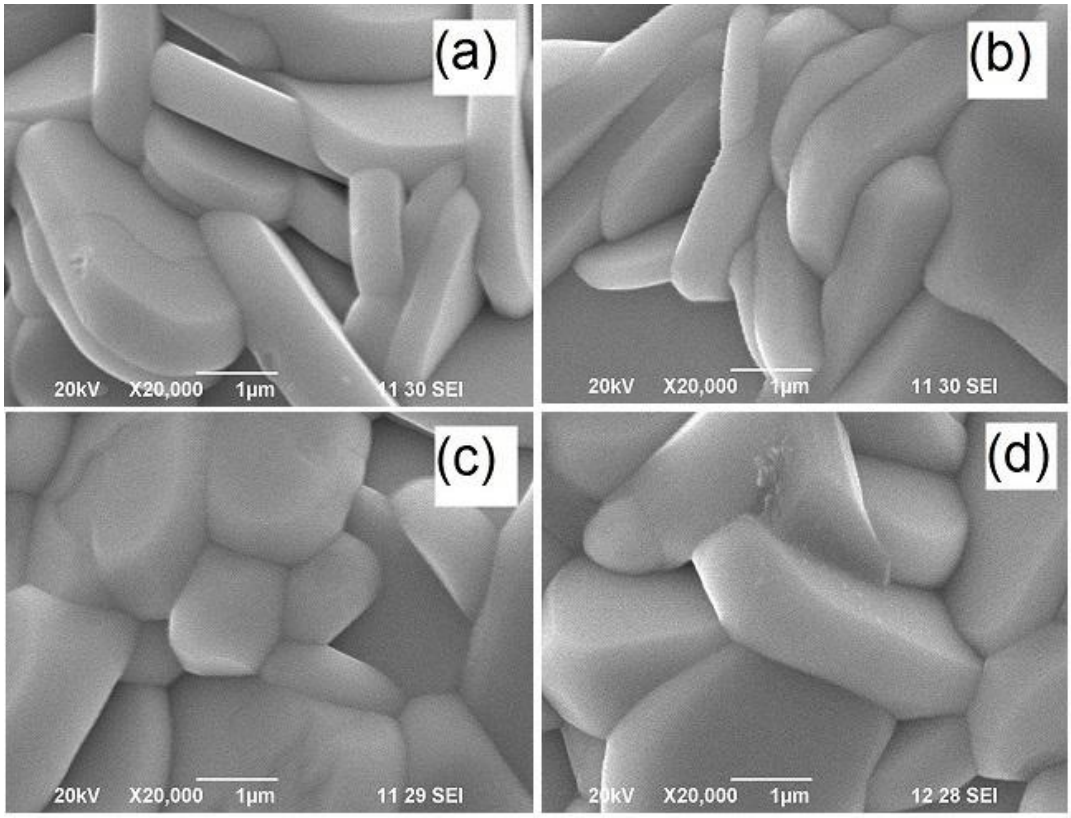

Figure 4.4 The scanning electron micrographs recorded on the surfaces of (a) 0 (b) 3 (c) 5 and (d) 10 mol% samarium doped SBT ceramics

4.4. Dielectric properties

The frequency dependence of the real (ε_r') and imaginary (ε_r'') part of the dielectric constant at 300 K for the SBSmT ceramic samples are shown in Figure 4.5 (a & b). In all these samples, the dielectric constant do not exhibit appreciable dispersion with frequency suggesting that the space charge effect is not significant at low frequencies [27].

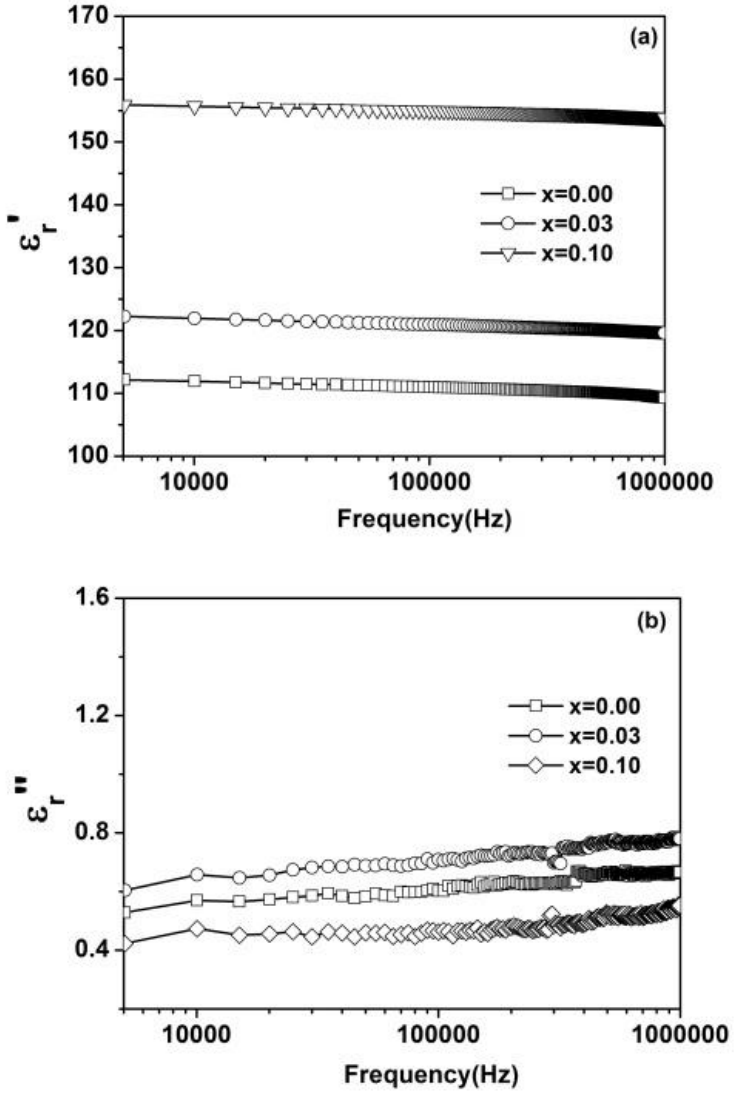

Figure 4.5. The frequency dependence of (a) ε_r' and (b) ε_r'' for different concentrations of samarium.

The dielectric constant and dielectric loss measured as a function of samarium content at 300 K are shown in Figure 4.6 (a & b). It is interesting to observe that the dielectric constant increases with increase in samarium content and reaches a maximum value of 155 at x = 0.10. The increase in dielectric constant with increase in samarium content could be attributed to the ionic size decrease from Bi^{3+} (0.117 nm) to Sm^{3+} (0.108 nm) which would have led to more structural distortion of the perovskite unit in the SBT crystal structure. This observation could also be corroborated due to the increase in the polar a - axis orientation which occurred mainly by the controlled c-axis grain growth. Interestingly, the dielectric loss of 10 mol% samarium doped SBT samples is lower than that of the undoped samples.

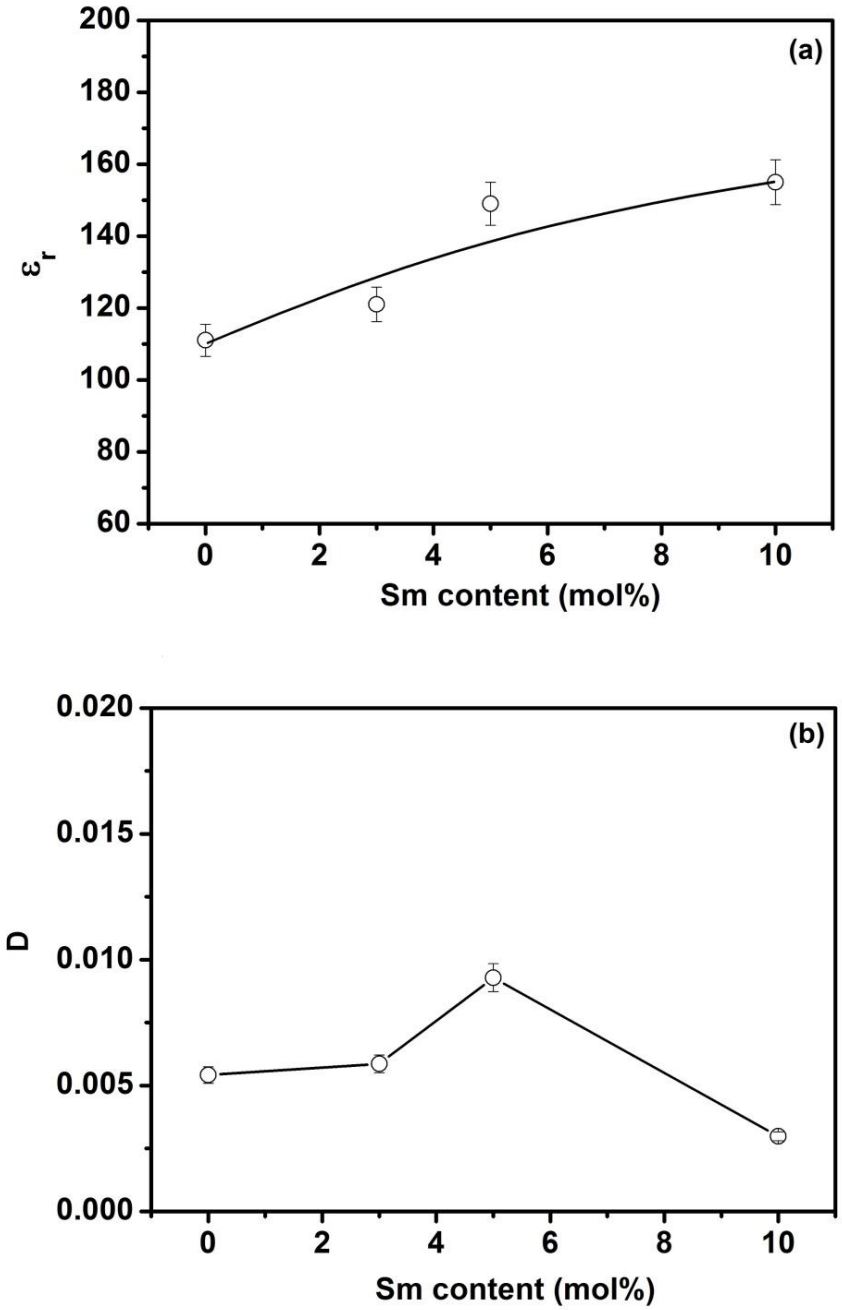

Figure 4.6. Variation of (a) dielectric constant and (b) dielectric loss as a function of samarium content at 100 kHz

4.5. Conductivity Studies

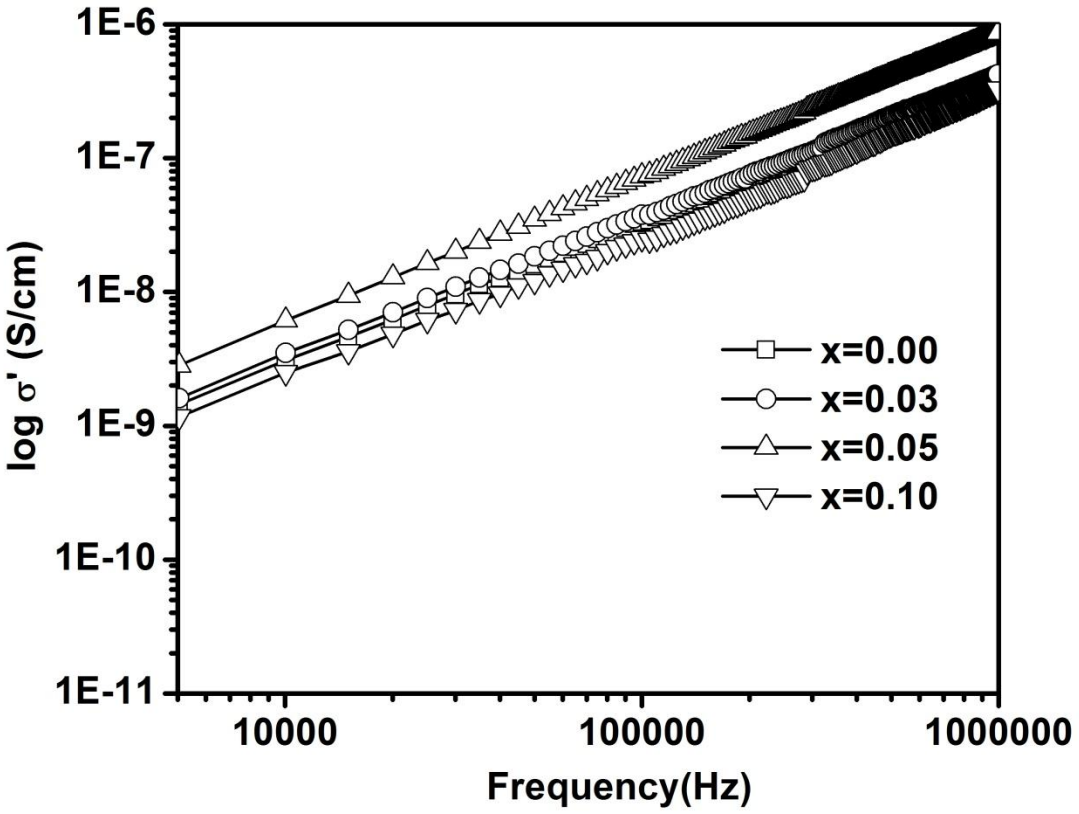

Figure 4.7. The frequency dependence of ac conductivity for various concentrations of samarium at 300 K

Figure 4.7 shows the variation of real part of the ac conductivity as a function of frequency at 300 K for SBSmT ceramic samples. The conductivity is found to increase linearly with the increase in frequency for all these samples. However, the trend of the curve does not change as a function of samarium content. The existence of electrical conductivity of the order of 10^{-7} to 10^{-9} S cm^{-1} in all these samples indicated that the oxygen ion vacancies might be the responsible charge carrier species for the conduction mechanism.

The electrical conductivity as a function of frequency ω in accordance with the Jonscher's power law is governed by the following expression

$$\sigma(f)= \sigma_{dc}[1+(\omega/ \omega_p)^n]$$

where σ_{dc} is the dc conductivity, ω and ω_p are the applied frequency and the relaxation frequency, respectively and n is the temperature dependent parameter and it can take the

value between 0 and 1. Generally, a long - range hopping behaviour of mobile charge carriers at high temperatures and low frequencies could be explained by Jonscher's universal law [28]. However, the linear dependence of conductivity relaxation process observed at low temperatures and high frequencies as depicted in Figure 4.8 implying an almost constant dielectric loss which could be described by the near constant loss (NCL) universal behaviour law $(\sigma(f) = A\omega$; where A is a constant) [29].

4.6. Ferroelectric properties

Figure 4.8 represents the polarization Vs electric field recorded at 300 K for different concentrations of samarium. Interestingly, the values of remnant polarisation computed from the hysteresis loop increase with increase in samarium content (P_r = 0.94μC/cm^2 for x = 0; P_r = 1.37 μC/cm^2 for x = 0.03; P_r = 4.04 μC/cm^2 for x = 0.05) that may be attributed to the increase in the structural distortion of the perovskite unit in the crystal structure of SBT and also this enhancement could be induced due to the slight increase in the polar a - axis orientation as corroborated by X - ray diffraction studies. Similarly, it is observed that the values of coercive field increase with increase in samarium content (E_c = 12.00 kV/cm for x = 0; E_c = 13.21 kV/cm for x = 0.03; E_c = 16.20 kV/cm for x = 0.05), indicating that a large field is required to switch the spontaneous polarisation along the c - axis of the crystal structure.

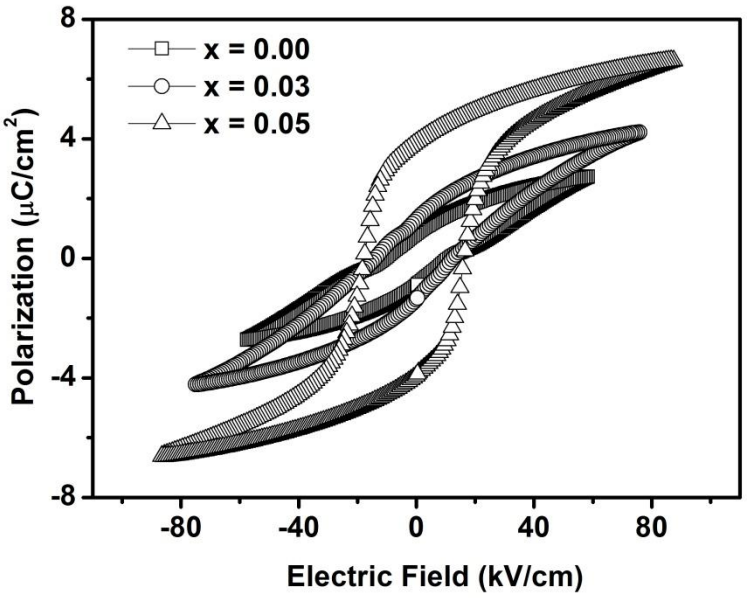

Figure 4.8. P *vs* E hysteresis loops recorded for various concentrations of samarium at 300 K.

4.7. Conclusions

The polycrystalline strontium bismuth samarium tantalate ceramics were successfully synthesized by molten salt synthesis route. The c - axis preferential orientation of the SBT grains is found to be samarium concentration dependent. Interestingly, the dielectric constant and remnant polarization of these ceramics increases with increase in samarium content. The electrical conductivity data revealed that the conductivity mechanism associated with these ceramics is essentially due to oxygen ion vacancies.

References

[1] T. Sivakumar, M. Itoh, *Chem. Mater.* **23,** 129 (2011)

[2] A.Z.Simõesc, E.C.Aguiara, C.S. Riccardia,E. Longoa, J.A.Varela, B. Mizaikoff, *Mater. Chem. Phys.***124**, 894 (2010)

[3] Sugandha, A.K. Jha, *Materials Characterization* **65**, 126 (2012)

[4] A. Srinivas, T. Sritharan,F.Y.C.Boey, *J. Appl. Phys* .**98**, 036104 (2005)

[5] J. P. B. Silva, S. A. S. Rodrigues, K. C. Sekhar, M. Pereira, M. J. M. Gomes, *J. Mater. Sci.: Mater. Electron.* **24**, 5097 (2013)

[6] W. Lee, O. Kahya, C.T. Toh, B. Ozyilmaz, J.-H. Ahn, *Nanotechnology* **24**, 475202 (2013)

[7] T. Sreesattabud, B.J. Gibbons, A.Watcharapasorn, S. Jiansirisomboon, *Ceram. Int.* **39**, S521 (2013)

[8] H. Wang, T. Matsunaga, H.-T. Lin, A.M. Mottern, *Smart Mater.Struct.* **21**, 025009 (2012)

[9] J. Pak, S. Park, K. Nam, G. Park, *Thin Solid Films* **518**, 5642 (2010)

[10] M. Zhu, L. Sun, W.W. Li, W.L. Yu, Y.W. Li, Z.G. Hu, J.H. Chu, *Mater. Res. Bull*. **45**, 1654 (2010)

[11] J. Glaum, M. J. Hoffman, *Am. Ceram. Soc.* **97**, 665 (2014)

[12] M. H. Tang, Z. H. Sun, Y. C. Zhou, Y. Sugiyama, H. Ishiwara, *Appl. Phys. Lett* . **94**, 212907 (2009)

[13] I. Coondoo, N. Panwar, V.S. Puli, R. S. Katiyar, *Integrated Ferroelectrics: An International Journal* **124**, 1 (2011)

[14] Q. Yang,J.X. Cao, Y. Ma, Y.C. Zhou,*AIP Advances* **3**, 052134 (2013)

[15] S. Zhang, Y. Wen, H.Zhang,*Powder Technology* **253**,464 (2014)

[16] H. He, J. Yin, Y. Li, Y. Zhang, H. Qiu,J. Xu, T. Xu, C. Wang, *Appl. Catal.* B**156-157**, 35 (2014)

[17] C. Sikalidas, Advances in Ceramics - Synthesis and Characterization, Processing and Specific Applications (InTech).75 (2011)

[18] T. Kimura, T.Yamaguchi, *Ceram. Int.* **9**, 13 (1983).

[19] T. Kimura, T.Takahashi, T.Yamaguchi, *J. Mater. Sci.* **15**, 1491 (1980).

[20] T. Kimura, T.Yamaguchi, *J. Mater. Sci.* **17**, 1863 (1982).

[21] T. Kimura, Y. Yoshido, *J. Am. Ceram. Soc.* **89**, 869 (2006).

[22] T. Sato, T. Kimura, *Ceram. Int.* **34**, 757 (2007).

[23] K. Babooram, Z.-G. Ye, *Chem. Mater.***18**, 532 (2006).

[24] S. Jin, I. M. M. Salvado, M.E.V. Costa, *Mater. Res. Bull.* **46**, 432 (2011).

[25] Y.M. Kan, G.J. Zhang, P.L. Wang, Y.B. Cheng, J. Eur. Ceram. Soc. **28**, 1641 (2008).

[26] Y. M. Kan, X. H. Jin, G. J. Zhang, P. L. Wang, Y. B. Cheng, D.S.J Yan, *J. Mater. Chem.* **14**, 3566 (2004).

[27] D. K. Pradhan, B. Behera, P.R. Das, *J. Mater. Sci.: Mater. Electron.* **23**, 779 (2012).

[28] Jonscher A. K. Dielectric Relaxation in Solids (Chelsea Dielectric Press, London, 1983).

[29] M. M. Kumar, Z.-G.Ye, *Phys. Rev. B* **72**, 024104 (2005).

[30] L. Sun, C.Fang, L.Chen, S.Huang, *J.Am.Ceram.Soc.* **90**, 3875 (2007).

CHAPTER 5

Temperature Dependent Dielectric and Electrical Conductivity Characteristics of Undoped and Samarium Doped $SrBi_2Ta_2O_9$ Ceramics

5. Temperature Dependent Dielectric and Electrical Conductivity Characteristics of Undoped and Samarium Doped $SrBi_2Ta_2O_9$ Ceramics

This chapter deals with the dielectric and electrical conductivity measurements carried out on undoped and samarium doped SBT ceramics at various frequencies and temperature of interest, whose fabrication, structural, microstructural and ferroelectric properties were dealt in the previous chapter. Undoped and samarium doped $SrBi_2Ta_2O_9$ ferroelectric ceramics have been fabricated by the molten salt synthesis route. The dielectric and electrical conductivity measurements were carried out in the 100 Hz - 1 MHz frequency range at various temperatures. A decrease in dielectric constant maximum (ε_m) and a downward shift in the Curie transition temperature (T_c) have been observed with the increase in samarium concentration. The frequency dependent real and imaginary parts of dielectric constant of these ceramics exhibited low frequency dielectric dispersion. Interestingly, temperature and frequency dependent dielectric constant plots indicated that the formation of oxygen ion vacancies are inhibited by samarium doping in SBT lattice. The activation energy values obtained from the Arrhenius plot have confirmed the existence of motion of oxygen ion vacancies in these ceramics.

5.1. Introduction

Layered ferroelectric materials such as $SrBi_2Ta_2O_9$ (SBT), $SrBi_2Nb_2O_9$ (SBN) and $BaBi_2Nb_2O_9$(BBN) have been recognized to be increasingly important materials for non-volatile ferroelectric random access memory device (NVRAM) applications [1-3]. Recently, strontium bismuth tantalate ($SrBi_2Ta_2O_9$) has received great attention owing to the inherent interesting properties of high fatigue endurance and low switching field [4]. This material belongs to a non-centrosymmetric crystal class and exhibits a ferroelectric to paraelectric transition around 573 K [5]. It has a layered structure with two TaO_6 octahedra sandwiched between Bi_2O_2 layers belonging to the Aurivillius family of ferroelectric oxides with the general formula $[Bi_2O_2]^{2+}$ $[A_{n-1}B_nO_{3n+1}]^{2-}$, where A site is in 12-fold coordination, B site is 6-fold coordinated and n is an integer ranging from 1 to 5 [6]. In this class of materials, there is an existence of bulk ionic conductivity arising out of oxygen ion vacancies and the oxygen vacancy driven space charge effects in the low frequency region at higher temperatures is an impediment to consider these materials for NVRAM device applications [7]. Under this situation, the dielectric constant measurements also do not reflect the intrinsic contributions particularly in the ferroelectric to paraelectric transition region.

Efforts have been made to tailor the physical properties of $SrBi_2Ta_2O_9$ ceramics by the substitution of alternative cations in the A-site and B-site of the perovskite layers [8-10]. It is also known that the Bi_2O_2 layers have a significant influence on the polar and electrical conductivity properties of bismuth based layered structures. Trivalent rare earth ion doping (Sm^{3+}, La^{3+}, Nd^{3+}) on the Bi^{3+} site of layered ferroelectric materials had an appreciable influence on the dielectric and reduction in the magnitude of electric conductivity triggered by the motion of oxygen ion vacancies in the crystal lattice [11-13]. The substitution of Bi^{3+} ion with the difference in the eightfold coordination ionic radii of Sm^{3+} ion in the crystal lattice of SBT would influence its physical properties. To the best of our knowledge, there are no systematic reports exist in the literature on the frequency and temperature dependent dielectric and electrical transport properties of undoped and samarium doped strontium bismuth tantalate ceramics fabricated by molten salt synthesis route. Hence, this chapter describes the dielectric and electrical conductivity measurements carried out on undoped and samarium doped SBT ceramics at various frequencies (100Hz - 1 MHz) and temperature of interest (303 K - 673 K).

5.2. Structural and microstructural analyses

The XRD patterns recorded for the samarium doped SBT ceramic samples revealed the formation of single phase layered perovskite structure without any impurity phases. The scanning electron micrographs of these ceramics revealed the plate shaped morphological grains. These grains are more or less tightly packed with the average grain size of 1 μm exhibiting the density of 95 % of the theoretical value. However, the detailed studies on the structural and microstructural aspects of these ceramics were already discussed in chapter 4.

5.3. Temperature and frequency dependent dielectric analyses

Figure 5.1 (a & b) shows the temperature dependent dielectric constant ($\boldsymbol{\varepsilon_r}$) and loss (D) measured at 100 kHz for different compositions, x = 0.00, 0.03, and 0.05.

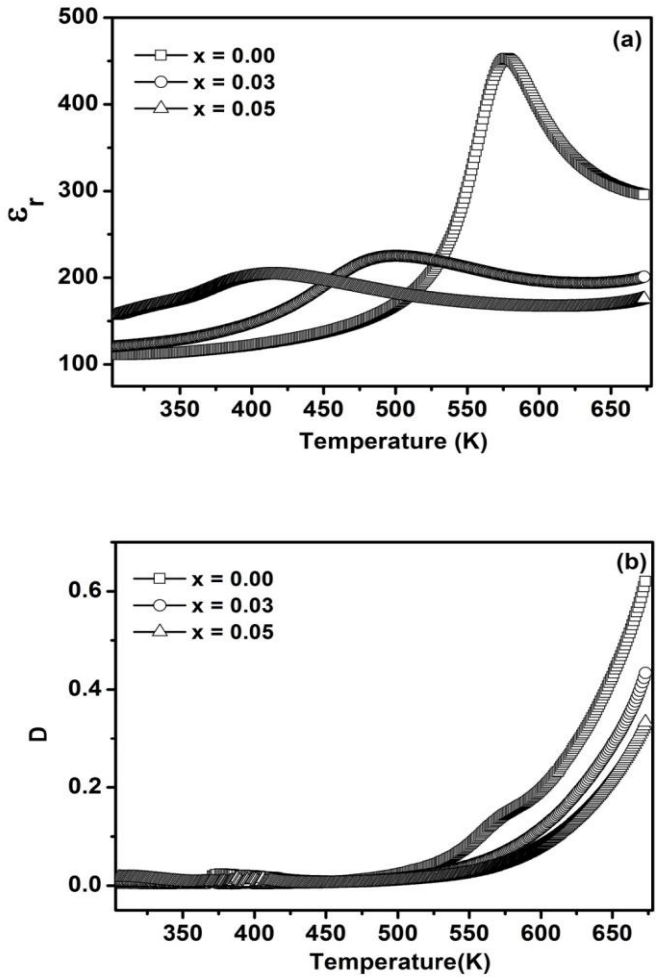

Figure 5.1. The temperature dependence of (a) ε_r and (b) D for different compositions of samarium at 100 kHz.

The undoped SBT ceramics exhibited a typical ferroelectric - paraelectric transition at 577 K (Curie transition temperature, $\boldsymbol{T_c}$) with the maximum dielectric constant ($\boldsymbol{\varepsilon_m}$) of 453. It is observed that the Curie transition temperature and the magnitude of the dielectric maximum decreases with increase in samarium doping content as indicated in Table 5.1.

Table 5.1 The Curie transition temperature (T_c) and peak dielectric constant (ε_m) of different compositions of samarium at 100 kHz.

Composition	$\boldsymbol{T_c}$(K)	$\boldsymbol{\varepsilon_m}$
x = 0.00	577	453
x = 0.03	501	225
x = 0.05	415	203

The plausible reason for the downward shift of Curie transition temperature and decrease in dielectric constant with increase in samarium content would be due to the reduction in the distortion of TaO_6 octahedra of SBT lattice [15]. On the other hand, the electron configuration state of Bi^{3+} ion indicates that it has one lone pair of $6s^2$ electrons coupled directly with perovskite layers in SBT crystal structure and these lone pair electrons will have larger tendency to participate in the polarization mechanism than bonding pair electrons with respect to the perovskite layer. Since the samarium cation does not have any lone pair electron and as a consequence the substitution of samarium would reduce the distortion extent of TaO_6 octahedra which normally results in the downward shift of $\boldsymbol{T_c}$ associated with the reduction in the magnitude of $\boldsymbol{\varepsilon_m}$ [16]. Interestingly, the tunability of $\boldsymbol{T_c}$ towards lower temperatures with samarium substitution had a significant influence on the remnant polarization in SBT ceramics as required for the better performance of ferroelectric memory device applications.

In Figure 5.1(b), the variation of dielectric loss as a function of temperature for all the compositions is sluggish till 523 K and thereafter it increases steadily with further increase in temperature. The steep increase in dielectric loss in the vicinity of high temperature regime might be due to the increased concentration of mobile oxygen ion vacancy charge carriers. Generally, these oxygen ion vacancy charge carriers are created in bismuth layered ferroelectric oxide based materials due to the volatilization of bismuth oxide at high temperatures during fabrication. It is interesting to observe that the dielectric loss decreases with the increase in samarium doping especially at elevated temperatures. This clearly reveals

that the Bi_2O_3 volatilization has been suppressed by the addition of samarium ion in the bismuth sites of SBT ceramics and thereby reducing the concentration of oxygen ion vacancy charge carriers [17].

The temperature dependence of dielectric constant measured at various frequencies for the compositions of x = 0.00, 0.03, and 0.05 is depicted in Figure 5.2 (a-c). In all the samples

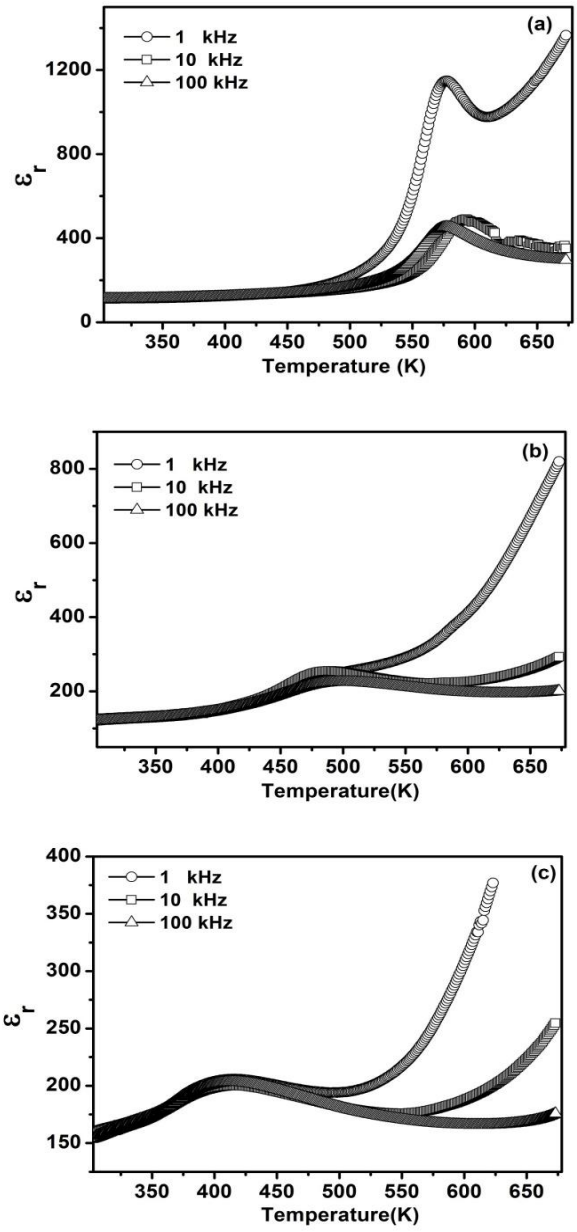

Figure 5.2. The temperature dependence of dielectric constant at various frequencies for the compositions (a) x = 0.00 (b) x = 0.03 and (c) x = 0.05.

studied, the dielectric constant exhibited a peak at the phase transition temperature for all frequencies and there is no noticeable shift in the position of the peak temperature (T_c)with frequency suggesting the normal ferroelectric behaviour of these samples. It is also noticed that the dielectric dispersion with frequency is significant at higher temperatures (i.e., well above T_c) and low frequencies in all the compositions. The lack of dispersion in the dielectric constant at high frequencies suggests that this phenomenon is coupled with space charge effects induced by oxygen ion vacancies.

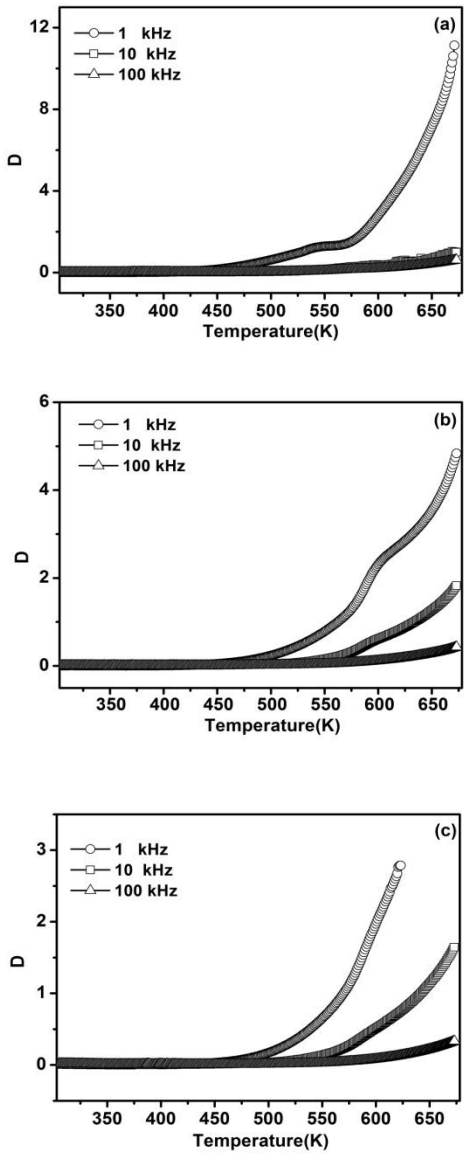

Figure 5.3. The temperature dependence of dielectric loss at various frequencies for the compositions (a) x = 0.00 (b) x = 0.03 and (c) x = 0.05.

Figure 5.3 (a-c) shows the temperature dependent dielectric loss measured at various frequencies for different samarium concentrations. The dielectric loss decreases with increase

in frequency for all the samples and it does not show any significant anomaly near the phase transition temperature. In addition, the dielectric loss is found to be increasing with increase in temperature especially at higher temperatures in all the compositions as observed in the temperature dependence dielectric constant plot. The increase in dielectric loss at higher temperatures might be attributed to the increase in charge carrier concentrations by the consequence of oxygen ion vacancy formation [18].

The frequency dependence of the real part of the dielectric constant ε'_r for the compositions, x = 0.00 and 0.05 at various temperatures is shown in Figure 5.4 (a & b). A plateau region in the high frequency part and strong low frequency dispersion is observed in both the plots.

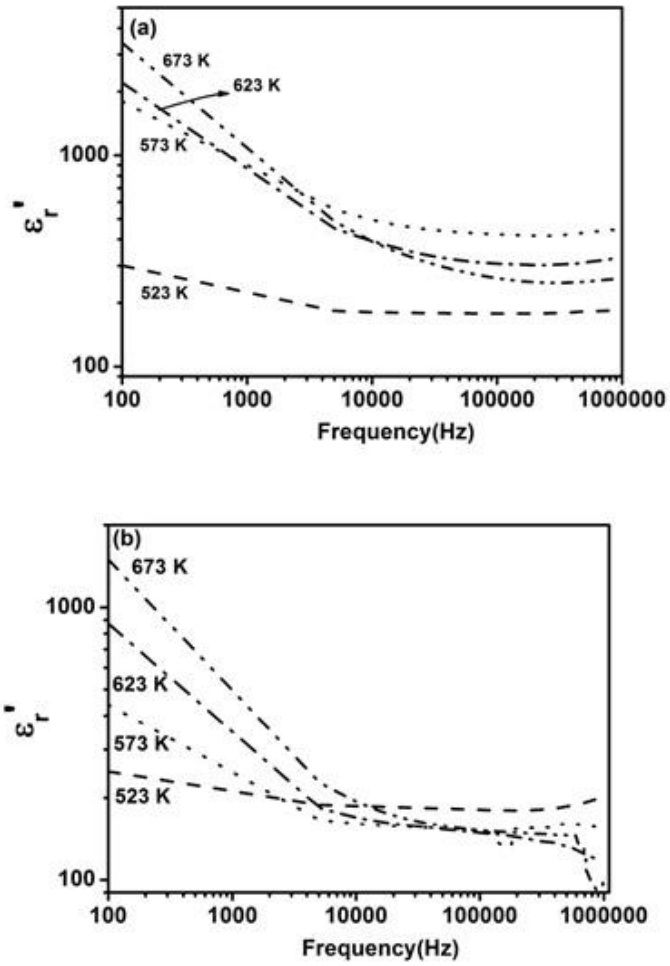

Figure 5.4. The frequency dependence of ε'_r and ε''_r (as an Inset) on a log - log scale at various temperatures for (a) x = 0.00 and (b) x = 0.05 ceramics.

This kind of behaviour is commonly encountered in lossy dielectric materials and is referred to as low frequency dielectric dispersion (LFDD) [19]. However, the low frequency dispersion at high temperatures is slightly stronger in undoped (x = 0.00) than samarium doped SBT sample (x = 0.05) which reveals that the incorporation of samarium ions in bismuth sites of SBT ceramics has suppressed the formation of oxygen ion vacancies arising out of the volatilization of bismuth oxide. The frequency dispersion of the imaginary part of the dielectric constant ε''_r (figure is not shown here) of the composition, x = 0.00 and 0.05 is stronger than that of the real part, ε'_r. The low frequency slope of the curve log ε''_r vs log f is close to -1, indicating the predominance of the dc conduction in this region. It is also interesting to observe that the magnitude of frequency dispersion of the imaginary part of the dielectric constant is lesser in samarium doped SBT sample compared to that of the undoped one.

5.4. AC conductivity studies

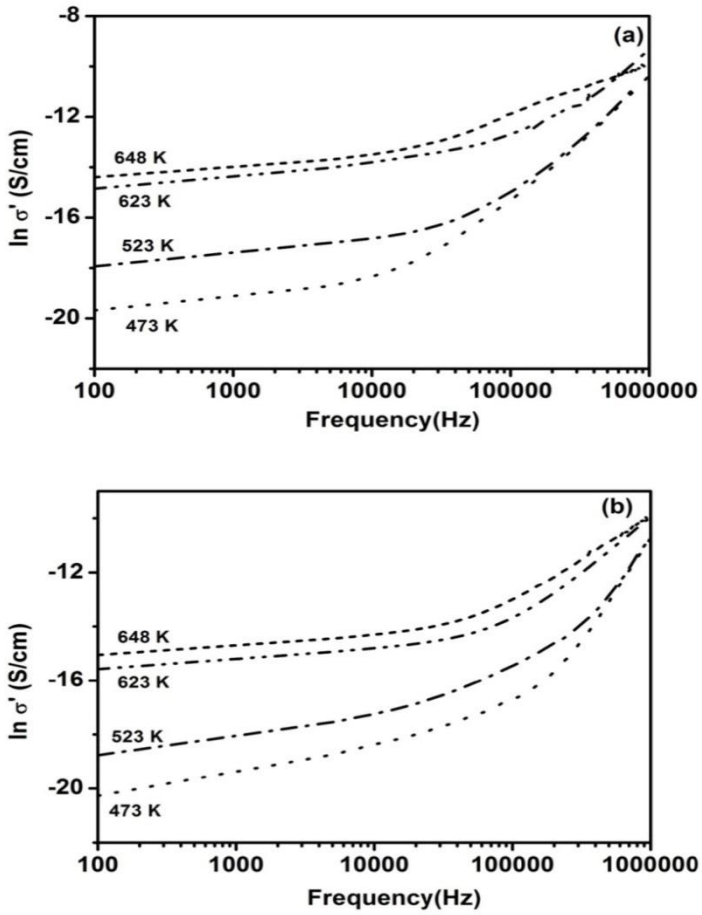

Figure 5.5. Variation of ac conductivity as a function of frequency at different temperatures for (a) x = 0.00 and (b) x = 0.05 ceramics.

Figure 5.5(a & b) shows the frequency dependent of the real part of ac conductivity at a few elevated temperatures. A convenient formalism to understand the physical mechanism of the frequency dependence of conductivity in a material is based on the power-law relation, proposed by Jonscher [20]. In the low frequency region, σ is independent of frequency and on increasing the frequency the conductivity increases, varying approximately as a power of frequency (ω^n) in both the samples. The onset of the dispersion tends to shift towards higher frequencies with increase in temperature. Interestingly, the conductivity values of the samarium doped ceramics are slightly lesser than those of the undoped SBT at all the temperatures under study and this might be attributed to the reduction in the concentration of the mobile charge carriers.

The Arrhenius plot derived from the conductivity values at various temperatures at 100 Hz of the composition, x = 0.00 and x = 0.05 is shown in Figure 5.6. The activation energies determined from this plot for x = 0.00 and x = 0.05 are 0.77 eV and 0.71 eV indicating the oxygen ion vacancy motion through the lattice.

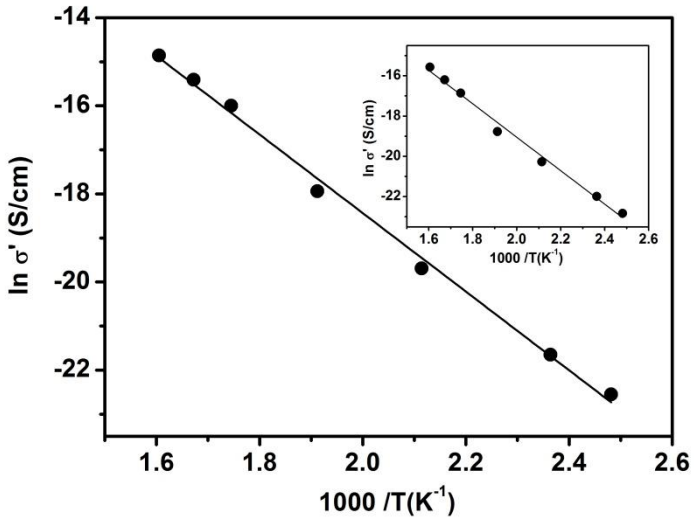

Figure 5.6. Arrhenius plot forac conductivity of x = 0.00 and x = 0.05 (as an Inset) ceramics

5.5. Conclusions

The dielectric and electrical conductivity properties of undoped and samarium (5 mol%) doped $SrBi_2Ta_2O_9$ ferroelectric ceramics synthesized by molten salt synthesis route were studied in the 100 Hz to 1 MHz frequency range at various temperatures (303 K - 673 K). There is a systematic downward shift of Curie transition temperature with an increase in

samarium content. A low frequency dielectric dispersion (LFDD) was encountered in these ceramics and the dispersion was stronger at low frequencies and higher temperatures. The electrical conductivity data indicated that the conductivity in these ceramics is essentially due to oxygen vacancies and the activation energy for the conduction in the high temperature region is found to be in the range of 0.70 eV.

References

[1] U. Chon, H.M. Jang, M.G. Kim, C.H. Chang, *Phys. Rev. Lett.* **89** (087601), 1 (2002).

[2] Roy, A. Dhar, S.K. Ray, *J. Appl. Phys.***104** (064103), 1 (2008).

[3] Sugandha, A.K. Jha, *Materials Characterization* **65**, 126 (2012).

[4] I. Coondoo, N. Panwar, V.S. Puli, R. S. Katiyar, *Integrated Ferroelectrics: An International Journal* **124**, 1 (2011).

[5] K. R. Whittle, N.C. Hyatt, Ian. M. Reaney, *Chem. Mater.* **20**, 6427 (2008).

[6] J.Mata, A.Dur´an, E.Mart´ınez, R. Escamilla, J. Heiras, J. M. Siqueiros, *J. Phys.: Condens. Matter.***18**, 10509- (2006).

[7] S.B. Desu, T.Li, *Materials Science and Engineering: B* **34**, L4, (1995).

[8] Y. Shimakawa,Y. Kubo, Y. Nakagawa, S. Goto, T. Kamiyama, H. Asano, F. Izumi,, *Physical Review B* **61**, 6559, (2000).

[9] Sugandha, A.K. Jha, *Ferroelectrics*, **459**, 160 (2014).

[10] Sugandha, A.K. Jha, *Ferroelectrics*, **447**, 136 (2013).

[11] B. Rajesh Kannan, B. HariharaVenkataraman, *Ferroelectrics Letters* Section **42,** 18 (2015).

[12] M. Roy, I.Bala, S.K. Barbar, S.Jangid, P.Dave, *J. Phys. Chem. Solids* **72**, 1347 (2011).

[13] S. Rachna, S. Bhattacharyya, S.M. Gupta, *J. Phys. Chem. Solids* **69**, 822 (2008).

[14] B.Rajesh Kannan, B.HariharaVenkataraman, *J. Mater Sci: Mater Electron.* **25**, 4943 (2014).

[15] R. Sridarane, B.J. Kalaiselvi, B. Akila, S. Subramanian, R.Murugan, *Physica B* **357**,439 (2005).

[16] L. Sun, C.Fang, L.Chen, S.Huang, *J. Am. Ceram. Soc.* **90**, 3875 (2007).

[17] B. Angadi, P. Victor, V.M. Jali, M.T. Lagare, R. Kumar, S.B. Krupanidhi, *Materials Science and Engineering B* **100**,93(2003).

[18] S. N. Padamavathi, Ch. Sameera Devi, M. Vithal, G. Prasad, G S. Kumar, *Ferroelectrics* **445**, 121 (2013).

[19] B.HariharaVenkataraman, K.B.R Varma, *Ferroelectrics*, **324**, 121 (2005).

[20] A.K. Jonscher, Dielectric Relaxation in Solids (Chelsea Dielectric Press, London, 1983).

CHAPTER 6

Structural, Microstructural and Dielectric Characteristics of Samarium Doped $BaBi_2Nb_2O_9$ Relaxor Ferroelectrics

6. **Structural, Microstructural and Dielectric Characteristics of Samarium Doped $BaBi_2Nb_2O_9$ Relaxor Ferroelectrics**

This chapter describes the fabrication and characterization of samarium doped barium bismuth niobate relaxor ferroelectric ceramics. Barium bismuth samarium niobate $Ba(Bi_{1-x}Sm_x)_2Nb_2O_9$ (x = 0, 0.03, 0.05, and 0.10) ceramics have been fabricated successfully via molten salt synthesis route. The X - ray diffraction analysis revealed the existence of bismuth layered perovskite phase with orthorhombic crystal structure in all the compositions studied. The dielectric and electrical conductivity properties were carried out in the 100 Hz – 1 MHz frequency range at 300 K. The dielectric constant and dielectric loss were found to decrease from 186 to 180 and 0.0966 to 0.0755 with increase in samarium content at 100 kHz.

6.1. Introduction

In recent years, bismuth layered structured ferroelectric materials (BLSFs) have been widely exploited for non-volatile random access memory (NVRAM) device applications owing to their high polarization fatigue resistance combined with low switching field [1,2]. The general formula of BLSFs is $(Bi_2O_2)^{2+}(A_mB_{m-1}O_{3m+1})^{2-}$, where A is a 12-coordination site and B is an octahedral coordination site with "m" indicating the number of octahedrons stacked along the c-axis between two neighbouring $(Bi_2O_2)^{2+}$ layers [3]. Most of the layered ferroelectric materials that include $SrBi_2Ta_2O_9$, $SrBi_2Nb_2O_9$ and $Bi_4Ti_3O_{12}$ belong to normal ferroelectrics whereas their barium based counterparts ($BaBi_2Ta_2O_9$ and $BaBi_2Nb_2O_9$) are relaxors in nature. These relaxor ferroelectric ceramics characterized by the diffused phase transition possess high fatigue endurance and polarization retention characteristics [4,5]. However, the drawbacks of these materials are high processing temperature and low remnant polarization [6]. In addition, the dc conductivity of these layered ferroelectric oxides are higher than that of perovskite materials. A proper substitution in $BaBi_2Ta_2O_9$ (BBT) and $BaBi_2Nb_2O_9$ (BBN) is expected to provide this material with enhanced physical properties that meets the requirements for its application in NVRAM devices [7,8]. It is widely accepted that the Bi_2O_2 layers have a significant influence on the polar and electrical conductivity properties of bismuth based layered structures [9]. There has been a lot of research conducted to enhance their properties by the substitution of the Bi^{3+} ions by alternate cations. Recently, trivalent rare earth ions doping in the layered ferroelectric structures have been paid considerable attention due to their profound influence on the physical properties [10,11]. For instance, doping with La^{3+} ions in $SrBi_2Nb_2O_9$ ceramics resulted in decrease in the Curie temperature and also an appreciable decrease in the dc conductivity [12]. It is expected that by substituting Bi^{3+} ion with the large difference in the eightfold coordination ionic radii of Sm^{3+} ion in the crystal lattice of BBN relaxor ferroelectrics could enhance its physical properties.

Most of the layered ferroelectric compounds are fabricated based on the conventional solid state reaction route which often leads to the compositional and structural inhomogeneities owing to the high calcination and sintering temperatures and thus worsening the microstructural and subsequently the electrical properties of the ferroelectric materials [13]. Molten salt synthesis (MSS) is proved to be one of the effective fabrication routes for synthesizing ceramic powders at relatively lower temperatures [14, 15]. Since there seems to

be no attempts made to synthesize samarium ion doped barium bismuth niobate compound via molten salt synthesis route, the effect of Sm^{3+} doping (on Bi^{3+} sites) on the structural, microstructural and electrical conductivity characteristics of BBN ceramics has been dealt in this chapter.

6.2. Barium Bismuth Niobate

Barium bismuth niobate (BBN) relaxor ferroelectrics have been recognised to be an increasingly important material for microelectromechanical and non-volatile random access memory device applications. This material has a layered crystal structure consisting of two NbO_6 octahedra stacked along the c-axis between two neighbouring $(Bi_2O_2)^{2+}$ layers (Figure 6.1)[16]. This layered structure is characterised by a high value of c-axis parameter in comparison with the lattice parameters a and b of the orthorhombic unit cell that leads to the high anisotropy nature of the crystal structure. The superior inherent characteristics of BBN material compared to lead based relaxor ferroelectrics are fatigue free and also non-toxic in nature. In this material, ferroelectric properties are originated from the displacement of Ba^{2+}ions along the a axis and the relaxor behaviour arises from the distortion of Ba^{2+} ions and Bi^{3+} ions in the crystal lattice.

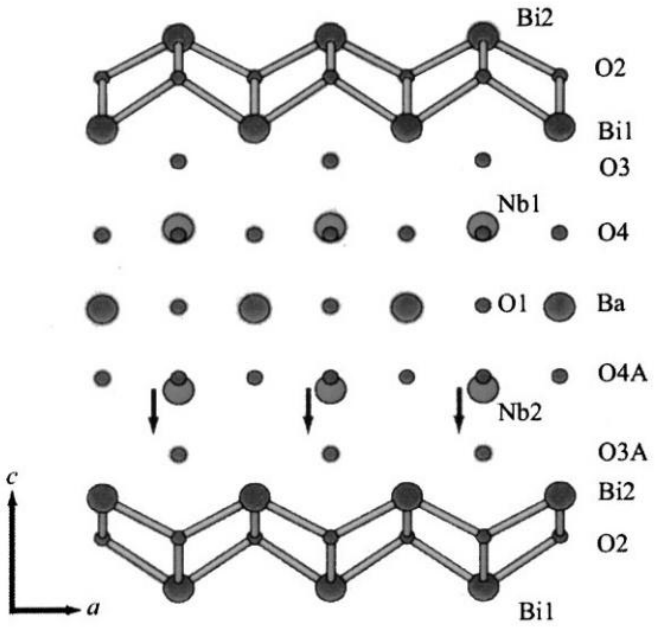

Figure 6.1. Crystal structure of $BaBi_2Nb_2O_9$

6.3. Structural Analyses

The polycrystalline barium bismuth samarium niobate (BBSmN) ceramic powders in the composition $Ba(Bi_{1-x}Sm_x)_2Nb_2O_9$ with x ranging from 0 to 0.10 (10 mol%) were synthesized by the molten salt synthesis route using KCl as a flux material. The starting reactants barium carbonate ($BaCO_3$), bismuth oxide (Bi_2O_3), samarium (III) oxide (Sm_2O_3) and niobium pentaoxide (Nb_2O_5) were thoroughly mixed with KCl in the molar ratio of 1:5. An excess amount of 5 wt.% bismuth oxide was added to the initial mixture to compensate bismuth vaporization at high temperatures. This admixture was calcined at 1073 K for 4 h in air with the heating and the cooling rate of 3 K/ min and subsequently these calcined powders were washed with hot deionized water for several times to remove the alkali metal salt. Further these powders were cold pressed at 300 K for few minutes at the pressure of 225 kg/cm^2 and subjected to the conventional sintering process at 1323 K for 10 h. The densities of the sintered ceramic samples were determined by the liquid displacement/Archimedian method. The structural phase formation of the calcined powders and sintered ceramic samples was confirmed via powder X-ray diffraction using CuKα radiation.

Figure. 6.2 shows the XRD patterns obtained for the various compositions of calcined $Ba(Bi_{1-x}Sm_x)_2Nb_2O_9$ (where x = 0, 0.03, 0.05 and 0.10) polycrystalline powders. These XRD patterns revealed the presence of single phase layered perovskite structure associated with few impurity peaks that correspond to the unreacted Bi_2O_3 reactant. All the remaining crystalline peaks of the layered perovskite BBN crystal structure could be indexed to an orthorhombic unit cell [17]. The obtained lattice parameters of all the compositions of the synthesized polycrystalline powders are listed in Table 6.1. It is observed that the values of

Table 6.1. Unit Cell Parameters Derived from X-ray Powder Diffraction Data.

Composition	a(Å)	b(Å)	c(Å)	V(Å^3)
x = 0.00	5.5677	5.5672	25.6404	794.7582
x = 0.03	5.5471	5.5477	25.5488	786.2304
x = 0.05	5.5355	5.5410	25.5356	783.2311
x = 0.10	5.5587	5.5568	25.5828	790.2102

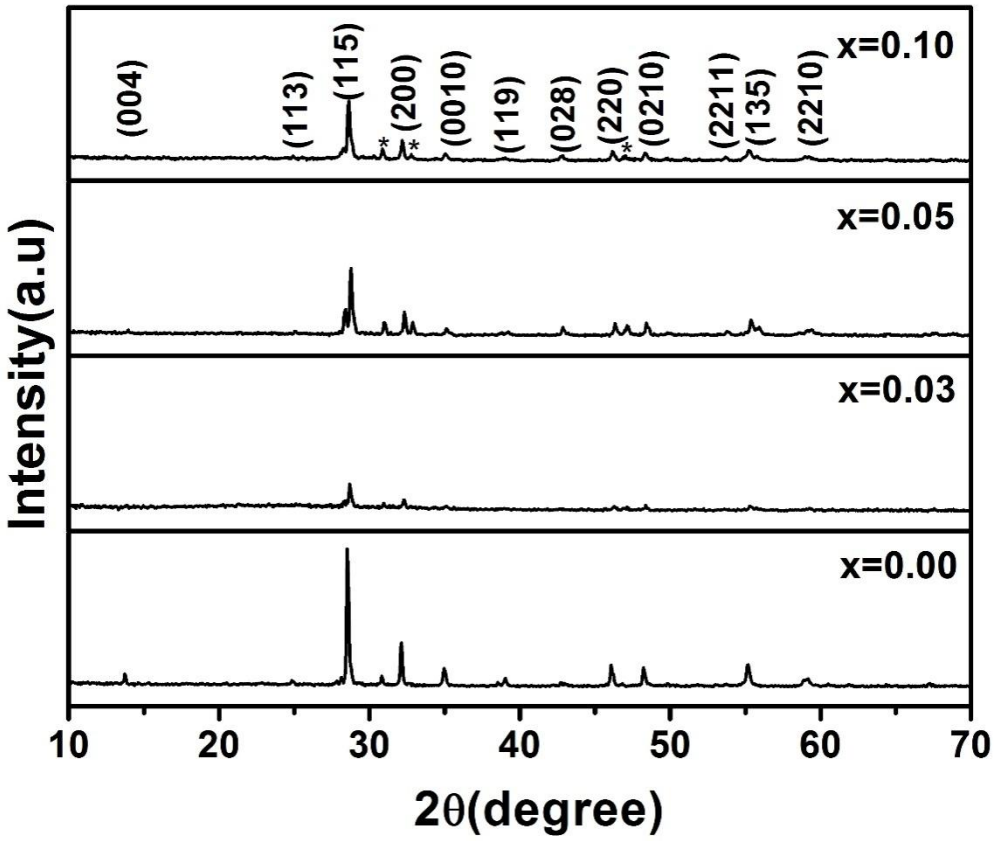

Figure 6.2. XRD patterns recorded for the polycrystalline powders of various concentrations of samarium.

lattice parameters (a, b & c) decrease slightly with increase in samarium content until x = 0.05, which could be attributed to the ionic size difference between $Sm^{3+}$and Bi^{3+}ions. The incorporation of smaller cation (Sm^{3+}) into the crystal lattice has also led in the shrinkage of the unit cell as indicated by the decrease in the magnitude of cell volume.

The XRD patterns recorded for the polycrystalline BBN ceramic samples containing different content of samarium sintered at 1323 K for 10 h are depicted in Figure 6.3. The d - spacings that are associated with all these XRD patterns of the sintered samples are found to be corresponding to the layered perovskite BBN crystal structure without any detectable impurity phase indicating the formation of solid solution between samarium and bismuth ions. The full width at half maximum (FWHM) of the Bragg peaks of these sintered samples are sharper compared to that of the respective BBSmN powder samples which reveals that there is an occurrence of grain growth during the sintering process.

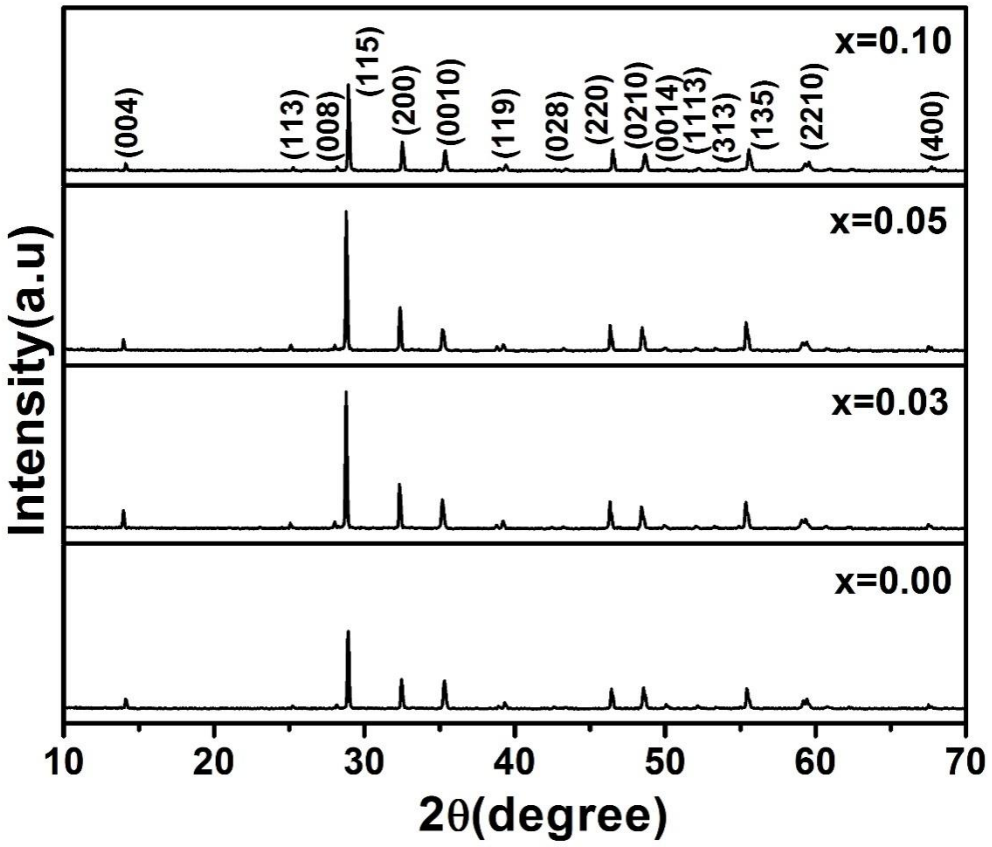

Figure. 6.3. XRD patterns obtained for the sintered BBN ceramics for different concentrations of samarium.

6.4. Microstructural Analyses

The scanning electron micrographs obtained for the sintered samples of BBN and BBSmN ceramics are shown in Figure 6.4. The SEM recorded for pure BBN ceramic samples reveals the existence of plate shaped grains with an average grain size of about 0.7 μm and the relative density of this ceramic sample is 91 % of the theoretical value. This plate like morphology is typical of Aurivillius family of oxides and is occurred due to the anisotropic nature of the crystal structure [18]. On the other hand, the micrographs corresponding to the samarium doped BBN ceramic samples indicated a decrease in intergranular porosity (i.e, the relative density value of all the samarium doped BBN ceramic samples is close to 93%) and also an increase in grain size from 0.70 μm to 1.4 μm as the samarium content increased from x = 0.03 to x = 0.10. This observation clearly suggested that the samarium doping has improved the sinterability and also grain growth of the BBN ceramics. These results are akin

to those reported in the literature for Dy^{3+} doped $Bi_4Ti_3O_{12}$ ceramics synthesized by the conventional solid state reaction route [19].

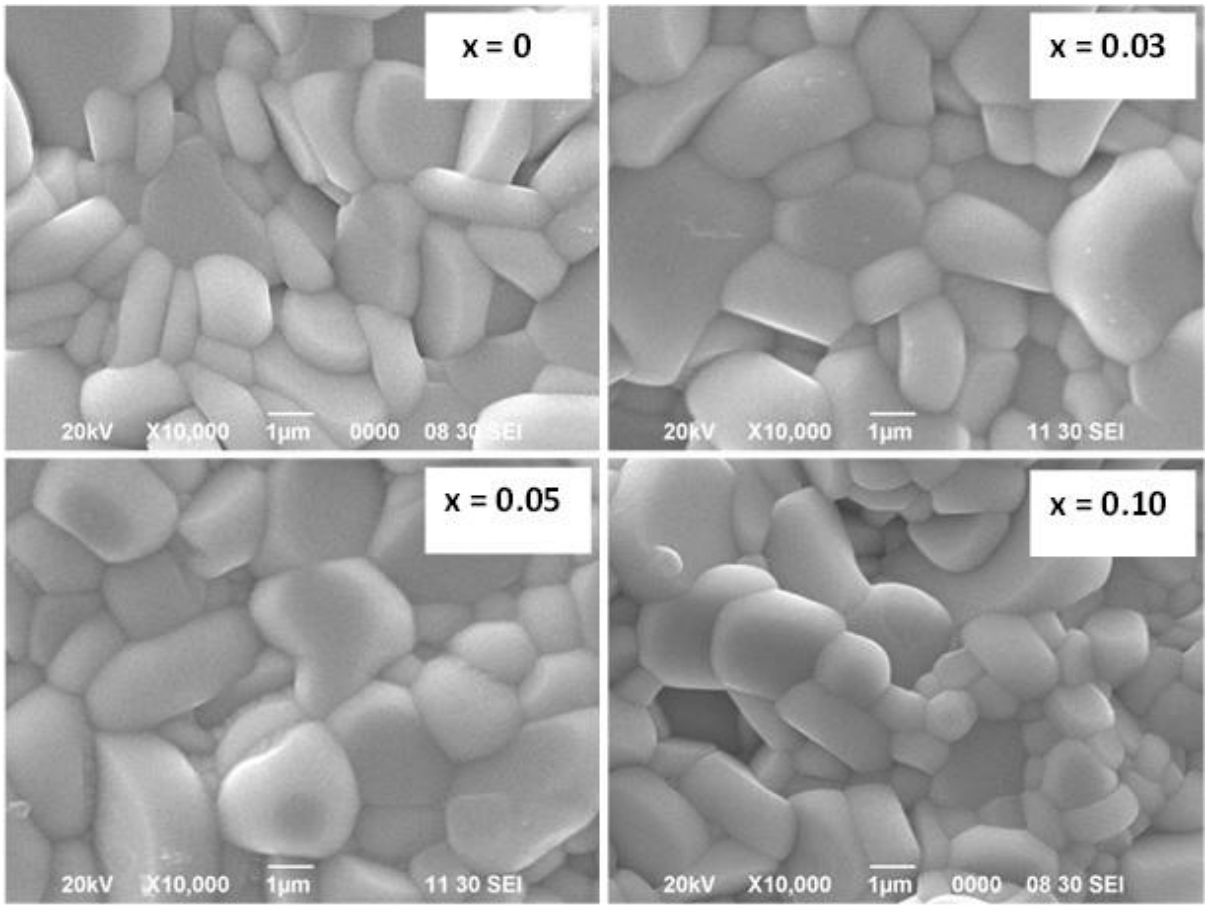

Figure 6.4. The scanning electron micrographs recorded on the surfaces of different concentrations of samarium doped BBN ceramics.

6.5. Dielectric and Conductivity Properties

The variation of real (ε'_r) and imaginary part (ε''_r) (as an inset) of the dielectric constant with frequency for different samarium compositions are represented in Figure 6.5. It is found that the value of the dielectric constant of all the ceramic samples in both the plots decreases with an increase in frequency. In bismuth layered structured ferroelectrics, the volatilization of Bi - O species in the crystal lattice creates the oxygen ion vacancies [20]. At low frequency, these charge carriers could migrate in the material in response to the applied field and thereby enhancing the space charge polarization mechanism that leads to the observed high dielectric constant [21]. But the space charge carrier species could not respond well to the applied field at high frequency which attributed to the reduction in the magnitude of the dielectric constant in the present study. Interestingly, the low frequency dielectric dispersion is found to be

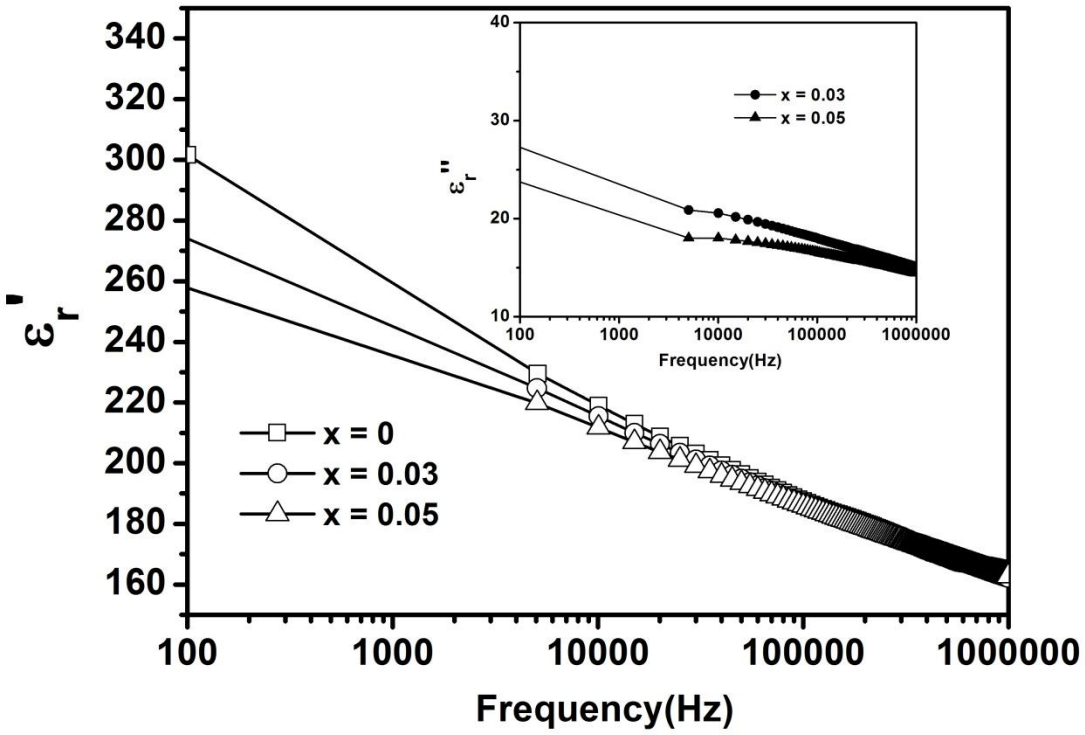

Figure 6.5. The frequency dependence of real and imaginary part of dielectric constant for various concentrations of samarium.

decreasing with the increase in samarium content. This observation clearly indicated that the samarium ion doping in to the BBN crystal lattice has suppressed the formation of oxygen ion vacancies during the fabrication process. The decrease in the concentration of oxygen ion vacancies would normally reduce the pinning of the domain walls and thereby increasing the number of available switching domains which would lead to the possibility in the enhancement of remnant polarization [22]. In addition, the dielectric constant (ε_r) and the dielectric loss (D) at 100 kHz decreased with an increase in samarium content as depicted in Figure 6.6.

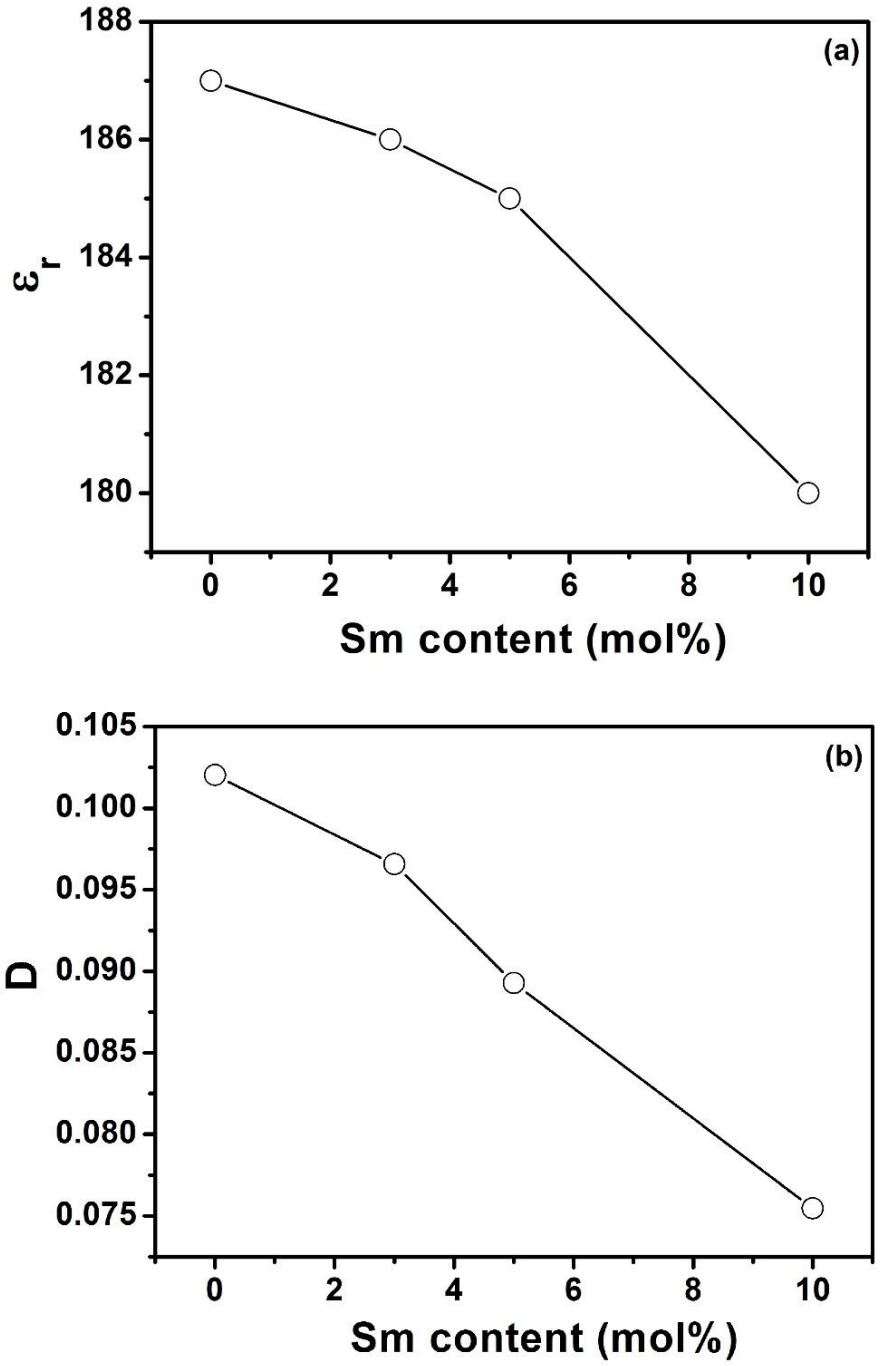

Figure 6.6. Variation of (a) dielectric constant and (b) dielectric loss as a function of samarium content at 100kHz.

The variation of real part of the ac conductivity as a function of frequency at 300 K for BBSmN ceramic samples is shown in Figure 6.7. The conductivity increases linearly with the

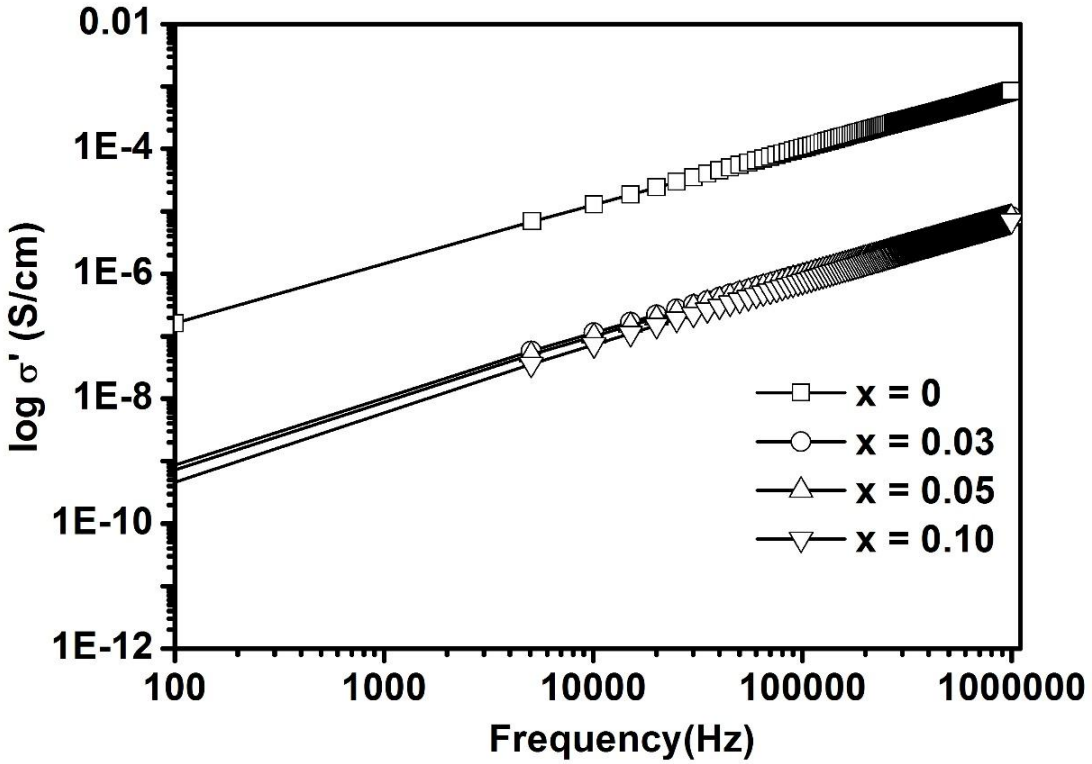

Figure. 6.7. The frequency dependence of ac conductivity for various concentrations of samarium at 300K.

increase in frequency for all these samples. This frequency dependent conductivity follows the Jonscher's universal power law [23]. It is also interesting to note that the magnitudes of the conductivity of all the samarium doped samples are lower than that of the undoped one. This observation clearly suggests that the doping of samarium ion in BBN ceramics controls the volatile nature of bismuth and thereby suppressing the formation of the oxygen ion vacancies which led to the observed reduction in the magnitude of the conductivity.

Ferroelectric hysteresis loop was recorded for different concentrations of samarium at 300 K. The values of remnant polarization (P_r = 0.11 μC/cm^2 for x = 0; P_r = 0.12 μC/cm^2 for x = 0.03; P_r = 0.06 μC/cm^2 for x = 0.05) and coercive field (E_c = 3.72 kV/cm for x = 0; E_c = 2.32 kV/cm for x = 0.03; E_c = 1.91 kV/cm for x = 0.05) were computed from the hysteresis loop and it is observed that there is no significant variation in remnant polarization and coercive field with increase in samarium content. However, the future plan of the research work includes a detailed investigation of the temperature dependent hysteresis behavior studies of these ceramics.

6.6. Conclusions

The partial substitution of bismuth by samarium on the structural and the relaxor behaviour of barium bismuth niobate layered ferroelectric ceramics has been investigated. These ceramics exhibited the well packed plate shaped grains of uniform microstructure. The samarium substitution resulted in lowering the dielectric maximum temperature and also the magnitude of dielectric maximum of BBN ceramics. The magnitude of the conductivity is found to vary linearly with frequency in all these ceramics.

References

[1] T. Sivakumar, M. Itoh, *Chem. Mater.* **23**, 129 (2011).

[2] A.Z Simões, E.C. Aguiara, C.S. Riccardi, E.Longo, J.A.Varela, B. Mizaikoff, *Mater. Chem. Phys.* **124,** 894 (2010).

[3] Y. Shimakawa, Y. Kubo, Y. Nakagawa, S. Goto, T. Kamiyama, H. Asano, F. Izumi, *Phys. Rev. B.***61,** 6559 (2000).

[4] C.A.P. de Araujo, J.D. Cuchiaro, I.D. McMillan, M.C. Scott, J.F. Scott, *Nature*, **374,** 627 (1995).

[5] J. Glaum, M. Hoffman, *J. Am. Ceram. Soc.* **97,** 665 (2014).

[6] G.C.C. da Costa, A.Z. Simoes, A. Ries, C. R. Forchini, M.A. Zaghete, J. A. Varela, *Mater. Lett.***58,** 1709 (2004).

[7] M. Adamczyk, L. Kozielski, M. Pilch, M. Pawełczykc, A. Soszyńskib, *Ceram. Int.* **39,** 4589 (2013).

[8] P. Dhak, D. Dhak, M. Das, P. Pramanik, *J Mater Sci: Mater Electron*, **22,** 1750 (2011).

[9] D.Damjanovic, Mayergouz, G.Bertotti(Eds.), *The Science of Hysteresis,* **vol.3**, Elsevier, Oxford,UK,(2005).

[10] N. Pavlović, V. Koval, J. Dusza, V.Srdi, *Ceram. Int.* **37,** 487(2011).

[11] J.D. Bobić, M.M.Vijatović Petrović, J.Banys, B.D.Stojanović, *Ceram. Int.* **39,** 8049 (2013).

[12] M. Verma, K. Sreenivas, Vinay Gupta, *J. Appl. Phys.* **105,** (024511) 1 (2009).

[13] D.G.Porob, P. A. Maggard, *Mater. Res. Bull.* **41,** 1513 (2006).

[14] S. Zhang, Y. Wen, H. Zhang, *Powder Technology* **253**, 464 (2014).

[15] H. He, J. Yin, Y. Li, Y. Zhang, H. Qiu, J. Xu, T. Xu, C. Wang, *Appl. Catal. B* **156-157,** 35 (2014).

[16] R. Machado, M. G. Stachiotti, and R. L. Migoni, A. H. Tera, *Physical Review B.* **70**, 214112 (2004).

[17] H. Zhang, H. Yan, M. J. Reece, *J. Appl. Phy*. **107,** 1 (104111) (2010).

[18] S. Jin, I. M Salvado, M.E.V. Costa, *Mater. Res. Bull.* **46,** 432 (2011).

[19] N. Thongmee, A. Watcharapasorn, S. Jiansirisomboon, *Ferroelectrics* **458,** 76 (2014).

[20] T. Hashimoto, H. Moriwake, *Phys. Rev. B* **78,** (092106)1 (2008).

[21] B. H. Venkataraman, K. B. R. Varma, *Solid State Ionics* **167,** 197 (2004).

[22] X. L. Zhong, J. B. Wang, L. Z. Sun, C. B. Tan, X. J. Zheng, and Y. C. Zhou, *Appl. Phys. Lett*. **90,** (012906) 1 (2007).

[23] A. K. Jonscher, *Dielectric Relaxation in Solids* (Chelsea Dielectric Press, London, 1983).

CHAPTER 7

Dielectric Relaxor and Conductivity Characteristics of Undoped and Samarium Doped Barium Bismuth Niobate Ferroelectric Ceramics

7. Dielectric Relaxor and Conductivity Characteristics of Undoped and Samarium Doped Barium Bismuth Niobate Ferroelectric Ceramics

This chapter presents the temperature and frequency dependence of dielectric and conductivity characteristics of undoped and samarium doped BBN relaxor ferroelectric ceramics whose fabrication, structural and microstructural properties have been discussed in the previous chapter. The polycrystalline $BaBi_2Nb_2O_9$ and $Ba(Bi_{0.9}Sm_{0.1})_2Nb_2O_9$ ceramics have been fabricated via the molten salt synthesis route. The temperature dependence of dielectric and electrical conductivity properties of BBN and BBSmN ceramics investigated at various frequencies have revealed the characteristic features of relaxor behaviour. The incorporation of Sm^{3+} for Bi^{3+} has induced a downward shift in the dielectric maximum temperature (438 K - 393 K) with the decrease in dielectric constant maximum (372 to 212) at 100 kHz. The estimated degree of diffuseness (γ) was found to be 2.17 for BBN and 1.93 for BBSmN ceramic samples. The activation energy obtained from the Arrhenius plot revealed the existence of motion of oxygen ion vacancy in these ceramics.

7.1. Introduction

Barium bismuth niobate (BBN) relaxor ferroelectrics have been recognised to be an increasingly important material for microelectromechanical and non - volatile random access memory device applications [1-5]. This material has a layered crystal structure consists of two NbO_6 octahedral stacked along the c-axis between two neighbouring $(Bi_2O_2)^{2+}$ layers [6]. The superior inherent characteristics of BBN material compared to conventional lead based relaxor ferroelectrics are fatigue free and also non - toxic in nature [7, 8]. In this material, ferroelectric properties originated from the displacement of Ba^{2+} ions along the a-axis and the relaxor behaviour arises from the distortion of Ba^{2+} ions and Bi^{3+} ions in the crystal lattice [9]. Generally, the relaxor ferroelectrics are characterized by the diffuse phase transition with strong frequency dependence. The dielectric and relaxor behaviour of ferroelectric ceramics could be tailored by the replacement of Bi^{3+} ions by suitable trivalent cations [10-15]. It was demonstrated that the partial substitution of lanthanum ions in $SrBi_2Nb_2O_9$ ferroelectric ceramics had a profound influence on the Curie temperature and also electrical conductivity which was caused by the presence of oxygen ion vacancies. Normally, the motion of these vacancies under an ac voltage results in entrapment at defect sites and consequently induces space charge effects which is considered to be an impediment for device applications. Since the practical devices operate in ac mode, understanding the conductivity mechanism of these ferroelectric materials under ac voltage is very essential. It was found that the trivalent rare earth ions doping (Sm^{3+}, La^{3+}, Nd^{3+}) on the Bi^{3+} site of layered ferroelectric ceramics had controlled the transport of oxygen ion vacancies in the lattice by suppressing the volatilization of bismuth oxide [16-18]. This prompted us to investigate the dielectric and conductivity behaviour of undoped and samarium doped BBN ceramics fabricated by molten salt synthesis route at various frequencies (100 Hz - 1 MHz) and temperatures of interest (303 K - 648 K).

7.2. Structural and microstructural studies

The careful analyses of the X-ray diffraction data revealed the formation of single phase layered perovskite structure of BBN and BBSmN polycrystalline ceramic powders without any impurity/secondary phases. The scanning electron micrographs of BBN and BBSmN ceramics revealed the presence of more or less tightly packed equiaxed plate shaped morphological grains. However, the detailed analyses on the structural and microstructural studies of these ceramics were already discussed in the previous chapter.

7.3. Dielectric Studies

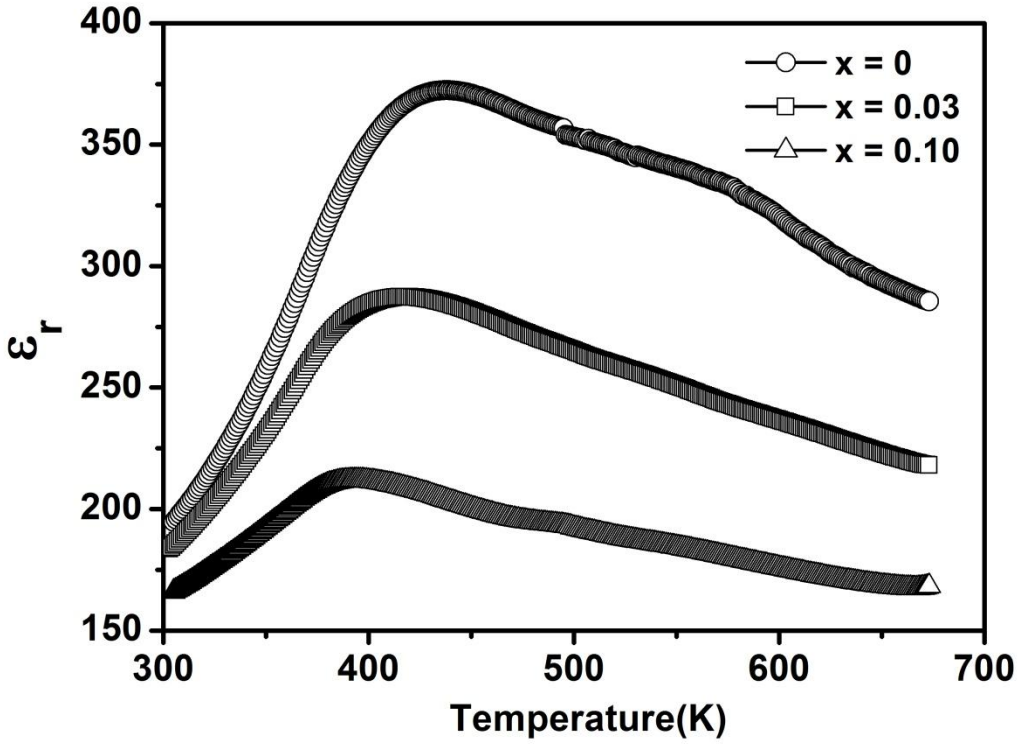

Figure 7.1. The temperature dependence of ε_r (at 100 kHz) for different concentrations of samarium.

Figure 7.1 shows the variation of the dielectric constant as a function of temperature at 100 kHz for the compositions x = 0, 0.03, and 0.10. The broadened peak which is encountered in the vicinity of the dielectric maximum temperature in all these samples revealed the diffused nature of the relaxor ferroelectrics and this peak broadening might occur due to the compositional fluctuations of the cations in the lattice structure. It is observed that the temperature of the dielectric maximum (T_m) shifts towards lower temperatures continuously with the increase in samarium content and further the magnitude of the dielectric maximum (ε_m) decreased with the incorporation of samarium in BBN ceramics. We believe that the possible explanation for the downward shift of T_m and reductions in the magnitude of $\varepsilon_m$with increase in samarium content could be attributed to the decrease in the distortion of NbO_6 octahedron of BBN ceramics. Bismuth has one lone pair electrons of $6s^2$ and these lone pair electrons have a tendency to occupy more space compared to the bonding pair electrons and thus induce more polarizability than bonding pair electrons in the crystal structure. Since the samarium cation does not have any lone pair electron, the substitution of samarium would

reduce the distortion of NbO_6 octahedron that might led to the downward shift of T_m associated with the reduction in the magnitude of ε_m[12, 23].

The temperature dependence of dielectric constant (ε_r) measured at various frequencies (1 kHz, 10 kHz and 100 kHz) for BBN and BBSmN ceramics is depicted in Figure 7.2 (a) and 7.2 (b).In Figure 7.2 (a), the undoped BBN ceramics exhibited a broad peak around 406K

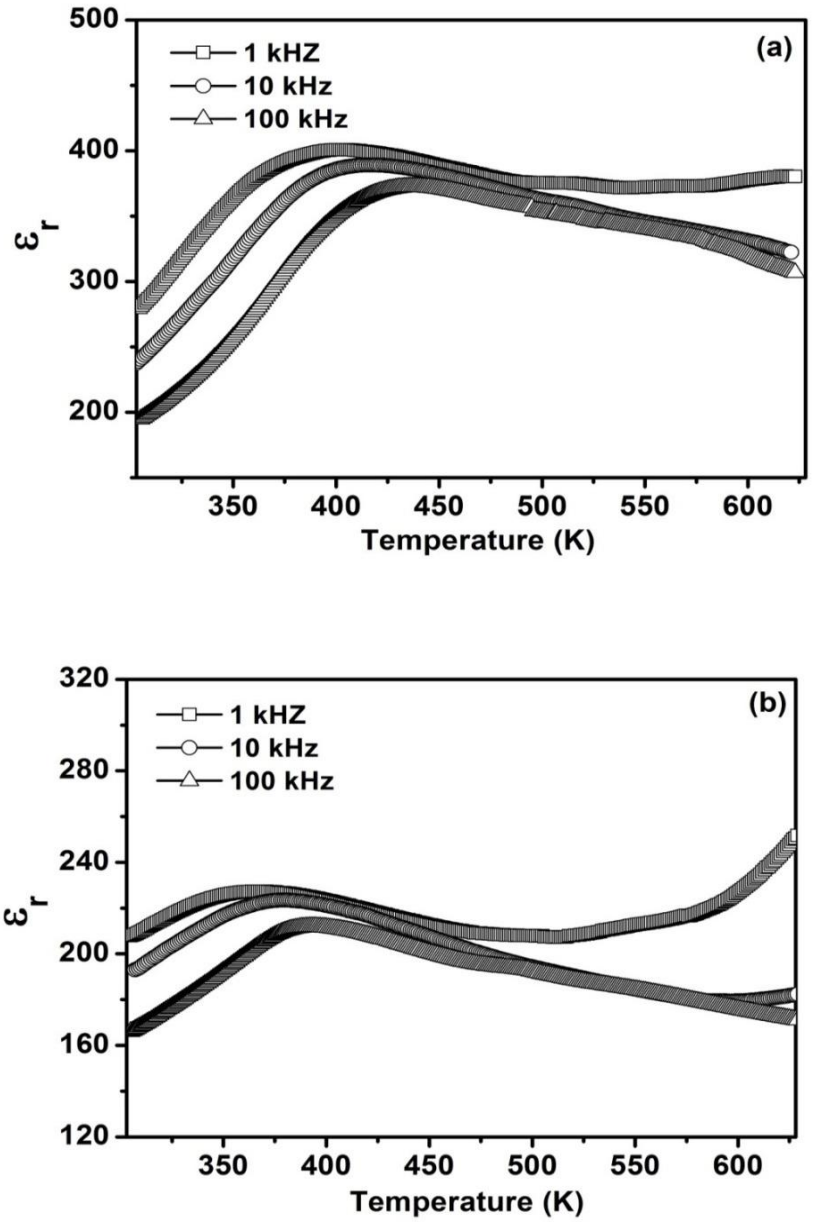

Figure 7.2. Variation of dielectric constant (ε_r) as a function of temperature for (a) BBN and (b) BBSmN ceramics.

at 1 kHz and there is a noticeable upward shift in the dielectric maximum temperature (T_m) with increase in frequency suggesting the characteristic features of relaxor ferroelectrics. It is also observed that the samarium doped BBN sample retained the relaxor behaviour accompanied by the characteristic frequency dispersion of the dielectric maximum temperature. In addition, there is a reduction in dielectric maximum (ε_m) and dielectric maximum temperature with the incorporation of samarium in BBN ceramics for all the frequency ranges under study (as indicated in Table 7. 1). This could be attributed to the decrease in the

Table 7.1. Dielectric properties of BBN and BBSmN ceramics

Frequency	**BBN ceramics**		**BBSmN ceramics**	
	$T_m(K)$	ε_m	$T_m(K)$	ε_m
1 kHz	406	400	367	227
10 kHz	416	389	381	224
100 kHz	438	372	393	212

distortion of NbO_6 octahedron of BBN ceramics [20]. The degree of frequency dispersion (ΔT_m) of dielectric maximum temperature is estimated by the difference between the T_m measured at 1 kHz and 100 kHz. The obtained values of frequency dispersion for BBN and BBSmN ceramics are 32 and 26. Generally relaxor behaviour of ferroelectric ceramics are characterized by the degree of diffuseness (γ) governed by the following mathematical relation

$$\left(\frac{1}{\varepsilon_r}\right) = \left(\frac{1}{\varepsilon_m}\right) + (C')^{-1}(T - T_m)^{\gamma}$$

where ε_m is the maximum value of dielectric constant, γ is the diffusivity parameter, C' the Curie-like constant, T_m is the dielectric maximum temperature [21]. The plot of $\log(1/\varepsilon_r - 1/\varepsilon_m)$ vs $\log(T - T_m)$ at 100 kHz for BBN and BBSmN ceramics is depicted in Figure 7.3 and the diffusivity parameter γ could be determined from the slope of the linear fit. The value of γ decreases from 2.17 for BBN to 1.93 for BBSmN ceramics implying that the substitution of samarium in BBN has decreased the diffuseness of the transition and thereby enhancing the ordering of the dipoles in the crystal lattice of BBN.

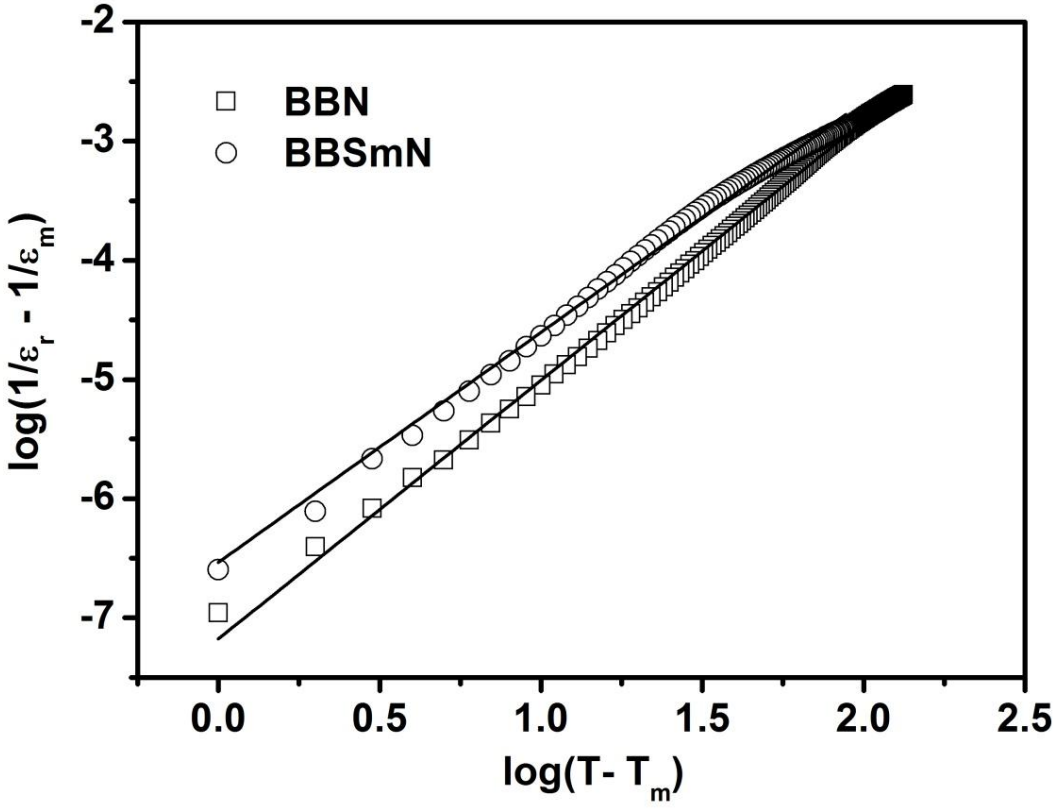

Figure 7.3. A plot of $\log(1/\varepsilon_r - 1/\varepsilon_m)$ vs $\log(T - T_m)$ at 100 kHz for BBN and BBSmN samples.

Figure 7.4 (a & b) shows the variation of dielectric loss (D) as a function of temperature at various frequencies for BBN and BBSmN samples. The temperature of maximum dielectric loss increases with an increase in the measured frequency for both the samples confirming the characteristics of relaxor behaviour. However, the frequency dispersion is clearly perceptible for BBN (shown as an inset in Figure 7.4(a)) than that of the BBSmN ceramics. In addition, there is a steep increase in the dielectric loss especially at elevated temperatures in both the samples as observed in the dielectric constant plot which might be ascribed to the increase in the charge carrier concentration induced by the consequence of oxygen ion vacancy formation [22].

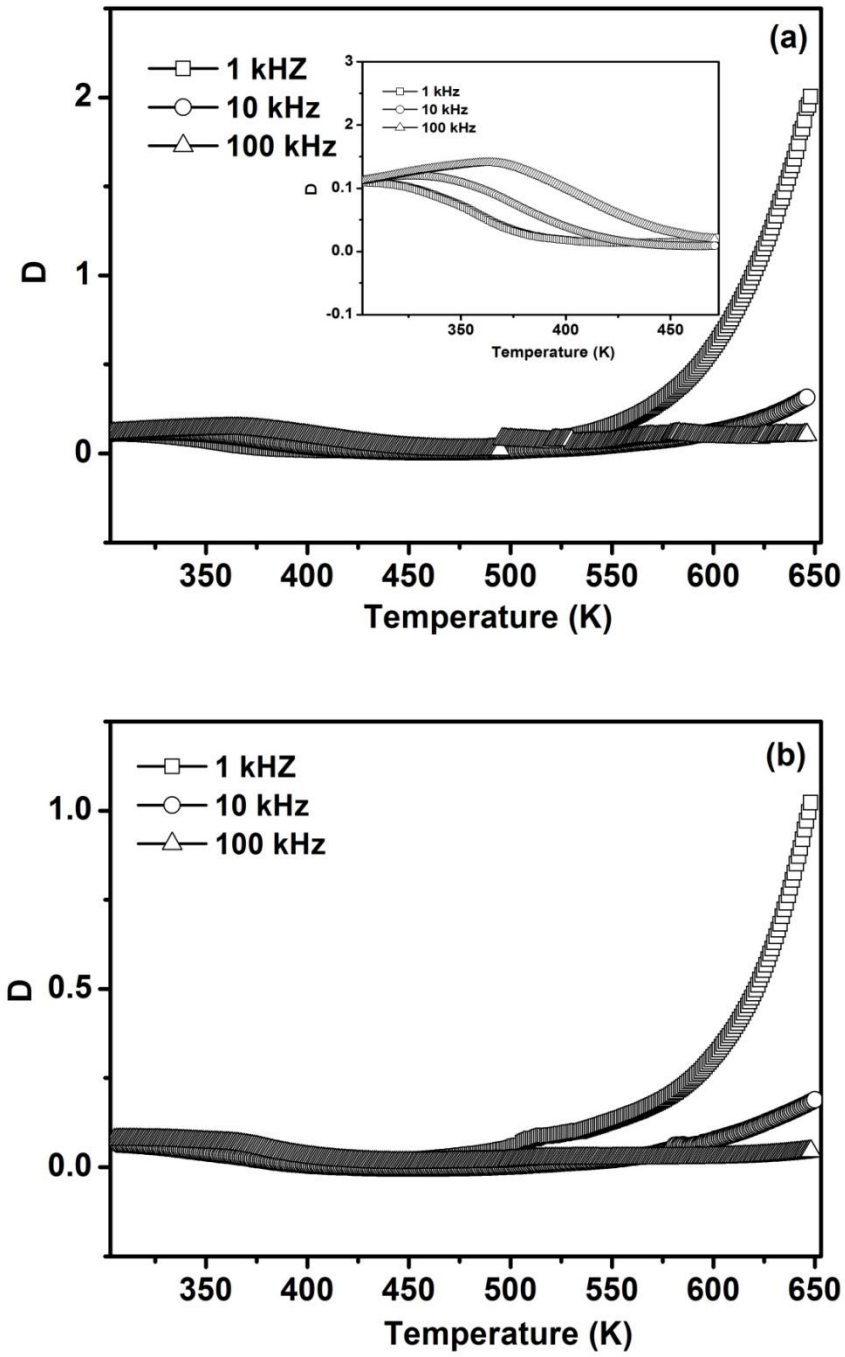

Figure 7.4. Variation of dielectric loss (D) as a function of temperature for (a) BBN and (b) BBSmN ceramics.

7.4. AC conductivity studies

Figure 7.5 (a) & 7.5 (b) shows the variation of frequency dependence of ac conductivity of BBN and BBSmN ceramics at different temperatures. In both the samples, the conductivity seems to be independent of frequency in the low frequency regime and afterwards it increases

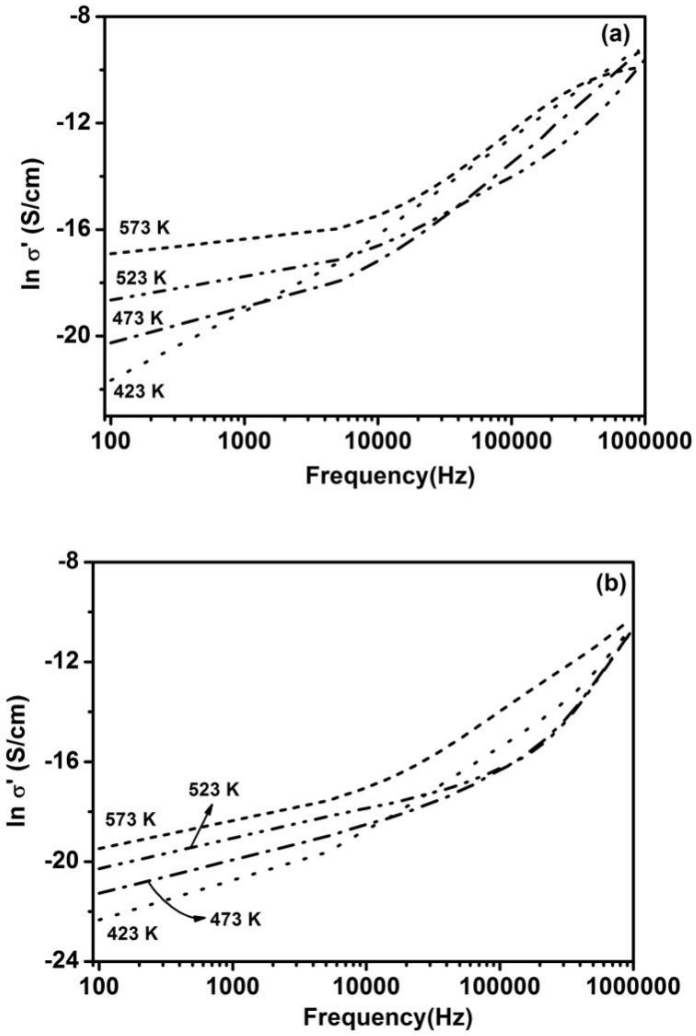

Figure 7.5. Variation of AC conductivity as a function of frequency at different temperatures for (a) BBN and (b) BBSmN ceramics.

with further increase in frequency as ω^n dependence. It is also observed from these plots that the onset of dispersion tends to be shifting towards higher frequencies with the increase in temperature.

The frequency dependence of conductivity in a material could be analysed by power law relation formalism, proposed by Jonscher [23] and it was observed that an excellent agreement between experimental and calculated values of conductivity for both BBN and BBSmN ceramics in the wide temperature range covered in the present investigations. For instance, the curve fitting obtained for BBN and BBSmN ceramics at 523 K is depicted in Figure 7.6 (a) & (b). The exponent $n(T)$ and the coefficient $A(T)$ were determined by curve fitting and are tabulated in Table 7. 2.

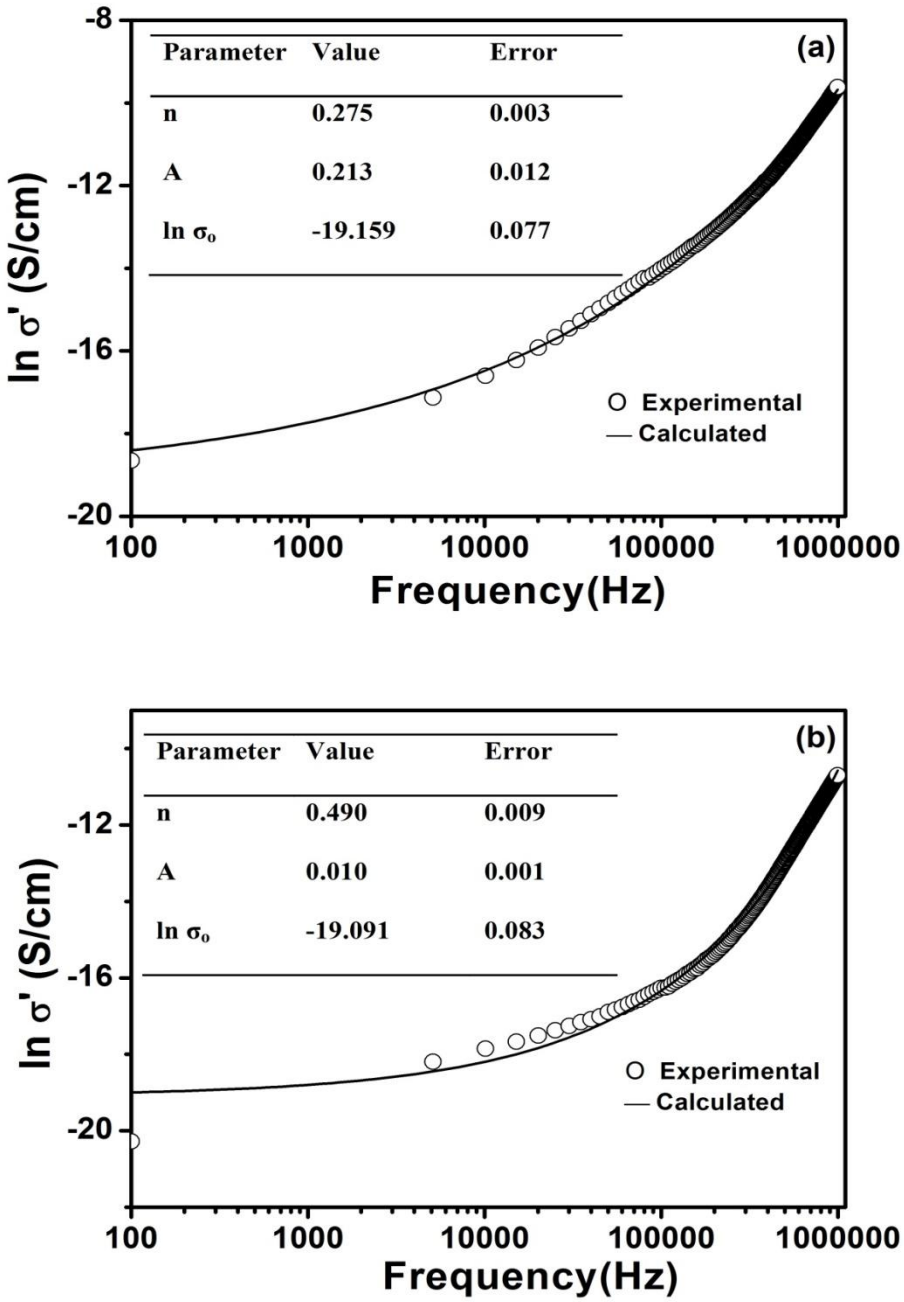

Figure 7.6. Experimental and theoretical fit for AC conductivity as a function of frequency at 523 K for (a) BBN and (b) BBSmN ceramics.

Table 7. 2. Exponent $n(T)$ and prefactor $A(T)$ for BBN and BBSmN ceramics

Temperature (K)	BBN ceramics		BBSmN ceramics	
	n	A	n	A
303	0.076	5.000	0.220	0.300
343	0.067	8.000	0.217	0.500
363	0.062	9.000	0.200	0.723
473	0.134	2.638	0.383	0.049
523	0.275	0.213	0.490	0.010

The exponent $n(T)$ initially decreases slightly with increase in temperature and shows a minimum around the vicinity of dielectric anomaly in both BBN and BBSmN ceramics and subsequently increases with further increase in temperature. According to the many body interaction models [23, 24], the observed minimum near T_m implies the strong interaction between the dipoles participating in the polarization mechanism. On the contrary, the prefactor $A(T)$ which determines the strength of polarizability exhibits a maximum in the vicinity of dielectric anomaly in these samples indicating the high magnitude of polarizability. However, the value of $A(T)$ for BBSmN is lesser than that of BBN in all the range of temperatures under study implying that the incorporation of samarium in the bismuth lattice leads to the reduction in polarizability and thereby diminishing the dielectric constant of BBSmN ceramics.

The Arrhenius plot derived from the conductivity values at various temperatures at 100 Hz for BBN and BBSmN (as an inset) ceramics is shown in Figure 7.7. The activation energies

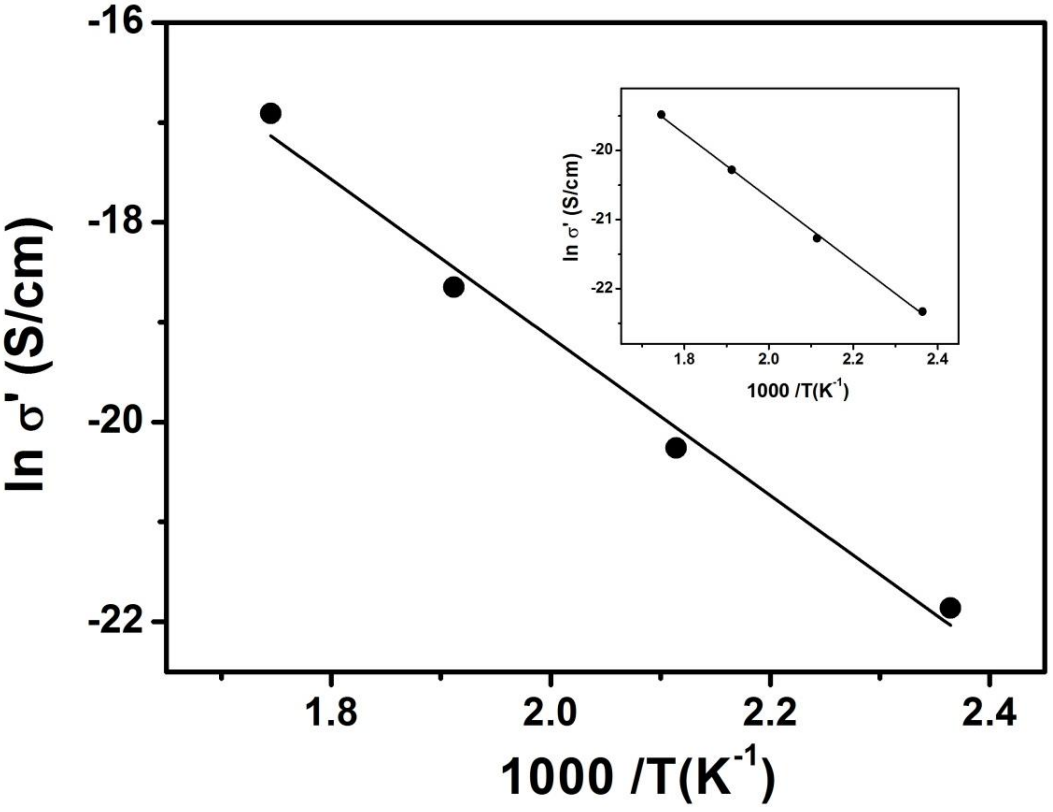

Figure 7.7 Arrhenius plot for AC conductivity of BBN and BBSmN (Inset) ceramics.

determined from these plots for BBN and BBSmN are of the order of 0.68 eV and 0.40 eV indicating the motion of oxygen ion vacancy through the lattice. Interestingly, the activation

energy of samarium doped BBN ceramics is identified to be lesser than that of undoped BBN which clearly suggests that the doping of rare earth samarium ion in the bismuth site of the crystal lattice has controlled the creation of oxygen ion vacancies arising out of the volatilization of bismuth oxide [25].

7.5. Conclusions

The dielectric and electrical conductivity behaviour of undoped and samarium doped $BaBi_2Nb_2O_9$ ceramics have been studied in the 100 Hz - 1 MHz frequency range at various temperatures. These ceramics have been found to exhibit the behaviour of relaxor ferroelectrics. The conductivity data fits well to the Jonscher's law in these ceramics and the parameters $A(T)$ and $n(T)$ have been determined. Interestingly, these parameters exhibited an anomaly in the dielectric phase transition region ($\approx T_m$) suggesting a coupling between charge carriers and lattice.

References

[1] T. Mazon, M.A. Zaghete, M.Cilense, J.A.Varela, *Ceram. Int.* **35**, 3143 (2009).

[2] D. Debasis, G.K. Tanmay, P.Panchanan, *Solid State Sci* .**9**, 57 (2007).

[3] M. Adamczyk, L.Kozielski, M.Pilch, *Ferroelectrics* **417**, 1 (2011).

[4] T. Shigyo, H.Itoh, J.Takahashi, *J. Mater. Sci: Mater. Electron.***21**, 302 (2010).

[5] M.Adamczyk, Z.Ujma, M.Pawelczyk, *J. Mater. Sci.***41**, 5317 (2006).

[6] H.C. Gupta, Archana, V.Luthra, *Vib. Spectrosc.***56**, 235 (2011).

[7] C.A.P. de Araujo, J.D. Cuchiaro, I.D. McMillan, M.C. Scott, J.F. Scott, *Nature*, **374**, 627 (1995).

[8] J. Glaum, M. Hoffman, *J. Am. Ceram. Soc*. **97**, 665 (2014).

[9] C. Karthik, K.B.R. Varma, *Mater. Sci. Eng., B* **129**, 245 (2006).

[10] Y.M. Kan, G.J. Zhang, P.L. Wang, Y.B. Cheng, *J. Eur. Ceram. Soc.* **28**, 1641 (2008).

[11] J.L.P. Flores, E.Chavira, J.R. Gasga, A.M. Gonzalez, A.H. Tera, *J. Eur. Ceram. Soc*. **23**, 839 (2003).

[12] K.R. Whittle, N.C. Hyatt, I.M. Reaney, Chem. Mater. **20**, 6427 (2008).

[13] V. B. Santos, J.-C. M'Peko, M.Mir, V.R. Mastelaro, A.C. Hernandes, *J. Eur. Ceram. Soc.***29**, 751(2009).

[14] P. Dhak, D. Dhak, M. Das, P. Pramanik, *J. Mater. Sci: Mater. Electron*. **22**, 1750 (2011).

[15] S. Rachana, S.Bhattacharyya, S.M. Gupta, *Mater. Sci. Eng., B* **175**, 207 (2010).

[16] J.D. Bobic, M.M. V. Petrovic, J.Banys, B.D.Stojanovic, *Ceram. Int*. **39**, 8049 (2013).

[17] M. Roy, I.Bala, S.K. Barbar, S.Jangid, P.Dave, *J. Phys. Chem. Solids* **72**, 1347 (2011).

[18] S. Rachna, S. Bhattacharyya, S.M. Gupta, *J. Phys. Chem. Solids* **69**, 822 (2008).

[19] L. Sun, C.Fang, L.Chen, S.Huang, *J.Am.Ceram.Soc* .**90**, 3875 (2007).

[20] M. Verma, K. Sreenivas, Vinay Gupta, *J. Appl. Phys*. **105**, 024511 (2009).

[21] C. Karthik, K.B.R. Varma, *J. Appl. Phys.* **101**, 014106 (2007).

[22] S. N. Padamavathi , Ch. Sameera Devi , M. Vithal , G. Prasad, G S. Kumar, *Ferroelectrics* **445**, 121 (2013).

[23] A.K. Jonscher, Dielectric Relaxation in Solids (Chelsea Dielectric Press, London, 1983).

[24] B.H. Venkataraman, K.B.R. Varma, *J.Phys. Chem. Solids* **64**, 2105 (2003)

[25] B. Angadi, P. Victor, V.M. Jali, M.T. Lagare, R. Kumar, S.B. Krupanidhi, *Mater. Sci. Eng., B* **100**, 93 (2003).

CHAPTER 8

Summary and Conclusions

8. Summary and Conclusions

8.1. Summary and Conclusions

Chapter 1 : Introduction

This chapter primarily describes the underlying phenomenon of dielectric and ferroelectric properties of materials. In addition to the principles and phenomena, the modelling of dielectric behaviour of ferroelectric materials by Jonscher's universal formalism has also been briefly discussed. Subsequently, the interesting aspects of the crystal structure and physical properties of Aurivillius family of layered ferroelectric ceramics, reported in the literature have been dealt.

Chapter 2 : Experimental Techniques

In this chapter, the experimental techniques that have been employed to synthesize and characterize the layered ferroelectric ceramic materials under investigations are described. The details pertaining the materials fabrication techniques adopted to fabricate polycrystalline ceramics is discussed. The structural and microstructural characterization of these materials was carried out by X - ray powder diffraction and scanning electron microscopy techniques. The dielectric and electrical conductivity measurements on these materials are reported. The ferroelectric properties of the materials under investigations were demonstrated by the Sawyer-Tower techniques.

Chapter 3 : Structural and Dielectric Properties of Strontium Bismuth Samarium Tantalate Layered Perovskites

Polycrystalline $Sr(Bi_{0.9}Sm_{0.1})_2Ta_2O_9$ (SBSmT) ceramics were fabricated via the promising low temperature molten salt synthesis route using potassium chloride (KCl) as a flux material. The mono-phasic perovskite crystal structure is confirmed by the X-ray powder diffraction patterns. The scanning electron microscopic studies revealed the presence of plate shaped morphological features of the SBSmT ceramics. Interestingly, the dielectric constant of the SBSmT ceramics in the frequency range of 100 Hz – 1 MHz could be tuned as a function of sintering duration. It is observed that the SBSmT ceramics sintered at 1323 K for 10 h exhibited higher dielectric constant (ε'_r= 76) at 100 kHz than those of ceramics sintered at other durations. The magnitude of the electrical conductivity of the order of 10^{-7} - 10^{-9}

S/cm at 300 K indicates that the conductivity mechanism might be attributed to the migration of oxygen ion vacancies in these ceramics.

Chapter 4 : Fabrication, Structural, Microstructural and Dielectric Properties of Samarium Doped Strontium Bismuth Tantalate Ceramics

This chapter comprises the fabrication and characterization of samarium doped strontium bismuth tantalate ceramics. Layered $Sr(Bi_{1-x}Sm_x)_2Ta_2O_9$ ceramics with x ranging from 0 - 0.10 (10 mol%) were fabricated by the low temperature molten salt synthesis route. X - ray powder diffraction studies revealed that the single phase orthorhombic layered perovskite structure is retained in all these compositions. Scanning electron microscopic studies on these ceramics confirmed the presence of well packed equiaxed plate shaped gra ins. The dielectric and electrical conductivity properties were studied in the 100Hz - 1 MHz frequency range at 300 K. Interestingly, the 10 mol% samarium doped $SrBi_2Ta_2O_9$ ceramics exhibited high dielectric constant (ε'_r = 155) and low dielectric loss (0.00298) compared to those of other compositions. The ferroelectric property of $SrBi_2Ta_2O_9$ ceramics is superior for higher concentration of samarium content. The electrical conductivity of undoped and samarium doped ceramics increased linearly with increase in frequency at 300 K.

Chapter 5 : Temperature Dependent Dielectric and Electrical Conductivity Characteristics of Undoped and Samarium Doped $SrBi_2Ta_2O_9$ Ceramics

This chapter deals with the dielectric and electrical conductivity measurements carried out on undoped and samarium doped SBT ceramics at various frequencies and temperature of interest, whose fabrication, structural, microstructural and ferroelectric properties were dealt in the previous chapter. Undoped and samarium doped $SrBi_2Ta_2O_9$ ferroelectric ceramics have been fabricated by the molten salt synthesis route. The dielectric and electrical conductivity measurements were carried out in the 100 Hz - 1 MHz frequency range at various temperatures. A decrease in dielectric constant maximum (ε_m) and a downward shift in the Curie transition temperature (T_c) have been observed with the increase in samarium concentration. The frequency dependence real and imaginary parts of dielectric constant of these ceramics exhibited low frequency dielectric dispersion. Interestingly, temperature and frequency dependence dielectric constant plots indicated that the formation of oxygen ion vacancies have inhibited by samarium doping in SBT lattice. The activation energy values

obtained from the Arrhenius plot have confirmed the existence of motion of oxygen ion vacancies in these ceramics.

Chapter 6 : Structural, Microstructural and Dielectric Characteristics of Samarium Doped $BaBi_2Nb_2O_9$ Relaxor Ferroelectrics

This chapter describes the fabrication and characterization of samarium doped barium bismuth niobate relaxor ferroelectric ceramics.Barium bismuth samarium niobate $Ba(Bi_{1-x}Sm_x)_2Nb_2O_9$ (x = 0, 0.03, 0.05, and 0.10) ceramics have been fabricated successfully via molten salt synthesis route. The X - ray diffraction analysis revealed the existence of bismuth layered perovskite phase with orthorhombic crystal structure in all the compositions studied. The dielectric and electrical conductivity properties were carried out in the 100 Hz - 1MHz frequency range at 300 K. The dielectric constant and dielectric loss were found to decrease from 186 to 180 and 0.0966 to 0.0755 with increase in samarium content at 100 kHz.

Chapter 7 : Dielectric Relaxor and Conductivity Characteristics of Barium Bismuth Niobate Ferroelectric Ceramics

This chapter presents the temperature and frequency dependence of dielectric and conductivity characteristics of undoped and samarium doped BBN relaxor ferroelectric ceramics whose fabrication, structural and microstructural properties have been discussed in the previous chapter. The polycrystalline $BaBi_2Nb_2O_9$ and $Ba(Bi_{0.9}Sm_{0.1})_2Nb_2O_9$ ceramics have been fabricated via the molten salt synthesis route. The temperature dependence of dielectric and electrical conductivity properties of BBN and BBSmN ceramics investigated at various frequencies have revealed the characteristic features of relaxor behaviour. The incorporation of Sm^{3+} for Bi^{3+} has induced a downward shift in the dielectric maximum temperature (438 K - 393 K) with the decrease in dielectric constant maximum (372 - 212) at 100 kHz. The estimated degree of diffuseness (γ) was found to be 2.17 for BBN and 1.93 for BBSmN ceramic samples. The activation energy obtained from the Arrhenius plot revealed the existence of motion of oxygen ion vacancy in these ceramics.

8.2. Future Scope of Work

The present investigations on various physical properties of samarium doped layered ferroelectric materials have provided a gateway for interesting prospects of future research.

- Suitably doped trivalent rare earth ion layered ferroelectric ceramics would open up the scope in enhancing the memory storage capacity of non - volatile random access devices.
- Fabrication of these materials in thin film form could be embedded as “Integrated Circuit” chip in random access memory that would cater rousing possibilities of utilizing the aforementioned ferroelectric materials for practical memory device applications.
- A detailed study on the temperature dependent impedance and ferroelectric properties on these ceramics in bulk/thin film form would provide unique insights in memory device fabrication technology.

9. **LIST OF PUBLICATIONS**

1. Dielectric and Electrical Conductivity Characteristics of Undoped and Samarium Doped Ferroelectric $SrBi_2Ta_2O_9$ Ceramics Derived From Molten Salt Synthesis Route
   B. Rajesh Kannan and B. HariharaVenkataraman
   Ferroelectrics, 493 (2016) 110-119.

2. Structural and dielectric properties of strontium bismuth samarium tantalate layered perovskites
   B. Rajesh Kannan and B. HariharaVenkataraman
   Ferroelectric Letters, 42 (2015) 18 - 26.

3. Effect of rare earth ion doping on the structural, microstructural and diffused phase transition characteristics of $BaBi_2Nb_2O_9$ relaxor ferroelectrics
   B. Rajesh Kannan and B. HariharaVenkataraman
   Ceramics International, 40 (2014) 16365.

4. Influence of samarium doping on structural and dielectric properties of strontium bismuth tantalate ceramics derived by molten salt synthesis route
   B. Rajesh Kannan and B. HariharaVenkataraman
   Journal of Materials Science : Materials in Electronics, 25 (2014) 4943.

5. An integrated use of Biopolymer-Ceramic composites towards capacitor and environmental application
   B. Rajesh Kannan, S. Kalidhasan, A. Santhana Krishna Kumar,N. Rajesh and B. HariharaVenkataraman
   Polymer - Plastics Technology and Engineering, 53 (2014) 626.

6. Dielectric relaxor and conductivity characteristics of undoped and samarium doped barium bismuth niobate ferroelectric ceramics
   B. Rajesh Kannan and B. HariharaVenkataraman
   Ferroelectric Letters (Accepted, 2016).

INTERNATIONAL/NATIONAL CONFERENCES

1. Trivalent Rare Earth Ion Doped Layered Ferroelectric Oxide Ceramic Materials for Electronic Storage Device Applications
   B. Rajesh Kannan and B. HariharaVenkataraman
   8th International conference on Materials for Advanced Technologies of Materials Research Society of Singapore, Singapore, June 28 - July 3, 2015

2. Electrical Properties of Barium Bismuth Samarium Niobate Ferroelectrics for Non - Volatile Random Access Memory Device Application
   B. Rajesh Kannan and B.HariharaVenkataraman

National Conference on Materials for Energy Conversion and Storage, VIT Chennai, India. March 19 - 21, 2015

3. Temperature - Dependent Dielectric and Electrical Characteristics of Undoped and Samarium Doped $SrBi_2Ta_2O_9$ Ferroelectric Ceramics
   B. Rajesh Kannan and B.HariharaVenkataraman
   14th Asian Conference on Solid State Ionics, National University of Singapore, Singapore. June 24 - 27, 2014, Proceedings of the 14th Asian Conference on Solid State Ionics **[ISBN: 978-981-09-1137-9]**

4. Rare Earth Doped $BaBi_2Nb_2O_9$ Ferroelectrics for Memory Storage Device Applications
   B. Rajesh Kannan and B.HariharaVenkataraman
   Indo- UK International workshop on advanced materials and their applications in Nanotechnology,
   BITS Pilani - Goa campus, Goa, India
   May 17 - 19, 2014

5. Microstructural and dielectric properties of undoped and samarium doped barium bismuth niobate ferroelectric ceramics synthesized by molten - salt flux route
   B. Rajesh Kannan and B. HariharaVenkataraman
   International Conference on Advanced Functional Materials, NIIST, Trivandrum
   February 19 - 21, 2014

6. Dielectric and electrical conductivity studies on undoped and samarium doped strontium bismuth tantalate ceramics
   B. Rajesh Kannan and B. HariharaVenkataraman
   10th National Conference on Solid State Ionics, IIT Kharagpur, India
   December 22 - 24, 2013

7. Effect of samarium substitution on the structural and dielectric properties of strontium bismuth tantalate ceramics
   B. Rajesh Kannan and B.HariharaVenkataraman
   National Conference on Physics and Chemistry of Solids, Khammam, India
   April 12 - 13, 2013

8. Molten salt synthesis and dielectric characterization of samarium ion doped $SrBi_2Ta_2O_9$ ferroelectric ceramics
   B. Rajesh Kannan and B. HariharaVenkataraman
   International Conference on Materials Science and Technology, Kottayam, India
   June 10 - 14, 2012

9. Study of the interesting properties of Biopolymer - Strontium Titanate Nanocomposites
   B. Rajesh Kannan, S. Kalidhasan, A. Santhana Krishna Kumar, N. Rajesh and B. HariharaVenkataraman
   International Conference on Nanoscience and Technology, Hyderabad, India
   January 20 - 23, 2012

Brief Biography of the Candidate

Rajesh Kannan B received his B.Sc. (2006) and M.Sc. degree (2008) from the Physics Department, Alagappa University, Karaikudi. In 2009, he joined Central Electrochemical Research Institute (CSIR-CECRI) Karaikudi and worked as a Project Assistant till April 2010. In October 2010, he joined as a Project Fellow based on the DST Fast - Track project in the Department of Physics, BITS -Pilani Hyderabad Campus and he registered for his Ph. D in August 2011 under the supervision of Dr. B. HariharaVenkataraman, Physics Department. His extensive research work on the fabrication and characterization of rare earth doped layered ferroelectric materials has yielded very interesting results and he has already published 5 papers in peer reviewed international journals and presented his research work in various reputed national and international conferences.

Brief Biography of the Supervisor

Dr. B. Harihara Venkataraman is an Assistant Professor in the Department of Physics, BITS - PILANI, Hyderabad Campus, Hyderabad. He was awarded Ph.D in Materials Science by Indian Institute of Science, Bangalore in 2006. He was a post-doctoral researcher at Nagaoka University of Technology, Nagaoka, Japan from June 2006 to September 2008. He has research expertise in glass/polymer nanocomposites, laser writing in glasses for optical based device applications, structure - property correlation studies in layered ferroelectric materials. He has published over 20 research articles in peer reviewed international journals and presented 15 papers in national and international conferences and written one book chapter. He received "Young Scientist Fast Track Project" from the Department of Science and Technology, New Delhi, 2010, Awarded "Centre of Excellence (COE) fellowship" for post - doctoral programme in Japan and also "Reviewer" in International Journals.